The role of IGF-1R signaling in the DNA damage response of Prostate Cancer

Kunal Lodhia
Oriel College

Department of Medical Oncology
University of Oxford
Weatherall Institute for Molecular Medicine





Contents

ABSTRACT 5

ACKNOWLEDGEMENTS 7

LIST OF FIGURES 9

LIST OF TABLES 11

ABBREVIATIONS 12

CHAPTER 1: INTRODUCTION 14

1.1 Prostate Cancer 14
1.1.1 Screening and Diagnosis of Prostate Cancer 15
1.1.2 Prostate Cancer Treatment 15

1.2 The Insulin-like growth factor (IGF) axis 17
1.2.1 IGF ligand and binding proteins 17
1.2.2 IGF-1R 18
1.2.3 IGF-1R Signalling Pathways 19

1.3 The role of IGF-1R in cancer biology 25
1.3.1 Expression of IGFs and IGF-1R in cancer 25
1.3.2 IGF-1R in malignant cell growth 28
1.3.3 Role of IGF-1R in apoptosis 30
1.3.4 Role of IGF-1R in metastasis 33

1.4 IGF-1R as a therapeutic target 35
1.4.1 Biomarker identification 38
1.4.2 The role of IGF-1R in the repair of DNA double strand breaks (DSBs) 40

1.7 Objectives of this project 45

CHAPTER 2: MATERIALS AND METHODS 46

2.1 Mammalian Cell Culture 46
2.1.1 General techniques 46
2.1.2 Cell Lines and Cell Culture 46
2.1.3 DNA transfection 47
2.1.4 Gene Silencing by RNA interference 48
2.1.5 Treatment with small molecule inhibitors 50
2.1.6 Treatment with IGF-1 ligand 50
2.1.7 Gamma Irradiation of cells 51

2.2 Protein Analysis 51
2.2.1 Collection and lysis of adherent cells 51
2.2.2 Cell Fractionation Methods 52
2.2.3 Western Blot 54
2.2.4 Immunoprecipitation 56
2.2.5 Co-Immunoprecipitation 56
2.2.6 Acid Elution of Immunoprecipitates 57

2.3 Procedures for DNA work 58
2.3.1 General Techniques 58
2.3.2 Quantification of nucleic acids 58
2.3.3 Preparation of plasmids 58
2.3.4 Digestion of DNA with restriction endonucleases 59
2.3.5 Gel electrophoresis of DNA 59

2.4 Procedure for RNA Extraction and Quantitative real-time PCR (qRT-PCR) 60
2.4.1 General Techniques 60
2.4.2 RNA Extraction from cultured cells 60
2.4.3 Reverse Transcription (RT) 61
2.4.4 qRT-PCR 61

2.4 Cell Based Assays 62
2.4.1 Growth Assays 62
2.4.2 Immunofluorescence Microscopy 63
2.4.3 Cell Cycle Analysis by Flow Cytometry 64

2.5 Mass Spectrometry (MS) Analysis 66
2.5.1. General techniques 66
2.5.2. In Gel Digest 66
2.5.3. In Solution digest 67
2.5.4 ZipTip Purification 68
2.5.5. Mass Spectrometry 68

2.6 Statistical Analysis 68

CHAPTER 3: INVESTIGATION OF THE HYPOTHESIS THAT ATM FUNCTION IS INFLUENCED BY IGF SIGNALLING IN HUMAN PROSTATE CANCER CELLS 70

3.1 The Role of IGF-1R in DNA Repair 70

3.2 Results 71
3.2.1 Inhibition of IGF-1R sensitises DU145 prostate cancer cells to Ionizing Radiation 71
3.2.2 Detection of a 350 kDa protein that is phosphorylated on a motif recognized by AKT in response to IGF-I 75
3.2.2 Use of siRNA and short hairpin approaches to investigate the IGF-induced 350kDa phospho-product 77
3.2.3 Probing for Phospho-AKT substrate motif immunoreactivity in ATM immunoprecipitates 79
3.2.4 Functional significance of AKT inhibition on radiosensitivity of DU145 83
3.2.5 Assay for radio-resistant DNA synthesis 86

3.2.5 Use of siRNA and inhibitors to study ATM dependent phosphorylation of downstream mediators 89

3.3 Discussion 91

CHAPTER 4: INVESTIGATING THE BINDING PARTNERS OF NUCLEAR IGF-1R 93

4.1 Introduction 93

4.2 Results 95
4.2.1 Immunoprecipitation of nuclear IGF-1R 95
4.2.2 Initial MS analysis 99
4.2.3 Further optimization of nuclear IGF-1R extraction and immunoprecipitation 104
4.2.4 Identification of potential IGF-1 ligand induced nuclear IGF-1R binding partners 113
4.2.5 Identification of potential DNA damage induced nuclear IGF-1R binding partners 120
4.2.5 General Transcription Factor II-I as a potential binding partner for nuclear IGF-1R 126

4.3 Discussion 130

CHAPTER 5: INVESTIGATION OF DNA REPAIR HITS IDENTIFIED IN A SYNTHETIC LETHALITY SCREEN USING IGF-1R INHIBITOR 132

5.1 Introduction 132

5.2 Results 133
5.2.1 Screen for proteins that regulate sensitivity to IGF-1R inhibition 133
5.2.2 Validation of RAD51 as a screen hit in DU145 prostate cancer cells 136
5.2.3 Investigating the effects of RAD51 depletion on sensitivity of IGF-1R inhibition in a panel of prostate cancer cell lines 140
5.2.4 Investigating the effects of RAD51 depletion on IGF-1 signalling 147
5.2.6 Investigating the effects of BRCA2 depletion or deficiency on sensitivity to IGF-1R inhibition 149
5.2.7 Investigating whether small molecule CDK1 inhibitor mimics effects of RAD51 depletion in enhancing sensitivity to IGF-1R inhibition 157

5.3 Discussion 163

CHAPTER 6: CONCLUSION AND FUTURE DIRECTIONS 165

BIBLIOGRAPHY 170

Abstract

The type 1 insulin like growth factor receptor (IGF-1R) is a cell surface receptor that mediates proliferation and cell survival. The aim of this project was to explore the contribution of the IGF-1R to the DNA damage response in human prostate cancer cells. Previous work from our group showed IGF-1R to be over expressed in prostate cancer. Furthermore, IGF-1R depletion enhances sensitivity of prostate cancer cells to DNA damaging agents, and IGF-1R depletion or inhibition delays DSB repair. Prior work in melanoma cells indicated that IGF-1R down-regulation enhances radiosensitivity and impairs the function of ATM, a key protein in the response to DNA DSB. This led to the initial hypothesis that IGF-1R signalling can influence ATM function, possibly via the PI3K-AKT pathway. Two putative AKT phosphorylation sites were identified on ATM and initial experiments detected a 350 kDa protein equivalent to the size of ATM, that was phosphorylated on RXRXXS/T motif(s) in response to IGF-1. However, it did not prove possible to identify this immunoreactivity in ATM immunoprecipitates, and AKT inhibition, although radiosensitizing, did not induce features of defective ATM function. Therefore this project was halted and two new projects exploring the role of IGF signalling in DNA repair were undertaken. The first project continues from work published from our laboratory showing that IGF-1R undergoes nuclear translocation in prostate cancer cells. The function of nuclear IGF-1R is unclear, and mass spectrometry (MS) was utilized to identify potential nuclear binding partners. Nuclear extraction and IGF-1R immunoprecipitation methods were modified in order to achieve optimal conditions for subsequent MS analysis. Three independent MS analyses have been performed aiming to identify binding partners of nuclear IGF-1R in cells grown in complete medium, cells that were serum-starved and IGF-1 treated, or exposed to irradiation-induced DNA damage. Candidate binding partners included transcription factors

such as Bruton's tyrosine kinase associated protein 135 (BAP-135) also known as general transcription factor II-I (TF II-I), suggesting possible involvement of nuclear IGF-1R in the regulation of transcription. Initial validation experiments suggested IGF-1 induced complex formation between IGF-1R and TF II-I, and also tyrosine phosphorylation of TF II-I in response to IGF-1, raising the possibility that IGF-1 influences TF II-I function. The second project is based on a high throughput screen completed by another member of our laboratory, that sought to identify DNA repair-related proteins that when depleted increased the sensitivity of prostate cancer cells to IGF-1R inhibition. One of the potential hits is RAD51, a recombinase central to the strand invasion step of homologous recombination (HR). Initial experiments validated RAD51 knockdown by the screen siRNAs, and showed that RAD51 depletion did indeed enhance sensitivity to a novel IGF-1R inhibitor in PTEN wild type prostate cancer cells. Loading of RAD51 onto single stranded DNA requires BRCA2, and in a PTEN wild type colorectal cell line model, lack of BRCA2 was shown to sensitize colorectal cancer cells to IGF-1R inhibition, compared to isogenic cells that expressed functional BRCA2. Finally, experiments also sought to mimic effects of RAD51 depletion using a small molecule CDK1inhibitor, R0-3306, recently shown to impair HR by inhibiting BRCA1 function. In prostate cancer cells, R0-3306 at the determined GI_{50} value (1 μM) suppressed formation of RAD51 foci, consistent with HR attenuation. Furthermore, CDK1 inhibition phenocopied the effects of RAD51 depletion, sensitizing prostate cancer cells to IGF-1R inhibition with a 2.4 fold reduction in GI_{50} value and 13 fold reduction in the GI_{80}. These data suggest that the sensitivity of human prostate cancer cells to IGF-1R inhibition can be enhanced by genetic and chemical approaches to suppress HR, and that BRCA mutant cancers may be intrinsically sensitive to IGF-1R inhibition. The ultimate aim of this work is to understand how IGF-1R biology influences DNA damage repair, in order to guide the development of new treatments for prostate cancer.

Acknowledgements

Firstly, I am very grateful to my supervisor, Dr. Val Macaulay, for her countless hours of hard work and support throughout my D.Phil. It has been a wonderful opportunity to complete my D.Phil. in her laboratory. I would also like to thank my co-supervisor, Dr. Tamara Aleksic, for not only her guidance with my work but also for her friendship. Both, Dr. Macaulay and Dr. Aleksic have been excellent mentors and helped me develop and grow not only as a scientist but as an individual. I am also fortunate to have worked with a great team of scientists and doctors: Meenali Chitnis, Philip Earwaker, Shan Gao, Mark Goodfellow, Hilde Jalving, Martin Kerr and Roger Ramcharan. You have all been the best colleagues and friends that I could have asked for and I greatly appreciate everything you have done for me.

I would also like to thank all the friends I have made at Oxford. I would especially like to thank Meenali Chitnis; you have been a constant source of motivation and inspiration. I will never forget our morning number 11, cell culture and FACS sessions, as well as our runs and squash matches. I will always remember the time we spent together with great fondness. I would also like to thank Philipp Schautschick for the great memories at formal halls, cooking at JMH, gym sessions, and travels. You have both been great friends and positive influences on my life and I am truly grateful for everything you have done for me.

Lastly, but not least, I would like to thank my mom, dad, and sister for their unconditional love and support. My family has been there for me in the good times and the hard times, yet there has not been a day of my life when I feel that I cannot count on them for support and the motivation to continually strive for excellence. I love you very much and thanks for everything.

Dedication:

I would like to dedicate my D.Phil to my grandparents: Bapuji, Ba, Nana and Nani

List of Figures

Chapter 1

Figure 1: Signalling downstream of the IGF-1R 21

Figure 2: Effects of IGF-1R signalling in cell cycle progression..... 30

Figure 3: Methods of targeting IGF-1R 37

Figure 4: DNA DSB repair pathways 42

Figure 5: Effects of IGF axis on DSB repair 44

Chapter 3

Figure 6: Effects of IGF-1R inhibition on IGF signalling and radiosensitivity of DU145 74

Figure 7: Investigation of possible IGF-induced phosphorylation by AKT on ATM ... 76

Figure 8: Effects of depletion of AKT or ATM on IGF-induced 350 kDa phospho-protein 78

Figure 9: Immunoprecipitation of endogenous ATM 81

Figure 10: Immunoprecipitation of overexpressed ATM..... 82

Figure 11: Effects of IGF-1R and AKT inhibition on radiosensitivity of DU145 cells . 85

Figure 12: Cell Cycle distribution following irradiation of DU45 cells..... 88

Figure 13: Effect of AKT and IGF-1R depletion or inhibition on downstream effectors of ATM 90

Chapter 4

Figure 14: Immunoprecipitation of nuclear IGF-1R 98

Figure 15: Analysis of large-scale IGF-1R IPs..... 101

Figure 16: Amino acid sequence of Bruton tyrosine kinase associated protein 135 (BAP-135) 104

Figure 17: Nuclear fractionation..... 106

Figure 18: Optimisation of nuclear extraction by different washing methods..... 109

Figure 19: Nuclear IGF-1R IP using in-house washing and lysis buffers..... 112

Figure 20: Testing fractionation and immunoprecipitation in IGF or solvent treated cells..... 118

Figure 21: IGF-1R interacts with chromatin of irradiated cells 122

Figure 22: Diagram of General Transcription Factor II-I 129

Figure 23: Investigating a potential interaction and post-translational modification on TFII-I by IGF-1R 129

Chapter 5

Figure 24: siRNA screen for synthetic/sickness lethality with IGF-1R inhibition 135

Figure 25: Validating RAD51 screen siRNA 137

Figure 26: Effects of RAD51 depletion on sensitivity to IGF-1R inhibition in DU145 cells 139

Figure 27: Characterisation of a panel of prostate cancer cell lines 142

Figure 28: RAD51 depletion by reverse transfection in prostate cancer cells 144

Figure 29: Effects of RAD51 depletion on sensitivity to IGF-1R inhibition in prostate cancer cell lines 145

Figure 30: Investigating RAD51 depletion affects on IGF-induced signalling 148

Figure 31: Initial stages of Homologous Recombination Repair 150

Figure 32: Assessment of BRCA2 screen siRNAs by quantitative real-time PCR .. 152

Figure 33: Characterization of DLD1 BRCA2 WT and Null cells 154

Figure 34: BRCA2 deficient cells fail to form radiation induced RAD51 foci 155

Figure 35: BRCA2 status affects sensitivity to IGF-1R inhibition 156

Figure 36: Effects of CDK1 in Homologous recombination DSB repair 158

Figure 37: Effects of CDK1 inhibition on viability of DU145 prostate cancer cells .. 160

Figure 38: CDK1 inhibition impairs RAD51 focus formation 160

Figure 39: CDK1 inhibition sensitises DU145 prostate cancer cells to IGF-1R inhibition 162

List of Tables

Chapter 2

Table 1: Human Cancer Cell Lines 47

Table 2: Short Interfering RNA used for Gene Silencing 49

Table 3: Cell Seeding and Transfection reagents for siRNA transfection 50

Table 4: Primary Antibodies for western blotting 55

Table 5: PCR Primers for qRT-PCR 62

Table 6: Primary Antibodies for Immunofluorescence 64

Chapter 4

Table 7: Proteins identified in IGF-1R (Band 12) and control (Band 13) immunoprecipitates. 103

Table 8: Potential IGF-1 induced IGF-1R binding partners 119

Table 9: Potential IGF-1R binding partners detected in non-irradiated and irradiated conditions 125

Chapter 5

Table 10: Effects of RAD51 depletion on sensitivity to IGF-1R inhibition 140

Table 11: Characterization of Prostate Cancer Cell Lines 142

Table 12: GI_{50} values and fold sensitization to IGF-1R inhibition in prostate cancer cell lines 146

Abbreviations

AKT	Protein Kinase B
ANOVA	Analysis of variance
AR	Androgen Receptor
AS	Allstars negative control
ATM	Ataxia Telangiectasia Mutated
ATP	Adenosine Triphosphate
ATR	Ataxia telangiectasia and RAD3-related protein
BCA	Bicinchoninic Acid
bp	base pairs
BRCA1	Breast Cancer type 1 susceptibility protein
BRCA2	Breast Cancer type 2 susceptibility protein
BrdU	Bromodeoxyuridine
BSA	Bovine Serum Albumin
CDK	Cyclin dependent kinase
CTG	CellTiter Glo
Da	Dalton
DMEM	Dulbecco's Modified Eagle's Medium
DMSO	Dimethyl sulphoxide
DNA	Deoxyribonucleic Acid
DNA-PKcs	DNA-dependent protein kinase, catalytic subunit
DSB	Double strand break
EDTA	Ethylene diamine tetraacetic acid
eGFP	Enhanced green fluorescent protein
EGFR	Epidermal Growth Factor Receptor
ERK	Extracellular-signal related kinase
EV	Empty vector
FCS	Foetal calf serum
GI_{50}	Concentration of inhibitor required to inhibit growth of cells to 50% of solvent
GSK3-α/β	Glycogen synthase kinase 3-alpha (α) and -beta (β)
Gy	Gray
ɣ-H2AX	Histone variant 2AX phosphorylated on serine 139
HR	Homologous Recombination
IC_{50}	Half maximal inhibitory concentration
IGF-I/2	Insulin-like growth factor 1/2
IGF-1R	Insulin-like growth factor receptor type 1
IR	Insulin receptor
IRS-1	Insulin receptor substrate-1
kDa	Kilodalton
MEK	Mitogen-activated protein kinase kinase
MRN	protein complex consisting of Mre11, Rad50 and NBS-1
mRNA	Messenger ribonucleic acid
mTOR	Mammalian target of rapamycin
NHEJ	Non-homologous end joining
nM	Nanomolar
p53	Protein 53
PARP	Poly(ADP-ribose) polymerase
PBS	Phosphate buffered saline
PBS-T	Phosphate buffered saline with 0.05% Tween-20

PCR	Polymerase chain reaction
PI	Propidium iodide
PI3K	Phosphatidyl inositol-3 kinase
PSA	Prostate-specific antigen
PTEN	Phosphatase and tensin homologue deleted on chromosome 10
qRT-PCR	Quantitative real-time polymerase chain reaction
RT	Reverse transcriptase
RTK	Receptor tyrosine kinase
RTKi	Receptor tyrosine kinase inhibitor
SDS	Sodium dodecyl sulphate
SF_{50}	Concentration required to inhibit survival by 50% of solvent control
shRNA	Short hairpin RNA
siRNA	Short interfering RNA
SSL	Synthetic sickness/lethality
TBS	Tris buffered saline
TBS-T	Tris buffered saline with 0.1% Tween 20
Thr	Threonine
Tyr	Tyrosine
µg	Microgram
VEGF	Vascular endothelial growth factor
WT	Wild Type

Chapter 1: Introduction

1.1 Prostate Cancer

The prostate is a gland located below the bladder in men. The size of the prostate is typically very small in younger males but grows in size with age. The prostate's primary responsibility is for the production for seminal fluid that helps transport sperm (http://www.nhs.uk/conditions/Prostate-disease/). Cancer of the prostate is the most common cancer affecting men in the UK and the second most common cause of death from cancer among men. In 2007, 36,100 new cases were diagnosed in the UK alone, accounting for a quarter of all new cases of cancer diagnosed in men in the UK (http://info.cancerresearchuk.org/cancerstats/). By 2009, there were 40,800 new cases being diagnosed in the UK, an increase of 4,700 new cases over two years (http://info.cancerresearchuk.org/cancerstats/). In America, prostate cancer is the second most common cancer affecting men, after lung cancer, with a projection of nearly 242,000 new cases in 2012 alone (http://www.cancer.org//ProstateCancer). The incidence of prostate cancer is increasing, but the number of deaths in the UK has not changed, with death rates of 23.9 and 23.8 per 100,000 diagnoses in 2008 and 2010, respectively (http://www.cancerresearchuk.org/cancerstats/).

Prostate cancer is unique in that its growth is largely dependent on androgen signaling (Friedlander and Ryan, 2012). Prostate cancer can be cured if diagnosed early, but metastatic prostate cancer is incurable. Metastases are most commonly found in bone, and metastatic disease is initially responsive to endocrine therapy, but inevitably becomes hormone resistant, and only shows modest response to chemotherapy (Tannock *et al.*, 2004). There is a need to develop therapies that will not only improve the quality of life but prolong survival rates.

1.1.1 Screening and Diagnosis of Prostate Cancer

Clinically, prostate cancer incidence has increased in men younger than 70, and this might be attributed to diet, alcohol consumption and environmental factors (Damber and Aus, 2008). Prostate cancer can be curable if diagnosed at its early stages. Prostate Specific Antigen (PSA), a protease secreted by the epithelial cells of the prostate, is used as a screen for diagnosis of prostate cancer (Damber and Aus, 2008). Attempts are being made to identify other factors, such as urine markers, that can be used in place of or in addition to PSA testing, to increase chances of diagnosing prostate cancer in its earlier stages, such as urine markers; however at the moment PSA is still the best marker (Muller and Brenner, 2006; Stenman *et al.*, 2005).

Diagnosis of prostate cancer is made by pathological analysis of tissue samples taken directly from the prostate. Typically, 8-12 core tissue biopsies are obtained for analysis using a rectal probe. Prostate tissues are graded using Gleason scores on a scale of 2 to 10, with 2 being the most well differentiated and least aggressive, and 10 being undifferentiated and the most aggressive (Aus *et al.*, 2005).

1.1.2 Prostate Cancer Treatment

Currently, stage, grade and PSA levels are the best prognostic indicators for patients with non-metastatic prostate cancer (Graefen *et al.*, 2004). The change in levels of total serum PSA over time is used routinely as a method of monitoring prostate cancer treatment (Damber and Aus, 2008).

There are a range of treatment options for localized prostate cancer, including active monitoring, radical prostatectomy, or hormone or radiotherapy. Choices for treatment are based on the characteristics of the cancer and life expectancy (Damber and Aus, 2008). Recent data suggests that active surveillance is appropriate in older men with low risk disease (Wilt *et al.*, 2012). Treatment with curative intent for localized prostate cancer usually uses radical surgery or radiotherapy as the standard treatment options and the efficacy of radiotherapy can be increased by combination with neoadjuvant or adjuvant hormone therapy (Thompson *et al.*, 2006; Van der Kwast *et al.*, 2007). Adjuvant androgen deprivation has also been shown to reduce the risk of progression after radiotherapy for locally advanced prostate cancer (Denham *et al.*, 2011).

There are several treatment options for metastatic prostate cancer but none are curative. Palliative hormone therapy is the standard treatment option (Singh and Srivastava, 2007); early studies using the synthetic estrogen diethylstilbestrol showed a delay in disease progression, but the survival advantage was complicated by the increased risk of cardiovascular toxicity (Damber, 2004). Current practice includes sequential use of Luteinizing-hormone-releasing hormone (LHRH) analoges to suppress the hypothalamic-pituitary drive to testosterone production, and antiandrogens such as bicalutamide (Tannock *et al.*, 2004). Chemotherapy was thought to be ineffective until a report showing that docetaxel alone or in combination with estramustine improved the survival of men with hormone resistant prostate cancer (Tannock *et al.*, 2004). New developments include the use of abiraterone to suppress adrenal androgen production (Fizazi *et al.*, 2012), the novel antiandrogen enzalutamide (MDV3100), and novel taxane cabazitaxel (Omlin and de Bono, 2012). However, responses to these novel agents are generally quite brief, and there remains a pressing need to develop more effective treatment options.

1.2 The Insulin-like growth factor (IGF) axis

The type 1 insulin like growth factor receptor (IGF-1R) is key molecule that transduces signals from extracellular ligand, leading to intracellular activation of pathways that regulate proliferation, survival and metastasis (**Figure 1**). The IGF axis includes the ligands IGF-1 and IGF-2, which activate transmembrane IGF-1R (Chitnis *et al.*, 2008). The bioactivity of IGF-1 and IGF-2 is regulated by IGF binding proteins (IGFBPs) and IGFBP-specific proteases (Denley *et al.*, 2005).

1.2.1 IGF ligand and binding proteins

IGF-1 and IGF-2 are similar in amino acid sequence and molecular structure, and hepatic secretion of IGF-1 is tightly regulated by growth hormone (Mathews *et al.*, 1986; Underwood *et al.*, 1994). IGFs are important for growth and have a key role in development, with IGF-2 playing a central role during embryonic development. However, mice harbouring a disrupted IGF-1 gene have a 40% reduction in body weight compared to wild type mice (Liu *et al.*, 1993), suggesting that in addition to IGF-2, IGF-1 is required for embryonic development. IGF-1 binds to IGF-1R with a 6 to 8 fold higher affinity than IGF-2 (Clemmons, 2007). IGF-2 also binds to IGF-2R which differs greatly from IGF-1R in structure, has no known signalling function and mediates internalization and degradation of IGF-2 (Pavelic *et al.*, 2002). IGF-2 knockout mice are viable but have marked reduction in bodyweight, approximately 60% of normal birth weight, while abnormal increase in IGF-2 results in overgrowth (DeChiara *et al.*, 1990; Eggenschwiler *et al.*, 1997).

IGF bioactivity is regulated by the family of 6 IGFBPs that are primarily synthesized in the liver. The most abundant IGFBP in serum is IGFPB3, which has the highest affinity for IGF-1 and IGF-2 (Shimasaki and Ling, 1991; Shimasaki *et al.*, 1991), and regulates the serum half-life of IGF-1 and IGF-2 (Laursen *et al.*, 2007). Some IGFBPs promote IGF bioactivity, for example IGFBP-2 and -5 are associated with metastasis and poor prognosis in breast cancer (Wang *et al.*, 2008). IGFBPs are negatively regulated by IGFBP-specific proteases, which cleave IGFBPs, reducing affinity for IGFs and enhancing IGF bioactivity (Collett-Solberg and Cohen, 1996). PSA is characterized as an IGFBP-3 protease, which can cause proteolysis of IGFBP-3, reducing its binding affinity for IGF-1 (Moschos and Mantzoros, 2002).

1.2.2 IGF-1R

The *IGF-1R* gene is located on chromosome 15 and is expressed in all types of cells except hepatocytes and T lymphocytes (Moschos and Mantzoros, 2002). Prostatic expression of the IGF-1R is up-regulated by androgens and growth hormone and regulated by insulin, IGF-1 and IFN-ɣ (Pandini *et al.*, 2005; Rubini *et al.*, 1994; Shalita-Chesner *et al.*, 2001).

The IGF-1R is a transmembrane receptor tyrosine kinase (RTK), initially translated as a single-chain polypeptide of 220 kDa with a 30 amino acid signal peptide at the N-terminus (Adams *et al.*, 2000). Following glycosylation and formation of dimers, the 220 kDa proreceptor undergoes further cleavage in the Golgi apparatus to produce a mature receptor containing two 135 kDa extracellular α-subunits and two 97 kDa transmembrane β-subunits, linked by disulfide bonds (Adams *et al.*, 2000; Ullrich *et al.*, 1986). The extracellular alpha subunit contains a ligand binding domain that has a 6-8 fold higher affinity for IGF-1 than for IGF-2, and also binds insulin at

micromolar concentrations (Forbes *et al.*, 2002). The transmembrane beta subunit contains the kinase domain that undergoes a series of autophosphorylations on tyrosine residues 1131, 1135 and 1136, upon binding of ligand (Adams *et al.*, 2000). These and other phosphorylations lead to a conformational change in the cytoplasmic domain that allows for downstream signalling cascades that are key to many aspects of the malignant phenotype, including growth, transformation, and protection from apoptosis.

1.2.3 IGF-1R Signalling Pathways

After ligand binding and autophosphorylation, activated IGF-1R is capable of initiating downstream signalling by recruitment and phosphorylation of intracellular substrates including insulin receptor substrate 1 to 4 (IRS-1 to IRS-4), Src homology and collagen domain protein (SHC) and growth-factor-receptor-bound protein 2 (Grb2) (**Figure 1**) (Chitnis *et al.*, 2008; Sehat *et al.*, 2007). Recruitment of IRS-1 initiates signalling via the phosphoinositide-3-kinase (PI3K)/AKT pathway and recruitment of SHC activates signalling via the RAS-RAF-extracellular signal-regulated kinase (ERK) pathway (**Figure 1**) (Pollak *et al.*, 2004).

Signalling via the AKT pathway begins when IRS-1 is recruited to phosphorylated tyrosine 950 on IGF-1R, which in turn leads to recruitment and activation of PI3K. This leads to the addition of a phosphate group to phosphatidyl inositol 3, 4-diphosphate (PIP_2), converting PIP_2 to phosphatidyl inositol-3,4,5 triphosphate (PIP_3). PI3K activity is reversed by the tumour suppressor protein phosphatase and tensin homolog (PTEN), which is capable of dephosphorylating PIP_3 to PIP_2 (Stambolic *et al.*, 1998). Production of PIP_3 leads to membrane translocation and activation of phosphoinositide-dependent kinase-1 (PDK-1) and downstream activation of protein kinase B (AKT) (Manning and Cantley, 2007). PDK-1 phosphorylates AKT on

threonine 308, and mammalian target of rapamycin (mTOR) complex 2 (mTORC2) phosphorylates AKT on serine 473 (Carnero, 2010). Activated AKT is a serine/threonine kinase that is capable of activating a wide range of substrates that regulate cell cycle progression, survival and growth (Manning and Cantley, 2007). AKT accomplishes this by phosphorylating substrates on the R-X-R-X-X-S/T-B motif, where X represents any amino acid, B represents a bulky hydrophobic residue and S/T is the phosphorylated serine or threonine (Alessi *et al.*, 1996). For example, AKT can inactivate the tumour suppressor tuberous sclerosis (TSC) complex 2 (TSC2), to enhance the activity of mTOR complex 1 (mTORC1) that promotes translation via inhibiting phosphorylation of 4EBP1 or activating p70 S6 Kinase (P70 S6K) (Laplante and Sabatini, 2012). AKT induces cell survival and protection from apoptosis by inhibitory phosphorylation of GSK3, FOXO, BAD and Caspase 9 (Downward, 2004; Sheppard *et al.*, 2012). **Figure 1** summarizes the key steps of IGF-1R signalling via the PI3K-AKT pathway.

Activation of the MAPK-ERK pathway begins when Shc is recruited to the IGF-1R β-subunit. Binding of Shc to the IGF-1R leads to recruitment of growth factor protein 2 (GRB2) and the mammalian homolog of son of sevenless (SOS). This cascade leads to activation of the GTPase, RAS, which subsequently activates the serine/threonine kinase, RAF. Activated RAF phosphorylates and activates mitogen-activated protein kinase 1/2 (MEK1/2), which phosphorylates and activates extracellular signal-regulated kinases 1/2 (ERK 1/2). ERKs play a role in cell proliferation and differentiation by regulating transcription of approximately 160 target genes (Yoon and Seger, 2006).

The IGF-1R is capable of activating several other signaling pathways, in addition to signaling via RAS-MEK and PI3K-AKT. Activated IGF-1R can phosphorylate janus

kinase 1/2 (JAK1/2), leading to phosphorylation of a family of signalling transducers and activators of transcription (STATs) that regulates growth, survival and differentiation (Zong *et al.*, 2000). Activated PI3K also promotes activation of Rac, a Rho GTPase, which leads to the activation of downstream effectors LIM kinase and cofilin, promoting cellular proliferation, motility and morphogenesis (Meyer *et al.*, 2005; Stachelscheid *et al.*, 2008).

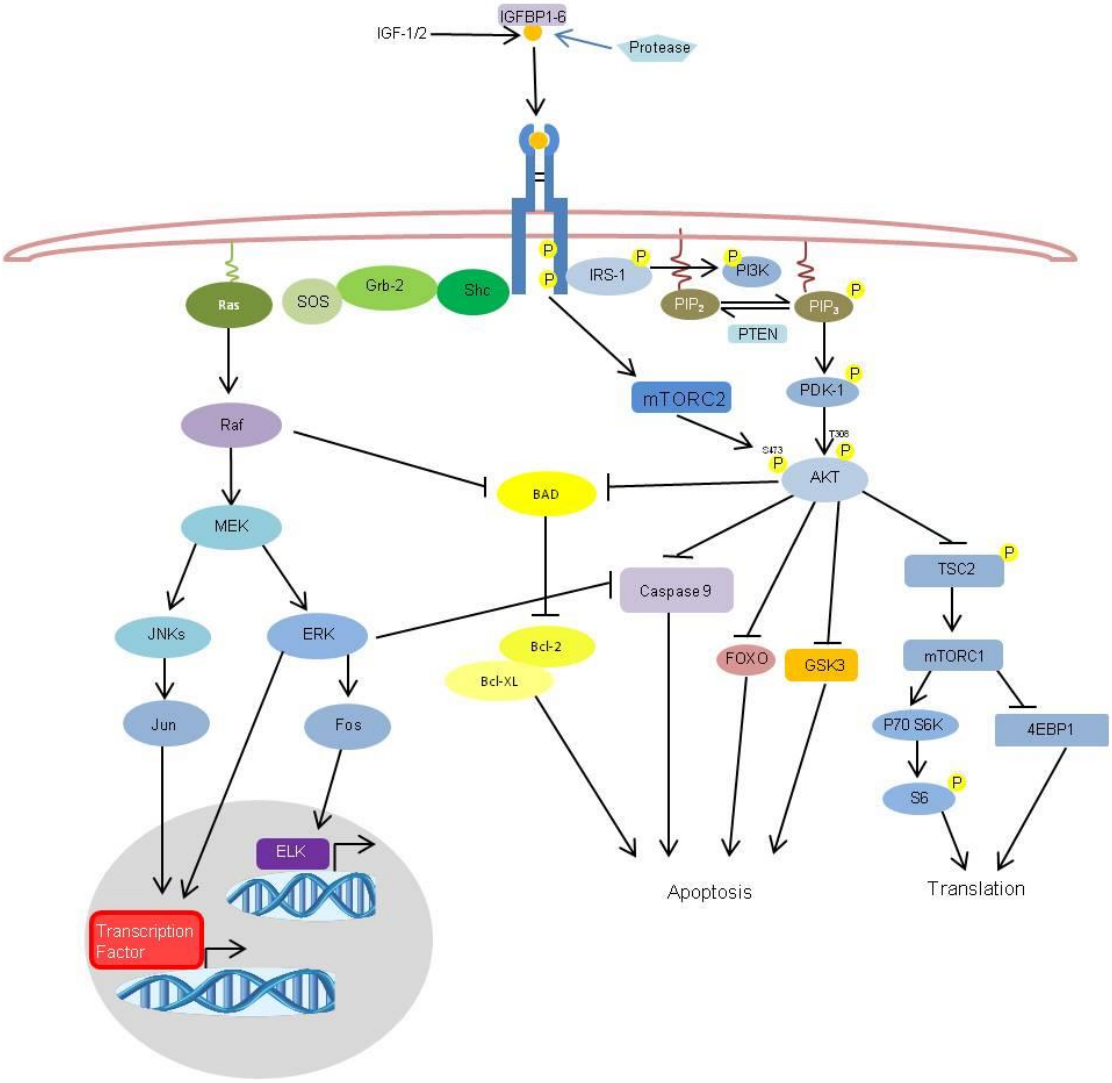


Figure 1: Signalling downstream of the IGF-1R

Signalling via the IGF-1R begins with binding of its ligands IGF-1, IGF-2 or insulin to the extracellular α-subunit and this in turn leads to phosphorylation of the intracellular β-subunits. Recruitment of the adaptor protein IRS-1 to the activated receptor initiates signalling via the PI3K-AKT pathway leading to such cellular responses as protection from apoptosis, proliferation and translation. Recruitment of adaptor protein SHC leads to activation of the RAS-MEK pathway leading to changes in gene expression. Diagram made from references cited in text.

1.2.3.1 Crosstalk between IGF-1R and insulin receptor

The Insulin receptor (IR) and IGF-1R evolved from a single ancestral receptor involved in the regulation of metabolism, growth and longevity (Djiogue *et al.*, 2012). The primary function of the IR is to regulate glucose uptake and metabolism, while the IGF-1R is involved in growth, cell cycle regulation, cell survival, tumorigenesis and metastasis. Although the two receptors have acquired different functions, the structure remains well conserved. The IR shares 70% homology in amino acid sequence with IGF-1R, and each receptor is translated as a single polypeptide chain, consisting of an α and β subunit, known as a half-receptor, that is then covalently linked into a tetrameric $\alpha_2\beta_2$ receptor (Ullrich *et al.*, 1986). Activated IR promotes uptake of glucose via phosphorylation of IRS, leading to high affinity binding of glucose transporters to the outer membrane of insulin-responsive cells (Saltiel and Kahn, 2001).

The human insulin receptor exists in two variants that are generated by alternative splicing of exon 11 (Seino and Bell, 1989). The two variants differ by 12 amino acids in the carboxy terminus of the alpha subunit, which are spliced out in IR variant type A (IR-A) (Benecke *et al.*, 1992). IR-B is the full length IR that plays a major role in the uptake of glucose. IR-A can be activated not only insulin but also by IGF-2, leading to proliferation and protection from apoptosis (Malaguarnera *et al.*, 2012). This suggests that the IR-A shares more similarity with the IGF-1R, and could play a crucial role in tumour development and biology. In addition, IR-A and IR-B can form hybrid receptors with IGF-1R, and these hybrid receptors may possess different ligand binding affinities (Pollak, 2012).

1.2.3.2 Crosstalk between IGF-1R and Epidermal Growth Factor Receptor (EGFR) Family

The EGFR (also known as HER1) is a member of the EGFR family of receptors, which includes four structurally similar RTKs (HER1 – HER4). Similar to the IR and IGF-1R, EGFR contains an extracellular ligand binding domain and a transmembrane domain that includes the cytoplasmic tyrosine kinase (Yarden, 2001). Upon binding of ligands epidermal growth factor (EGF) and transforming growth factor alpha (TGF α), the EGFR forms homodimers or heterodimers with other HER receptors. Dimerized receptors are activated by autophosphorylations, which initiate downstream signalling pathways including PI3K-AKT, JAK-STAT and the RAS-ERKs (Ono and Kuwano, 2006).

Like IGF-1R, EGFR plays a role in cell proliferation and protection from apoptosis, and shares many downstream signalling pathways (Ono and Kuwano, 2006). Previous work from our group detected complex formation between the IGF-1R and EGFR by reciprocal co-immunoprecipitation, and the stability of IGF-1R protein is reportedly regulated by EGFR (Riedemann *et al.*, 2007). Blocking EGFR results in increased IGF-1R activity and conversely, depleting IGF-1R results in increased EGFR activation. Thus, activation of EGFR or IGF-1R is reported as a mechanism to enhance resistance to inhibition of either receptor (Cortot *et al.*, 2012; Riedemann *et al.*, 2007; Wheeler *et al.*, 2010).

1.2.3.3 Crosstalk between IGF-1R and Androgen Receptor

The androgen receptor (AR) is a nuclear receptor that is activated by binding of dihydrotestosterone, leading to a conformational change that renders the AR capable of interacting not only with specific DNA elements but also with basal transcription factors, such as general transcription factor II-IF (McEwan and Gustafsson, 1997). The AR is also capable of interacting with other signalling pathways through protein-

protein interactions. There is crosstalk between the AR and the IGF axis in that the AR can bind to the IGF-1 promoter to increase the expression levels of IGF-1 (Wu *et al.*, 2007). The AR can also upregulate IGF-1R via nongenotropic pathways involving AR binding to Src (Pandini *et al.*, 2009). Moreover, studies in prostate cancer cells have shown that IGF-1, IGF-2 and EGF alone can activate AR to different extents in the absence of androgen, and in the presence of androgen and IGF-1 or EGF there is enhanced activation of AR transcriptional activity (Culig *et al.*, 1996; Orio *et al.*, 2002). Growth factor induced enhancement of AR activity could be inhibited by the antiandrogen hydroxyflutamide, suggesting that this increase is androgen-dependent (Orio *et al.*, 2002). Recent data indicate that AR transcriptional activity is activated by downstream PI3K and AKT inhibition, and conversely, AR inhibition leads to PI3K-AKT activation in PTEN-deficient mouse and human prostate cancer models (Carver *et al.*, 2011).

1.3 The role of IGF-1R in cancer biology

Cancer is a disease in which normal cells acquire one or more genetic mutations that result in a malignant phenotype. These mutations often lead to favourable growth conditions and the ability to invade and metastasize to distant sites. Mutated genes that allow cells to acquire a function that promotes cancer development are termed oncogenes, while mutated genes that lead to a loss of function that inhibit cancer formation are known as tumour supressors. *Hanahan and Weinberg* described six "hallmarks of cancer" that enable normal cells to acquire the malignant phenotype (Hanahan and Weinberg, 2000). These six characteristics are: 1) self-sufficiency in growth signals, 2) insensitivity to anti-growth signals, 3) tissue invasion and metastasis, 4) limitless replicative potential, 5) sustained angiogenesis and 6) evading apoptosis (Hanahan and Weinberg, 2000). Subsequently, two additional hallmarks of cancer have been added: reprogramming of energy metabolism and evading immune destruction (Hanahan and Weinberg, 2011).

The role of IGFs and IGF-1R signalling has been widely studied in cancer biology, revealing that activation of IGF-1R signalling leads to several of the "hallmarks of cancer", including: cell motility, proliferation, and cell survival, which are all essential in tumour development and progression (Baserga *et al.*, 1997; Pollak, 2012).

1.3.1 Expression of IGFs and IGF-1R in cancer

It has been established that high circulating levels of IGF-1 are associated with risk of developing cancers of the colon (Rinaldi *et al.*, 2010), breast (Key *et al.*, 2010), ovary (Yee *et al.*, 1991), lung (Yu *et al.*, 1999) and prostate (Chan *et al.*, 1998; Roddam *et al.*, 2008). Recent data also show a link between high IGF-1 levels and prostate cancer mortality (Rowlands *et al.*, 2012). In addition to being produced by the liver and peripheral tissues, IGFs are also expressed by cancer cells, although factors that

regulate autocrine production of IGF-1 by tumours are not well understood. Mouse IGF-1 is regulated by estrogen by direct binding of estrogen receptor α (ERα) to the estrogen-responsive element (ERE) in the mouse IGF-1 promoter (Hewitt *et al.*, 2010). Although no ERE is known in the human IGF-1 promoter, chromatin immunoprecipitation (ChIP) analysis shows binding of ERα to the human IGF-1 promoter, and in ovarian and breast cancer cells, estrogen activates IGF-1 mRNA expression (Sasaki *et al.*, 2008). Mutations in the breast cancer susceptibility gene 1 and 2 (BRCA1 and BRCA2) have been shown to elevate IGF-1 expression and furthermore, siRNA mediated BRCA1 depletion increases intracellular IGF-1 in primary human mammary gland cells (Hudelist *et al.*, 2007).

Previous work from our laboratory and others has shown that IGF-1R is frequently overexpressed in established cancers including colon (Tricoli *et al.*, 1986), lung (Minuto *et al.*, 1986), melanoma (Kanter-Lewensohn *et al.*, 1998), bladder (Rochester *et al.*, 2007) and kidney (Yuen *et al.*, 2007). Furthermore, work in our laboratory examined IGF-1R expression in 54 primary prostate tissue samples and found that IGF-1R expression is up-regulated at the protein and mRNA levels in primary prostate cancer, and commonly persists in metastatic disease (Hellawell *et al.*, 2002). Further work from our laboratory studied IGF-1R expression in serial samples of prostate cancer, and showed that IGF-1R expression remains high throughout disease progression (Turney *et al.*, 2011). IGF-1R expression by prostate cancer can be influenced by AR via enhanced c-Src activity, which subsequently activates ERK 1/2 and stimulates IGF-1R promoter activity (Pandini *et al.*, 2009). BRCA1 has also been shown to differentially regulate *IGF-1R* gene transcription in an AR-dependent manner (Schayek *et al.*, 2009). PTEN is mutated in approximately 33% of all prostate cancers (Mutter, 2001) and PTEN status was shown to suppress IGF-1R expression at the level of translation (Zhao *et al.*, 2004a). The IGF-1R promoter is

also targeted by several oncogenes including c-myb, and tumour suppressors such as tumour protein 53 (p53), to influence IGF-1R expression at the transcriptional level (Ohlsson *et al.*, 1998; Reiss *et al.*, 1991). P53 mutations have been reported in approximately 20% of prostate cancers, moreover the rate of p53 alterations increases with prostate cancer progression (Schlomm *et al.*, 2008). The tumour suppressor p53 is a nuclear transcription factor that plays an important role in tumour biology, and regulating cell cycle progression, genome stability and apoptosis, all aspects of the "Hallmarks of Cancer" (Oren, 1999). It has been shown that wild-type p53 negatively regulates IGF-1R expression by suppressing activation of the IGF-1R promoter, while mutant p53 leads to increased IGF-1R promoter activity (Ohlsson *et al.*, 1998; Werner *et al.*, 1996). However, in p53 wild type melanoma cells that overexpress IGF-1R, inhibition of p53 led to IGF-1R downregulation, followed by cell death (Hussein, 2004; Kanter-Lewensohn *et al.*, 2000). The oncoprotein murine double minute 2 (MDM2) is a key regulator of p53, and overexpression of MDM2 results in decreased levels and activity of p53 (Kubbutat *et al.*, 1997). Under conditions when p53 is inhibited, MDM2 has been shown to be redistributed and bind to IGF-1R, leading to its ubiquitination and degradation (Girnita *et al.*, 2003).

The Von Hippel Lindau (VHL) protein (pVHL) interacts with hypoxia inducible factors (HIFs) under normal physiological conditions in the presence of oxygen. Under these conditions pVHL ubiquitinates HIF1α and causes its degradation. In the absence of oxygen, the pVHL does not bind to HIF1α, allowing HIF1α to dimerize with HIF1β, activating the transcription of genes involved in cellular metabolism and glucose uptake (Kaelin, 2007). Previous work in our laboratory showed that the tumour suppressor gene VHL negatively regulates IGF-1R expression in renal cancer cells (Yuen *et al.*, 2007).

1.3.2 IGF-1R in malignant cell growth

In prostate cancer IGFs have been shown to act as important regulators of epithelial cell growth and differentiation, as well as prostate cancer development (Roberts, 2004). IGF-1 and IGF-1R play an important role in regulating cell cycle progression, principally by promoting the transition through G1 into S phase (**Figure 2**). This is accomplished largely by IGF-1 induced up-regulation of cyclin D1, reported to be the rate limiting factor in the G1-S transition (Sherr, 1996; van der Burg *et al.*, 1988). Type D-cyclins (D1, D2 and D3) bind to cyclin dependent kinases (CDK) 4 and 6, and this activated complex is capable of phosphorylating retinoblastoma protein (RB) (Sherr, 1996; Symeonidou *et al.*, 2012). Phosphorylated RB releases E2F transcription factors, which in turn promote S-phase progression by activating the transcription of cell cycle genes (Sherr, 1996). One of the important transcriptional targets of the activated Cyclin D1/CDK4 complex is cyclin E, which forms a complex with CDK2 during late G1 and is required for entry into S-phase (Frederick and Wood, 2004). The ability of IGF-1R to regulate cyclin D1 expression is mediated by both the MAPK-ERK and PI3K-AKT pathways (Lavoie *et al.*, 1996a; Lavoie *et al.*, 1996b; Sherr, 1996). CDK activity is regulated by interactions with a family of CDK inhibitory proteins (CIPs), the CIP/KIP family, which includes $p21^{CIPI}$ and $p27^{KIP1}$ (Denicourt and Dowdy, 2004). Over-expression of any of the CIP/KIP family members can lead to cell cycle arrest, for example forced expression of $p27^{KIP1}$ in phases other than G0 and early G1, results in disruption of the cyclin D1/CDK4 complex and G1 arrest (Denicourt and Dowdy, 2004). In contrast to IGF-1R, IGFBP3 has been shown to lead to G1 arrest in renal 786-O, epithelial adenocarcinoma cells A549 and breast MCF7 breast cancer cells, by decreasing cyclin E1 expression and increasing p21 expression (Wu *et al.*, 2012a). The effects of IGF-signalling on the cell cycle are summarized in **Figure 2**.

IGF-1R has been shown to be crucial for anchorage independent growth, a characteristic of malignant cells, and required for tumorigenesis and metastasis. Normal cells will undergo apoptosis if they lose contact with other cells or with the substratum, however, transformed cancer cells exhibit anchorage-independent growth *in vitro* (Shin *et al.*, 1975). Anchorage-independent growth can be acquired by various cellular changes, including ectopic expression of IGF-1R and IRS-1 (Baserga, 1999). Work from many laboratories has demonstrated that a certain amount of IGF-1R must be expressed on the cell surface before anchorage independent growth can occur (Baserga, 1999; Larsson *et al.*, 2005; Zhang *et al.*, 2006). This suggests that as cancers acquire the anchorage independence necessary for metastasis, the cancer may be becoming more IGF-1R dependent (Larsson *et al.*, 2005).

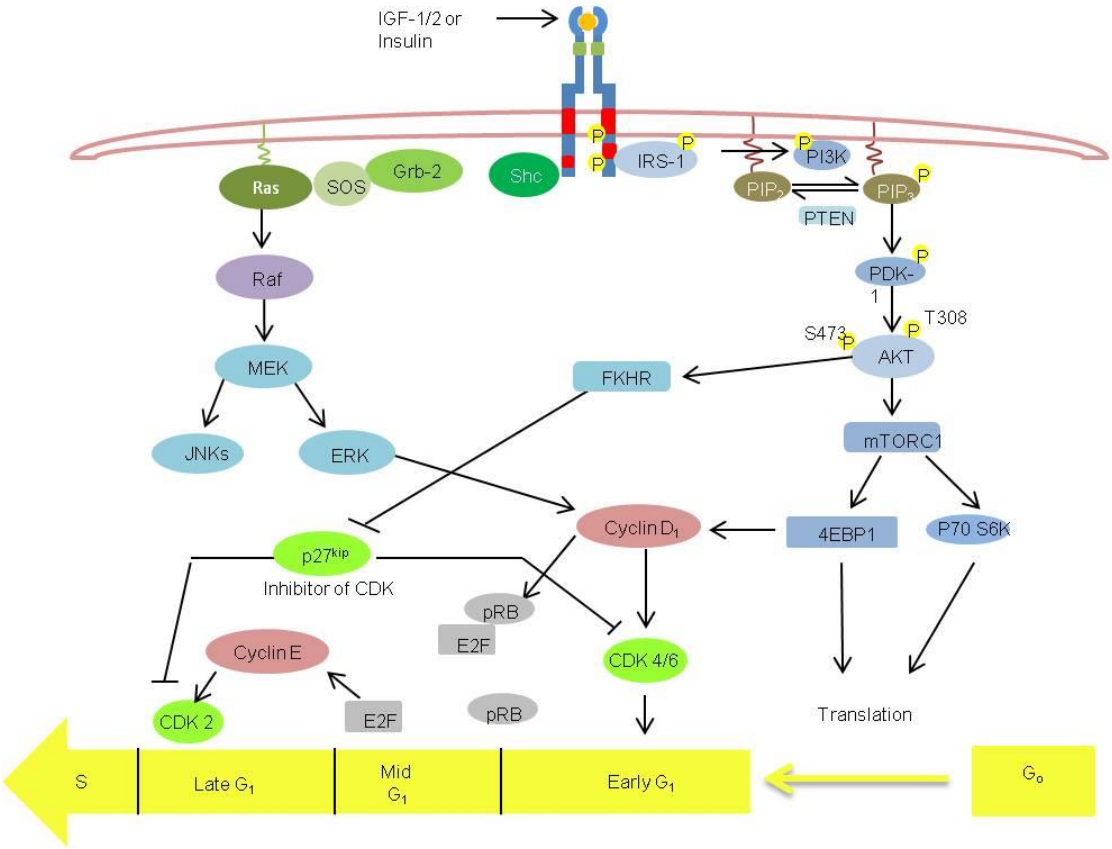


Figure 2: Effects of IGF-1R signalling in cell cycle progression

IGF-1R signalling can effect cell cycle progression through control of several cycle checkpoints. Its major direct effects occur by controlling progression through G1 and entry into S phase, by inducing expression of cyclin D1, and inhibitory regulation of cyclin dependent kinase inhibitor, $p27^{kip}$.

1.3.3 Role of IGF-1R in apoptosis

Resisting cell death is one of the hallmarks of cancer. There are four major identified forms of cell death that are differentiated by morphology: apoptosis, necrosis, autophagy, and mitotic spindle catastrophy (Kroemer *et al.*, 2009). Apoptosis is the major and most well-characterised form of cell death and is a highly regulated process that typically involves the disassembly and repackaging of the cellular components (Alison and Sarraf, 1992). Apoptosis begins with activation of death ligand (TNFα, TNF-related apoptosis-inducing ligand (TRAIL) and Fas ligand (FasL)) and death receptors, results in the formation of a complex of caspase-8, Fas-associated protein with death domain (FADD), and receptor-interacting serine-

threonine kinase 1 (RIP1) (Sola *et al.*, 2013). Activated caspase-8 cleaves and thus inactivates RIP1; however if caspase-8 is inhibited or absent, RIP1 recruits RIP3 and initiates necrosis (Wu *et al.*, 2012a). Necrosis is morphologically characterised by a swelling of cellular organelles and rupture of plasma membrane ultimately leading to the loss of cellular contents (Kroemer *et al.*, 2009). Initiation of necrosis leads to enhanced cellular metabolism, which is accompanied by increasing production of reactive oxygen species (ROS) (Ouyang *et al.*, 2012). Excessive production of ROS can lead to mitochondrial membrane permeabilization and subsequently programmed necrosis (Kroemer *et al.*, 2009; Wu *et al.*, 2012b). Mitotic spindle catastrophe occurs either during or shortly after a dysregulated or failed mitosis, which often results in the formation of micronucleation, the presence of chromosome fragments that have not been evenly distributed between daughter cells, or multinucleation, the presence of two or more nuclei (Castedo *et al.*, 2004; Vakifahmetoglu *et al.*, 2008). Autophagy is characterised by the sequestrating of cytoplasm organelles and material into autophagosomoes for bulk degradation by lysosomes and is morphologically defined by massive autophagic vacuolization of the cytoplasm (Denton *et al.*, 2012; Kroemer *et al.*, 2009) IGFs have been implicated in regulating autophagy by activating mTOR kinase, resulting in inhibition of the proteins required for the initial steps of the autophagy such as autophagy- related gene-1 (Atg1) complex (Neufeld, 2010). However, the mode of cell death most closely associated with the IGF axis is apoptosis.

The IGF axis has been shown to play an important role in cell survival by protection from apoptosis, and depletion or inhibition of IGF-1R can lead to apoptosis *in vitro* (Jernberg-Wiklund and Nilsson, 2007; O'Connor *et al.*, 1997). Classically, apoptosis is activated by the intrinsic, mitochondrial pathway, or extrinsic pathway which begins with activation of pro-apoptotic receptors on the cell surface (Elmore, 2007). As the

name suggests, the intrinsic pathway is initiated within the cell, usually as a result of negative stimuli such as absence of growth factors, hormones and cytokines, or positive stimuli such as radiation, toxins, hypoxia, viral infection and free radicals (Kooijman, 2006). These stimuli lead to internal signalling that causes the pro-apoptotic Bcl2 proteins, Bad, Bax, and Bid to oligomerize, opening pores in the mitochondrial membrane, causing the release of cytochrome c (Ott *et al.*, 2002; Saelens *et al.*, 2004). In the cytosol, cytochrome c binds to and activates the apoptotic protease activating factor 1 (Apaf-1) and procysteine-dependent aspartate-specific protease 9 (procaspase-9); this complex is known as an apoptosome (Hill *et al.*, 2004). Clustering of procaspase-9 leads to activation of caspase-9 and downstream activation of caspase-3 and/or caspase-7 (Li and Yuan, 2008). Caspase-3 activates the execution pathway that involves activation of endonucleases for DNA fragmentation and chromosomal degradation, and proteases that degrade nuclear and cytoplasmic proteins (Elmore, 2007).

By contrast, the extrinsic pathway signals by transmembrane death receptors that are part of the tumour necrosis factor (TNF) or Fas receptor family (Locksley *et al.*, 2001). Activation of TNF or Fas receptors recruits adaptor proteins and leads to proteolytic cleavage and activation of caspase-8 and caspase-10, which in turn leads to activation of caspase-3 and the execution pathway (Kischkel *et al.*, 1995).

Increased activity and overexpression of IGF-1R has been shown to protect cancer cells from apoptosis by regulating the intrinsic pathway at the transcriptional and post-transcriptional level. Firstly, signalling via the PI3K-AKT pathway leads to activation of the cAMP-responsive element binding (CREB) protein, which in turn increases CREB transcriptional activity and increases expression of Bcl-2 and Bcl-XL (Du and Montminy, 1998; Kooijman, 2006; Pugazhenthi *et al.*, 2000). Secondly,

activated IGF-1R leads to activation of AKT, which phosphorylates and inactivates several pro-apoptotic proteins including Bad. In its inactive state, Bad localizes at the mitochondrial wall and binds to Bcl-2 (Alison and Sarraf, 1992; Danial, 2008).

1.3.4 Role of IGF-1R in metastasis

Another hallmark of cancer is the ability of cancer cells to invade and metastasize. The migration of cancer cells from a primary tumour to a distant organ is known as metastasis, and the expression of IGF-1R is associated with development of lung metastases in synovial sarcomas, liver metastasis in uveal melanoma and lymph node metastasises in gastric cancers (All-Ericsson *et al.*, 2002; Jiang *et al.*, 2004; Xie *et al.*, 1999). In prostate cancer, IGF-1, IGF-1R and its signalling components play a role in the development of bone metastases (Bubendorf *et al.*, 2000). Metastatic prostate cancer cells preferentially adhere to bone marrow endothelial cells and this process is shown to be dependent on the expression of Cadherin 11, which tends to be overexpressed in primary cancer (Chu *et al.*, 2008; Sikes *et al.*, 2004). Once adhered, metastatic prostate cancer cells are stimulated by the high levels of bone-derived growth factors including IGF-1 (Menagh *et al.*, 2010).

Typically, metastasis from a primary tumour is a multistep process that involves lymphangiogenesis and angiogenesis, degradation of extracellular matrix (ECM), cellular migration through blood vessels, cell survival and proliferation in the circulation, and ability to grow at the secondary site (Hanahan and Weinberg, 2011; Nguyen *et al.*, 2009). IGF-1R signalling has a role in many of these steps (Samani *et al.*, 2007). Angiogenesis is the process by which developing tumours overcome the lack of oxygen and nutrient rich blood supply by secreting chemicals to induce the formation of new vessels. Under normoxia, a family of prolyl-hydroxylase domain (PHD)-containing enzymes hydroxylate HIF-1α. Hydroxylated HIF-1α is recognized

by the Von Hippel-Lindau (VHL) protein and subsequently ubiquitinated, thus marking it for proteolytic degradation (Greer *et al.*, 2012). Under hypoxic conditions or in VHL null cells, HIF-1α is stabilized and promotes the expression of proteins that facilitate the cellular response to hypoxia, including vascular endothelial growth factor (VEGF) (Carmeliet and Jain, 2000). Under normoxia, IGF-1 and IGF-2 can lead to increased synthesis of HIF-1α and expression of VEGF in colon cancer cells, by signaling via PI3K and ERK1/2 (Fukuda *et al.*, 2002). Studies have also shown that IGFs are capable of inducing expression of HIF-1α, which is required for expression of genes encoding IGF-2, IGFBP2 and IGFBP3 (Feldser *et al.*, 1999).

Cancer cells can also induce lymphangiogenesis, the formation of new lymphatic vessels, and this process is mediated by the VEGF receptor 3 (VEGFR-3) ligands VEGF-C and VEGF-D (Mandriota *et al.*, 2001; Stacker *et al.*, 2001). In breast, colon and prostate cancer, increased expression of VEFG-C correlates with increased risk of metastasis to regional lymph nodes (Nisato *et al.*, 2003). IGF-1R signalling via PI3K can act as a positive regulator of VEFG-C expression, lymphatic endothelial cell proliferation migration and lymphatic metastasis (Bjorndahl *et al.*, 2005; Tang *et al.*, 2003).

Another potential limiting factor for metastasis is degradation of extracellular matrix (ECM), which is facilitated by a family of proteinases known as the matrix metalloproteinases (MMPs) (Zhang *et al.*, 2003). MMPs are synthesized and secreted as inactive pro-MMPs, and activity of MMPs are tightly regulated by the tissue inhibitors of MMPs (TMPs) (Kleiner and Stetler-Stevenson, 1999). The membrane type 1-MMP (MT1-MMP), which is expressed in the majority of invasive tumours, binds to proMMP-2 and TMP-2, leading to MMP-2 cleavage and activation, and subsequently to ECM proteolysis (Samani *et al.*, 2007). IGF-1R signalling via

the PI3K-AKT pathway has been shown to regulate tumour invasion, at least in part by inducing expression of MT1-MMP and MMP2 (Zhang *et al.*, 2003).

1.4 IGF-1R as a therapeutic target

The diverse roles of IGF-1R in the development of the malignant phenotype has made it a very attractive therapeutic target. Therapeutically, the two main approaches being developed are anti-IGF-1R monoclonal blocking antibodies (mAbs) that block receptor-ligand interaction, and small molecule tyrosine kinase inhibitors (TKIs) that inhibit tyrosine kinase activity (**Figure 3**) (Hendrickson and Haluska, 2009; Yee, 2012; Yuen and Macaulay, 2008).

The first assessment of IGF-1R targeted treatment used αIR-3, a mouse monoclonal antibody (mAb), which blocked IGF-1 binding to IGF-1R and inhibited growth of estrogen-independent breast cancers (Arteaga *et al.*, 1989; Kull *et al.*, 1983; Rohlik *et al.*, 1987). Subsequent clinical developments have focused on IGF-1R specific mAbs that selectively inhibit IGF induced IGF-1R signalling and lead to IGF-1R internalization and degradation (Hewish *et al.*, 2009). Nine mAbs have been evaluated clinically, including: AVE1642, BIIB022, cixutumumab, dalotuzumab, figitumumab, ganitumumab, R 1507, robatumumab and h10H5 (Yee, 2012). Clinical trials using these antibodies have shown single agent activity in uncommon cancers such as Ewings sarcomas, but little benefit as single agent in common cancers. The low levels of single agent activity of IGF-1R inhibition might be at least in part due to redundancy in signaling via the insulin receptor or other growth factor receptors (Buck *et al.*, 2010). However, in combination with other forms of therapy such as chemotherapy or other biological agents, they have shown patient benefits (Hewish *et al.*, 2009; Yee, 2012; Yuen and Macaulay, 2008). For example, the combination of

IGF-1R antibody with chemotherapy with genotoxic agents has led to significant increase in response rates, with little added toxicity, in non-small cell lung cancer (NSCLC) (Gualberto and Karp, 2009; Karp *et al.*, 2009). However, this approach failed to prolong survival in unselected patients, leading to premature discontinuation of Phase 3 trials (Basu *et al.*, 2011).

There are currently nine small molecule inhibitors targeting IGF-1R being evaluated clinically: BMS-754807, Insm-18 (NDGA), XL-228, OSI-906 (linsitnib), GSK-1904529A, ABDP, A-928605, AXL1717 (PPP) and KW-2450 (Yee, 2012). Small molecule inhibitors offer several potential advantages over blocking antibodies. Inhibitors can be administered orally and have a shorter half-life than antibodies, in the order of hours rather than days (Buck and Mulvihill, 2012). This property can be exploited to allow for dosing flexibility, which can be helpful in optimizing the scheduling of IGF-1R inhibition with other agents. Moreover, the small molecule inhibitors target the tyrosine kinase domain of the IGF-1R, which shares a high degree of homology with the Insulin receptor kinase domain and this allows for not only targeting of IGF-1R but also IR-A that can mediate tumor growth. Initial clinical experience suggests that co-inhibition of IR-B is tolerable (Pollak, 2012).

The key issues for successful clinical use of IGF-1R inhibiting drugs are firstly, the need to identify biomarkers that predict sensitivity to IGF-1R inhibition, and secondly to understand how IGF-1R influences the DNA damage response, in order to combine IGF-1R inhibition effectively with chemotherapy and radiotherapy.

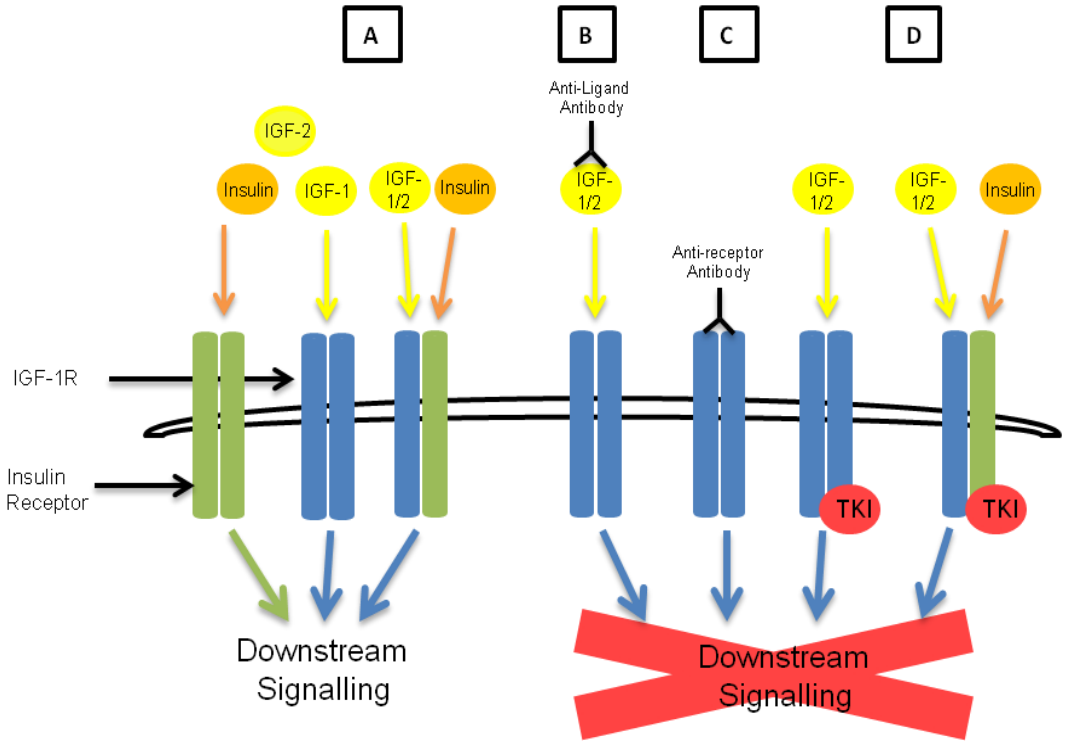


Figure 3: Methods of targeting IGF-1R

A) Signalling via the IGF axis can occur via IGF-1 homodimers and IGF-1R/IR hybrid receptors (blue, IGF-1R; green IR). Targeting IGF-1R can be achieved by B) ligand binding antibodies, C) receptor binding antibodies or D) small molecule tyrosine kinase inhibitors (TKI). Diagram modified from (Buck and Mulvihill, 2011)

1.4.1 Biomarker identification

1.4.1.1 Circulating IGF-1

Several studies have suggested that high circulating IGF-1 correlates with sensitivity to IGF-1R antibody, but many studies have not found this (Gualberto *et al.*, 2011; Juergens *et al.*, 2011).

1.4.1.2 Nuclear IGF-1R

It is now well recognized that RTKs can translocate to the nucleus, and this was first shown for EGFR (Lin *et al.*, 2001; Massie and Mills, 2006; Wang *et al.*, 2010). Nuclear EGFR is capable of directly regulating gene transcription and also interacts with DNA-dependent protein kinase catalytic subunit (DNA-PKcs), a protein central to DNA repair by non-homologous end joining (NHEJ) (Dittmann *et al.*, 2005; Lin *et al.*, 2001).

Following activation, IGF-1R is known to be internalized by clathrin and caveolin-mediated endocytosis (Huo *et al.*, 2003; Salani *et al.*, 2010). Upon internalization, IGF-1R is transported to recycling endosomes where it is either recycled and shuttled back to the cell surface or transported to lysosomes for degradation (Romanelli *et al.*, 2007). Work from our laboratory showed that IGF-1 can lead to ligand-dependent internalization and nuclear translocation of full-length IGF-1R subunits in prostate cancer cells (Aleksic *et al.*, 2010). Similar observations were reported in melanoma cells by Larsson's laboratory, who also reported that IGF-1R nuclear translocation requires SUMOylation on three evolutionarily conserved lysine residues (K1025, K1100, K1120) in the beta subunit (Sehat *et al.*, 2010). Typically, proteins that are transported to the nucleus contain a nuclear localisation sequence (NLS), which allows binding to importins for translocation through nuclear pores (Hoelz *et al.*, 2011). The IGF-1R does not contain an NLS, therefore the exact mechanism by

which IGF-1R traffics to the nucleus is unknown. Similarly, the function of nuclear IGF-1R is unclear. *Sehat et. al.* conducted a ChIP-sequencing experiment and identified IGF-1R binding sites in the genome, but these were few (~500) and most were remote from known genes (Sehat *et al.*, 2010). Recent studies have shown that nuclear IGF-1R can bind to LEF1 transcription factor and increase the promoter activity of LEF1 target genes including cyclin D1, which might be an additional mechanism by which IGF-1R promotes proliferation (Warsito *et al.*, 2012). In addition, IGF-1R/INSR hybrid receptors are reported to localize to the nucleus of corneal epithelial cells (Wu *et al.*, 2012c).

Work from our laboratory showed that higher levels of nuclear IGF-1R were associated with poor prognosis in renal cancer, suggesting that nuclear IGF-1R contributes to an aggressive phenotype (Aleksic *et al.*, 2010). We are currently testing whether there is any association with clinical data in prostate cancer. Recently, *Asmane et. al.* examined nuclear IGF-1R in tumours from phase I and II patients treated with different anti-IGF-1R antibodies, and showed that the presence of nuclear staining was significantly associated with an increase in progression free survival and overall survival (Asmane *et al.*, 2012). This suggests that exclusive nuclear IGF-1R staining might serve as a predictive biomarker for sarcoma patients likely to benefit from IGF-1R monoclonal antibody therapy (Asmane *et al.*, 2012).

1.4.1.3 Screens for predictive biomarkers

Several groups have taken an unbiased approach to identify markers that correlate with sensitivity to IGF-1R inhibition. Approaches include identification of predictive gene signatures in breast and colorectal cancer (Litzenburger *et al.*, 2011; Pitts *et al.*, 2010), and siRNA screens. A study on childhood sarcoma cell lines used the small molecule IGF-1R inhibitor BMS-536924 and screened a siRNA library to deplete 88 RTKs and 31 Insulin/IGF signaling pathway proteins and identified ribosomal S6 and

macrophage-stimulating 1 receptor tyrosine kinase (MSTR1R) as mediators of resistance to BMS-536924 (Potratz *et al.*, 2010). Work in our laboratory also used an unbiased siRNA screen to identify factors that regulate sensitivity to a novel small molecule IGF-1R inhibitor (AZ12253801) in DU145 prostate cancer cells and MCF7 breast cancer cells (Dr. Shan Gao, 2012, University of Oxford, D.Phil. thesis July 2012). Several repair proteins were found to mediate resistance to IGF-1R inhibition in DU145 prostate cancer cells and MCF7 breast cancer cells, and the top hit, a poorly characterized component of the WNT pathway, is the subject of ongoing work in our group.

1.4.2 The role of IGF-1R in the repair of DNA double strand breaks (DSBs)

Cells have complex signalling networks to detect and repair DNA damage. One of the most cytotoxic lesions, the double strand break (DSB), is detected by large proteins including Ataxia Telangiectasia mutated (ATM) (Lavin, 2008). Following induction of DSBs, ATM rapidly phosphorylates the histone variant H2AX (ɣH2AX) leading to its recruitment at the site of damage, and initiating signalling pathways regulating cell cycle, induction of apoptosis or repair of DSBs (Dickey *et al.*, 2009). DSBs repair occurs by two major repair pathways: non-homologous end joining (NHEJ) or homologous recombination (HR) (**Figure 4**) (Jackson, 2002). The majority of DSBs are repaired by NHEJ, which is typically regarded as error-prone due to end processing or insertion. Repair by NHEJ is initiated with the binding of Ku 70/80 to the DNA ends; this in turn leads to the recruitment of activated DNA-PK (Chen *et al.*, 2007; Walker *et al.*, 2001). Ku 70/80 and DNA-PK with the assistance of Artemis, initiate DNA end resection and processing (Pawelczak *et al.*, 2011). The DNA end processing leads to blunt ends and typically involves the deletion of a small DNA sequence prior to joining, making NHEJ error prone. Ligation of the blunt DNA ends

occurs by a complex involving XRCC4 and DNA Ligase IV (Ahnesorg *et al.*, 2006; Calsou *et al.*, 2003; Karimi-Busheri *et al.*, 2007; Koch *et al.*, 2004).

In contrast to NHEJ, homologous recombination (HR) is a high fidelity process that requires a sister chromatid as a template for DSB repair, and this typically occurs during late S and G_2 phases of the cell cycle (Jackson, 2002). HR begins with the binding of CtIP, SIRT6, BRCA1 and Mre11-RAD50-NBS1 (MRN) complex at the DSB ends, and these proteins are capable of initiating resection in the 5' to 3' direction (Kass and Jasin, 2010). Resection leads to the formation of a single stranded 3' overhang that is subsequently coated by replication protein A (RPA), which prevents the formation of secondary structure in the single stranded region of the DNA (Krejci *et al.*, 2012). Phosphorylation of RPA by checkpoint kinases, ATM and Mec1, and by cell-cycle dependent kinases (CDKs) is important for recruitment of RAD51 to the site of damage (Shi *et al.*, 2010; Zou and Elledge, 2003). RPA is subsequently displaced by the RAD51 nucleofilament that is loaded on the 3' overhang with the assistance of RAD52, and BRCA2 (Gudmundsdottir *et al.*, 2004; Kojic and Holloman, 2004; Yang *et al.*, 2002). BRCA2-induced stabilization of the RAD51 nucleoprotein is regulated by CDKs (Esashi *et al.*, 2005; Esashi *et al.*, 2007). RAD51 is capable of searching the genome for homologous sister chromatid sequence and catalyzing the strand invasion step of HR, to form a displacement loop (D-loop). In synthesis-dependent strand annealing, the 3' end of the D-loop is extended, and then dissociates to anneal to the other DNA end. Alternatively, capture of the second DNA end by the D-loop can lead to formation of Holliday Junctions that are resolved by cleavage and rejoining reactions (Kass and Jasin, 2010; Sung and Klein, 2006).

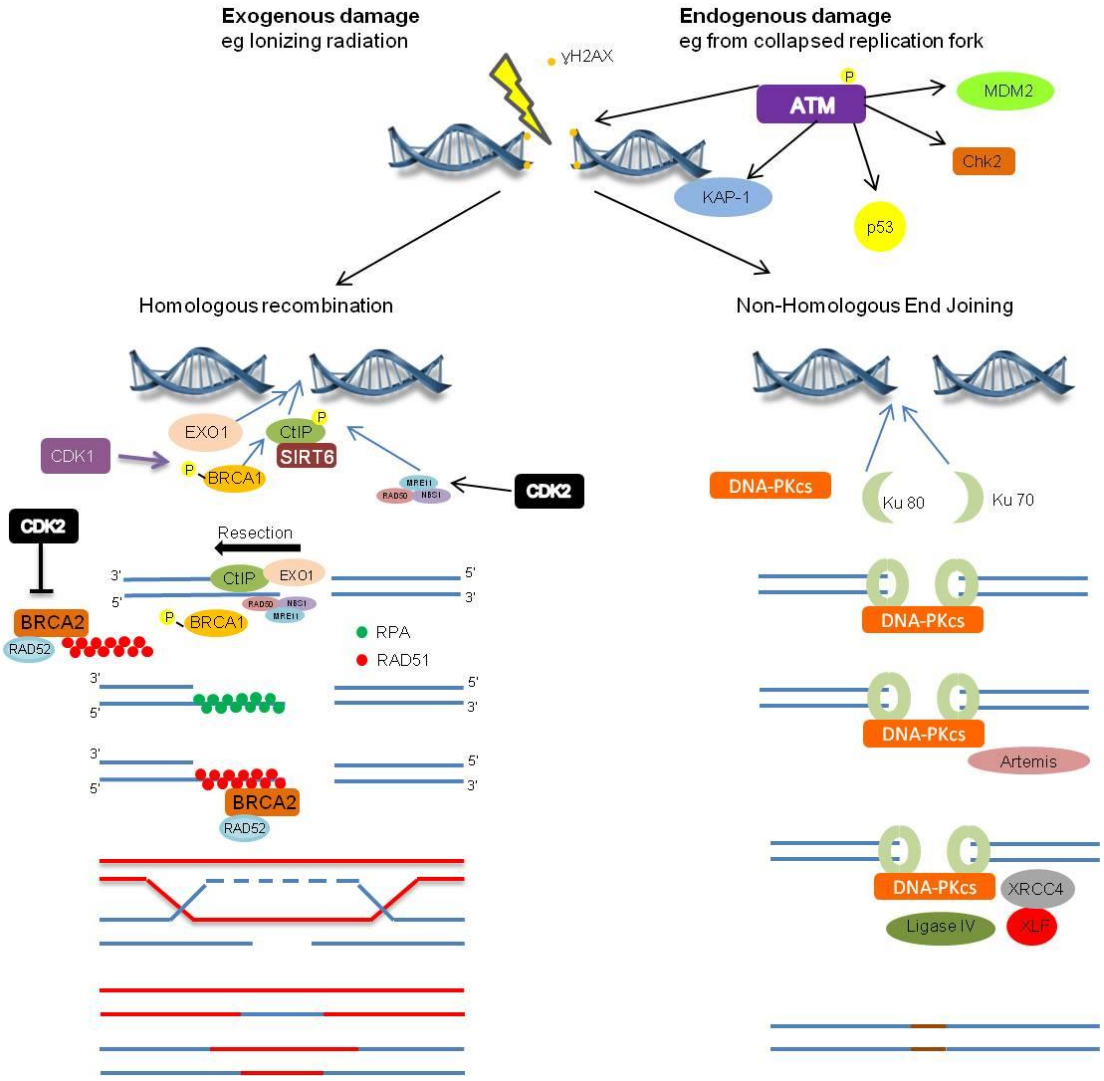


Figure 4: DNA DSB repair pathways

DNA DSB can be induced by exogenous and endogenous factors. Once damage has occurred, sensing molecules such as ATM are rapidly phosphorylated and lead to phosphorylation and recruitment of γH2AX and the activation of other proteins involved in cell cycle regulation and chromatin remodelling. Subsequent repair can occur by two major repair pathways: Non-homologous end joining (NHEJ) or homologous recombination (HR). Diagram made from references sited in text.

IGFs are well known to influence chemosensitivity by protecting tumour cells from apoptosis (Dunn *et al.*, 1997). Mouse embryo fibroblasts lacking IGF-1R are more susceptible to radiation-induced apoptosis, whereas isogenic cells over-expressing IGF-1R show inhibition of apoptosis (Tezuka *et al.*, 2001). There is also evidence that IGF-1R signalling can influence DNA repair more directly. Previous work from our laboratory showed that down-regulation of IGF-1R caused delayed tumour

growth and enhanced radiosensitivity in mouse melanoma cells, and this effect was associated with impaired activation of ATM (Macaulay *et al.*, 2001). In human prostate cancer cells, our group demonstrated that IGF-1R depletion enhanced sensitivity to cytotoxic drugs that induce DSBs, but not to chemotherapeutic agents that kill cells without damaging DNA (Rochester *et al.*, 2005). These data suggest that IGFs could influence chemosensitivity by means other than regulation of apoptosis, and also suggest that IGFs may influence the response to DNA damage. To begin to understand the mechanism by which IGF-1R depletion impairs the DNA damage response, murine melanoma, human breast and human prostate cancer cells were treated with chemical inhibitors or siRNA to inhibit or deplete components of the IGF axis (**Figure 5**). In human breast cancer cells, radiation-induced PI3K inhibition or depletion of IRS-1 or AKT2 led to a reduction in CHK2 phosphorylation (Riedemann and Macaulay unpublished), suggesting that IRS-1-PI3K-AKT signalling may influence ATM activation and function (**Figure 5**).

IGF-1R activation is reported to influence the homologous recombination pathway via direct interaction of the docking molecule IRS-1 with RAD51 (Trojanek *et al.*, 2003). This interaction was shown in serum-starved 3T3-like mouse fibroblasts, holding RAD51 in a cytoplasmic localisation. IGF-1 stimulation was shown to attenuate this interaction, allowing RAD51 to traffic to the nucleus and form foci in response to DNA damage. In the absence of IGF-1, or failure of the IGF-1R to properly tyrosine phosphorylate IRS-1, localisation of RAD51 to the site of DNA damage was diminished (Trojanek *et al.*, 2003). Others have reported that AKT is activated by DNA damage, and that PI3K-AKT inhibition can enhance tumour cell radiosensitivity (Bozulic and Hemmings, 2009; Prevo *et al.*, 2008). In contrast, studies from the Lopez laboratory showed that AKT1 activation leads to cytoplasmic retention of BRCA1 and RAD51 thus impairing HR (Plo *et al.*, 2008). Subsequently, activation of

AKT1 in BRCA1-deficient cells was shown to impair Chk1 nuclear localization and disrupt interaction of Chk1 and RAD51, leading to impaired HR (Jia *et al.*, 2012).

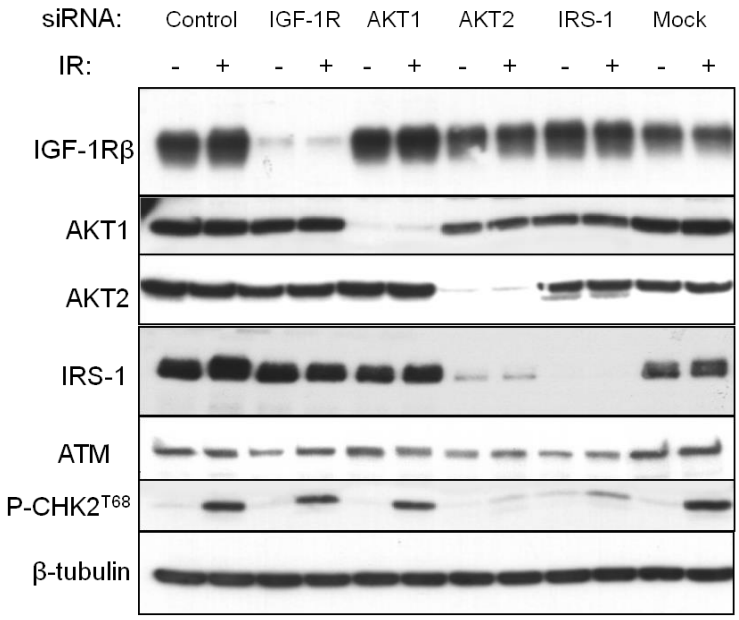


Figure 5: Effects of IGF axis on DSB repair

MCF7 breast cancer cells were transfected with non-silencing control siRNA, or siRNA to deplete components of the IGF axis. After 48 hours, cells were irradiated, and one hour later lysed for western blotting. Depletion of IRS-1, and AKT2 appeared to suppress radiation induced Chk2 phosphorylation (experiment done by Riedemann and Macaulay).

Thus at the start of this project, work from our group implicated involvement of IRS-1 and AKT2 in the activation of ATM, but there was conflict in the literature regarding the role of AKT in the DNA damage response.

1.7 Objectives of this project

The aim of this project is to investigate the potential that IGF signalling can influence the cellular response to DNA damage in human prostate cancer cells. The initial aim of this project was:

1) Investigate the hypothesis that depletion or inhibition of IGF-1R or AKT can radiosensitize prostate cancer cells, at least in part via effects on ATM

Subsequently two further projects were initiated in parallel but will be presented sequentially.

2) To identify potential binding partners of nuclear IGF-1R by mass spectrometry in order to understand the function of nuclear IGF-1R
3) Validation of RAD51 as a hit in a screen for proteins that regulate sensitivity to IGF-1R inhibition

The long term aim of this work is to assess the potential of the IGF-1R as a therapeutic target in prostate cancer, and specifically to understand how to combine IGF-1R inhibitors with DNA damaging therapies.

Chapter 2: Materials and Methods

2.1 Mammalian Cell Culture

2.1.1 General techniques

All cell culture was performed in cell culture hoods, and cultures were maintained in sterile, mycroplasma-tested media in tissue culture grade flasks, dishes and plates (Falcon or Nunc). All cell lines were incubated in a humidified atmosphere of 5% CO_2 and 95% air or 10% CO_2 and 90% air.

2.1.2 Cell Lines and Cell Culture

All cell lines used for this work are listed in **Table 1**. Cells were cultured in appropriate media from Invitrogen Gibco (see table 1) and supplemented with 10% foetal calf serum (FCS, PAA laboratories), 100 units/mL penicillin and 0.1 mg/mL streptomycin. HeLa shLacZ and HeLa shATM cells were obtained from Dr. Wojciech Niedzwiedz (Weatherall Institute of Molecular Medicine, Oxford, UK) with consent from Dr. Yossi Shiloh (Tel Aviv University, Tel Aviv, Israel). DLD-1 colorectal cancer cells expressing wild-type BRCA2 (+/-) and isogenic BRCA2 deficient (-/-) cells were generated by Dr. Scott Kern (Laboratory of Cellular and Molecular Biology, NIH, Baltimore, Maryland, USA) and obtained with consent via Dr. Fumiko Esashi (Sir William Dunn School of Pathology, Oxford, UK). All other cell lines were obtained from Cancer Research UK Central Cell Services. For routine passage, cells were disaggregated using 3 mM EDTA in PBS, pelleted by centrifugation at 1200 rpm for 5 min, resuspended in complete medium and reseeded. For cryopreservation and banking, cells were disaggregated and pelleted as above, and resuspended in 1 mL of 5% dimethyl sulphoxide (DMSO) with 95% FCS and aliquoted into sterile Nunc vials. Vials were frozen in a “Mr Frosty” container to cool by 1^{o}C per minute to -80^{o}C before being transferred to liquid nitrogen for long term storage. Cells were

recovered from liquid nitrogen by rapidly thawing the vial at 37° C and transferring the 1 mL cell suspension into a sterile culture flask with complete medium (with 10% FCS) for culture. The medium was changed 24 hours later to remove DMSO.

Cell Line	Origin	Medium	Additional Culture Requirements, Comments
DU145	Prostate Cancer	RPMI1640	5% CO_2
22Rv1	Prostate Cancer	RPMI1640	5% CO_2
PC3	Prostate Cancer	Hams F12	5% CO_2
LNCaP	Prostate Cancer	RPMI1640	5% CO_2
MCF7	Breast Cancer	DMEM	5% CO_2
HEK 293T	Human Embryonic Kidney Cells	DMEM	10% CO_2, Transformed by expression of the large T antigen from SV40 virus
HeLa shATM	Cervical Cancer	DMEM	10% CO_2
HeLa shLacZ	Cervical Cancer	DMEM	10% CO_2
DLD-1 BRCA2 +/-	Colorectal Cancer	RPMI1640	5% CO_2
DLD-1 BRCA2 -/-	Colorectal Cancer	RPMI1640	5% CO_2

Table 1: Human Cancer Cell Lines

2.1.3 DNA transfection

2.1.3.1 DNA transfection with Calcium Phosphate

Plasmid DNA (5 µg) was introduced into HEK 293T cells using the Calcium Phosphate method (Invitrogen, Cat No K2780-01). Twenty-four hours prior to transfection, cells were plated at a density that resulted in 40-60% confluence the next day. On the day of transfection, 5 µg of ATM plasmid and 36 µL of 2 M $CaCl_2$ were added to MilliQ water to a final volume of 300 µL. The mixture was very slowly added to 300 µL of 2X Hepes Buffered Saline (HBS) and incubated for 30 minutes at room temperature before adding dropwise to a 10 cm dish containing 10 mL of medium. Cells were analyzed 48 hours post transfection.

2.1.3.2 Plasmid transfection using Lipofectamine LTX with Plus

Plasmids were introduced into DU145 p-DR-GFP cells using Lipofectamine LTX with Plus reagent (Invitrogen, Cat No 15338-100). Twenty-four hours prior to transfection, cells were plated at a density that resulted in 40-60% confluence the next day. On the day of transfection a mixture of 0.75 µg p-CMV-Sce-I (provided by Phil North, CRUK, WIMM) and 0.25 µg pDsRed2-Mito (BD Clontech) were incubated with the equivalent volume of plus reagent (ie: 1 µL plus reagent per 1 µg DNA) in 500 µL of Opti-MEM (Invitrogen Gibco) for 5 minutes at room temperature. Following incubation, 3.5 µL Lipofectamine LTX transfection reagent was added and the transfection mix was further incubated for 25 minutes at room temperature before adding dropwise to cells growing in complete medium. The volumes given are for cells growing in a 6 cm dish and were scaled up or down accordingly. Cells were typically analyzed by flow cytometry 72 hours post transfection.

2.1.4 Gene Silencing by RNA interference

2.1.4.1 Forward Transfection using Oligofectamine

Twenty-four hours prior to transfection, cells were plated in 10 cm dishes at a density that resulted in 30-40% confluence the next day. Oligofectamine (Invitrogen), a lipid mediated transfection reagent, was used to introduce siRNA (**see Table 2**) into cells. This was done by first separately incubating 13.65 µL of 20 µM siRNA stock (final concentration 100 nM) with 1516.65 µL of Opti-MEM (Invitrogen), and 12.3 µL Oligofectamine with 410 µL Opti-MEM for 10 minutes. Following incubation at room temperature for 10 minutes, the siRNA and oligofectamine were mixed and incubated at room temperature for 25 minutes. During this incubation cells were washed twice with PBS. After removing the final PBS wash, 710 µL of Opti-MEM was added to each dish, and then complexes were added dropwise to cells. Four hours later, 11

mL of complete medium with 273 µL of FCS (to bring FCS to 10% final concentration) were added. Cells were typically analyzed 48 hours post transfection.

Name	Target	Source	Catalogue Number
AllStars Negative Control	Human Nonsilencing Control	Qiagen	1027281
Hs_AKT1_7	Human AKT1	Qiagen	SI00299159
Hs_AKT2_5	Human AKT2	Qiagen	SI00299166
Hs_ATM_5	Human ATM	Qiagen	SI00299299
Hs_IGF-1R_1	Human IGF-1R	Qiagen	SI00017521
Hs_IRS1_4	Human IRS-1	Qiagen	SI00078652
Hs_RAD51_1	Human RAD51	Qiagen	SI00045010
Hs_RAD51_7	Human RAD51	Qiagen	SI02663682
Hs_BRCA2_6	Human BBRCA2	Qiagen	SI02653434
Hs_BRCA2_7	Human BRCA2	Qiagen	SI02653595

Table 2: Short Interfering RNA used for Gene Silencing

2.1.4.2 Reverse Transfection using DharamaFECT

Cells were reverse transfected with siRNA using DharamaFECT transfection reagent (Dharmacon, USA). For reverse transfection into a 96 well plate, 24 µL of 20 µM stock siRNA and 7.2 µL of DharmaFECT transfection reagent were diluted in 1920 µL of appropriate medium, without FCS and antibiotics (**see Table 3** for cell lines and DharmaFECT transfection reagent). DharmaFECT transfection reagent 1 was used for DU145 cells and the transfection mix was incubated for 30 minutes at room temperature before transfering 20 µL to each well of a u-clear 96-well plate (Grenier Bio-One). To each well was added 2,000 DU145 cells per well in 80 µL of appropriate growth medium (without antibiotics). Following 7 hours incubation of siRNA complex with cells, the transfection medium was removed and replaced with 100 µL of complete medium (with FCS and antibiotics). Following 48 hours incubation, wells were treated with AZ12253801 at 0-300 nM. Cell viability was assessed by CellTiter-Glo (CTG) Luminescent assay (Promega) (described below).

Cell Type	Number of Cells per well	DharmaFECT transfection reagent
DU145	2,000	1
22Rv1	4,000	1
PC3	2,000	2
LNCaP	2,000	2
MCF7	4,000	1
DLD-1 BRCA2 +/-	2,000	N.A.
DLD-1 BRCA2 -/-	2,000	N.A

Table 3: Cell Seeding and Transfection reagents for siRNA transfection

2.1.5 Treatment with small molecule inhibitors

IGF-1R inhibition was achieved using a small molecule ATP-competitive IGF-1R tyrosine kinase inhibitor AZ18853801 provided by AstraZeneca (Alderly Park, United Kingdom). AZ12253801 was dissolved in DMSO to a stock concentration of 10 mM, aliquoted and stored at -20^{o}C. Small molecule inhibitors of ATM (cat # 118500), AKT inhibitor X (cat # 124020), and CDK1 (cat# RO-3306) were purchased from Calbiochem, dissolved in DMSO to a stock concentration of 10 mM, aliquoted and stored at -20^{o}C. For individual experiments inhibitors were further diluted in complete medium.

2.1.6 Treatment with IGF-1 ligand

Activation of IGF receptor was achieved using human R^{3} IGF-1 (Sigma-Aldrich, St. Louis, Mo, USA). IGF-1 stock was made by dissolving 1 mg of lyophilized powder in 1 mL of 10 mM hydrochloric acid (HCl). Stock solution (110 µM) was aliquoted and stored at -80^{o}C. Prior to use, adherent cells were washed twice with PBS and allowed to incubate for 24 hours in serum free medium. The following day cells were treated with IGF-1 diluted to 10-50 nM in serum free medium. Control cells were treated with an equivalent volume of 10 mM HCl diluted in serum-free medium.

2.1.7 Gamma Irradiation of cells

Adherent cells grown in complete cell culture medium were irradiated in 6 well plates, 10 cm or 15 cm dishes with 0-20 Gy using a Cesium-137 source in an IBL 637 chamber (CIS Bio International, France).

2.2 Protein Analysis

2.2.1 Collection and lysis of adherent cells

2.2.1.1 Whole Cell Extracts

Culture medium was aspirated from dishes and adherent cells were washed twice with ice cold PBS. Adherent cells were scraped in 1 mL of PBS and pelleted by centrifugation at 3,000 rpm for 5 min. After aspirating PBS, cells could be stored at -20^{o}C following snap freezing in dry ice with 100% ethanol for one minute. Cells were lysed in IGF-1R lysis buffer [50 mM HEPES pH 7.6, 100 mM NaCl, 10 mM EDTA, 1% Triton X-100, 4 mM sodium pyrophosphate, 2 mM sodium orthovanadate, 10 mM NaF] or radio-immunoprecipitation assay (RIPA) lysis buffer [20 mM Tris pH7.5, 1 mM EDTA, 100 mM NaCl, 1% Triton X-100, 0.5% sodium deoxycholate, 0.1% sodium dodecyl sulphate (SDS)]. All lysis buffers were supplemented with ETDA-free protease inhibitor cocktail, 1.5 mM Pefabloc SC Plus (Roche), phosphatase inhibitor complex II (Sigma, P5726) and complex III (Sigma, P0044). Samples were incubated with lysis buffer for 30 minutes on ice and insoluble material was pelleted by centrifugation at 13000 rpm for 15 minutes at 4^{o}C.

2.2.2 Cell Fractionation Methods

2.2.2.1 Fractionation using Sucrose Gradient

Culture medium was aspirated from dishes and adherent cells were washed twice with ice cold PBS. Adherent cells were scraped in 1 mL of PBS and pelleted by centrifugation at 3,000 rpm for 5 min at 4°C. Cells were resuspended in 5 mL of hypotonic Buffer A [10 mM HEPES pH 7.9, 10 mM KCl, 1.5 mM Mg_2Cl, 0.5 mM DTT, supplemented with ETDA-free protease inhibitor cocktail, 1.5 mM Pefabloc SC Plus] per ten 15 cm dishes. The cell suspension was incubated on ice for 5 minutes to allow cells to swell before transferring to a pre-chilled Dounce tissue homogenizer (Fisher Scientific, FB56691). The cell suspension was homogenized 20 times before visualising 20 µL in a haemocytometer with trypan blue to check that no intact cells remained. Once greater than 99% of cell membranes were disrupted, nuclei were pelleted by centrifugation at 1000 rpm for 5 minutes at 4°C. One millilitre of supernatant ('non-nuclear' components) was saved for western blotting, and the nuclear pellet was resuspended in 3 mL of solution S1 [0.25 M sucrose, 10 mM $MgCl_2$, supplemented with ETDA-free protease inhibitor cocktail, 1.5 mM Pefabloc SC Plus] and layered over 3 mL of solution S2 [0.35 mM sucrose, 0.5 mM $MgCl_2$, supplemented with ETDA-free protease inhibitor cocktail, 1.5 mM Pefabloc SC Plus] in a pre-chilled 15 mL falcon. Samples were centrifuged through the sucrose gradient at 2500 rpm for 5 minutes at 4°C and the supernatant was discarded. The pellet was resuspended in 3 mL of solution S2, layered over 3 mL of solution S3 [0.88 mM sucrose, 0.5 mM $MgCl_2$, with protease inhibitors] in a pre-chilled 15 mL falcon tube and centrifuged at 3000 rpm for 10 minutes at 4°C. The supernatant was discarded and the nuclear pellet was incubated for 30 minutes in nuclear lysis buffer (NLB) [1% NP-40, 20 mM HEPES pH 7.5, 0.5 mM EDTA, 300 mM NaCl, 100 mM NaF, 10 mM β-glycerophosphate and 1 mM sodium orthovanadate, protease inhibitor cocktail (Roche), Pefabloc (Roche), and phosphatase inhibitor cocktail II and III

(Sigma)]. Nuclear lysates were analysed by western blotting (**as in section 2.2.3**) and used for immunoprecipitation (**as in section 2.2.4)**.

2.2.2.2 Fractionation with Panomics Kit

Nuclear extracts were prepared using the Nuclear Extraction Kit (Panomcis, Cat# AY-2002). Briefly, culture medium was aspirated from dishes and adherent cells were washed twice with ice cold PBS at 4^{o}C. Adherent cells were scraped in 1 mL of PBS and pelleted by centrifugation at 3,000 rpm for 5 min. Disruption of the cell membrane was achieved by incubating the cell pellet from five 15 cm dishes in 1 mL of hypotonic Panomics buffer A [per 1 mL of buffer A added 10 µL of DTT, 10 µL Protease Inhibitor, 10 µL Phosphatase Inhibitor complex I, Phosphatase Inhibitor complex II] on ice for 10 minutes. Nuclei were pelleted by centrifugation at 14,000 rpm for 3 minutes at 4^{o}C. The supernatant, containing membrane and cytoplasmic proteins, was transferred to a fresh eppendorf tube and nuclei were resuspended in NLB (as in 2.2.2.1), incubated on ice for 30 minutes and insoluble proteins were pelleted by centrifugation at 13000 rpm for 15 minutes at 4^{o}C and analysed by western blotting (**as in section 2.2.3**).

2.2.2.3 Fractionation using in-house buffers

Adherent cells were washed, scraped into PBS and pelleted by centrifugation as above. Hypotonic swelling of cells was achieved by incubating the cell pellet from ten 15 cm dishes in 5 mL of in-house hypotonic buffer [10 mM Tris-Cl pH 7.5, 10 mM KCl, 1 mM EDTA, 1 mM EGTA, 2 mM $MgCl_2$, with protease inhibitors]. The cell suspension was transferred to a pre-chilled Dounce homogenizer and homogenized 20 times before checking with trypan blue to ensure complete disruption of cell membranes. The suspension was then centrifuged at 1500 rpm for 5 minutes at 4^{o}C. A sample of supernatant was saved for western blotting, and the nuclear pellet was washed three times with 3 mL nuclear wash buffer [150 mM NaCl, 20 mM HEPES pH

7.5, 0.5 mM EDTA, 0.1% Tween-20, 4 mM sodium pyrophosphate, 2 mM sodium orthovanadate, 10 mM sodium fluoride, with protease inhibitors]. Nuclei were pelleted by centrifugation at 1000 rpm for 5 minutes at 4ºC between each wash. After the final wash, nuclei were resuspended in NLB, incubated on ice for 30 minutes and analysed by western blotting (**as in section 2.2.3**).

2.2.3 Western Blot

Soluble protein was quantified against bovine serum albumin (BSA) standards using the Pierce Bicinchoninic Acid (BCA) assay and analysed on a plate reader at 562 nm (μQuant Universal Microplate Spectrophotometer, NorthStar Scientific). Equal amounts of protein, (typically 30-50 μg) were made up to a fixed volume using lysis buffer and were denatured in 3X Laemmli Buffer (70 mM Tris pH 6.8, 5% (v/v) β-mercaptoethanol, 40% (v/v) glycerol, 3% (w/v) SDS, 0.05% (w/v) Bromophenol Blue) at 95˚C for 5 minutes. Samples were separated by molecular weight by SDS polyacrylamide gel electrophoresis on 5-10% polyacrylamide gels. Proteins were transferred to Hybond C extra nitrocellulose membrane (Amersham Pharmacia Biotech) in semi-dry transfer buffer [48 mM Tris, 39 mM glycine, 20% methanol, 1.3 mM SDS, final pH 9.2] using a semi-dry transfer apparatus (Hoefer SemiPhor Transfer Unit, Amersham Biosciences) at a constant current of 40 milliamperes per 8X10 cm gel for 3 hours at room temperature. Following transfer, membranes were blocked in order to reduce nonspecific protein binding, with either 5% w/v non-fat dairy milk (Marvel) or BSA (Sigma) in TBS-T (Tris-buffered saline (TBS) with 0.1% Tween 20, Sigma) for one hour at room temperature. Primary antibodies used in this project are described in **Table 4**. Primary antibodies were diluted as described in Table 4 and incubated overnight at 4ºC on a shaking platform. After washing three times with TBS-T for 10 minutes, membranes were incubated with goat anti-rabbit or

goat anti-mouse secondary antibody conjugated to horse-radish peroxide (DAKO, Ely, UK) for one hour at room temperature. Membranes were washed four times for 10 minutes with TBS-T and proteins were detected using an Enhanced Chemiluminescence kit (ECLplus, Amersham Pharmacia Biotech).

Antibody	Source	Primary Dilution	Blocking Buffer	Molecular Weight
Total AKT	Cell Signaling (#9272)	1:1000	5% BSA	60 kDa
Androgen Receptor	Cell Signaling (3203)	1:1000	5% NFDM	110 kDa
Total ATM (D2E2)	Cell Signaling (#2873)	1:1000	5% BSA	350 kDa
Phospho- ATM (S1981)	Rockland (600-401-398)	1:1000	5% NFDM	370 kDa
β Actin	Abcam (ab8224)	1:10000	5% NFDM	42 kDa
β Tubulin	Sigma (T-4026)	1:10000	5% NFDM	55 kDa
Calnexin	BD Transduction Laboratories	1:2000	5% NFDM	90 kDa
Chk2	Cell Signaling (#2662)	1:1000	5% NFDM	62 kDa
Total ERK 1/2	Cell Signaling (4695)	1:2000	5% NFDM	42 & 44 kDa
Flag M2	Sigma (F1804)	1:1000	5% NFDM	-
Golgin-84	BD Transduction Laboratories	1:500	5% NFDM	84 kDa
IGF-1R β Subunit	Cell Signaling (#3027)	1:1000	5% NFDM	95 kDa
IRS-1	Cell Signaling (#2382)	1:1000	5% BSA	180 kDa
KAP-1	Bethyl Laboratories	1:2000	5% NFDM	100 kDa
Lamin-A (133A2)	Abcam (ab8980)	1:5000	5% NFDM	74 kDa
MEK 1/2	Cell Signaling (4694)	1:2000	5% NFDM	45 kDa
Myosin IIb	Cell Signaling (#3404)	1:1000	5% BSA	230 kDa
Phospho-AKT (Ser473)	Cell Signaling (#4051)	1:1000	5% BSA	60 kDa
Phospho-AKT Substrate (RXRXXS*/T*)	Cell Signaling (#10001)	1:1000	5% BSA	-
Phospho-Chk2 (Thr68)	Cell Signaling (#2661)	1:1000	5% BSA	62 kDa
Phospho-GSK3 α/β (Ser21/9)	Cell Signaling (#9331)	1:1000	5% BSA	46 & 51 kDa
Phospho-IGF-1R β (Tyr1135/1136)	Cell Signaling (#3024)	1:1000	5% BSA	95 kDa
Phospho-KAP-1 (S824)	Bethyl Laboratories	1:2000	5% BSA	100 kDa
Phospho-ERK 1/2	Cell Signaling (4377)	1:2000	5% BSA	42 &44 kDa
PTEN	Cell Signaling (9559)	1:0000	5% NFDM	54 kDa
RAD51 (4B4)	Abcam (ab213)	1:1000	5% NFDM	37 kDa
Sodium Potassium ATPase (464.8)	Abcam (ab8344)	1:2000	5% NFDM	35 kDa

NFDM = Non-Fat Dairy Milk
BSA = Bovine Serum Albumin

Table 4: Primary Antibodies for western blotting

2.2.4 Immunoprecipitation

Typically 1-5 mg of total protein was used for immunoprecipitation. Protein volumes were equalized using RIPA lysis buffer so that each immunoprecipitation was performed in 1 mL final volume. Protein A or protein G agarose beads (Sigma) were prepared by weighing lyophilized beads and swelling in ten times volume of ice cold PBS for 30 minutes on ice. Beads were washed three times with ice cold PBS, and resuspended to the starting volume with PBS. Lysates were first pre-cleared to reduce nonspecific binding with 1 µg of random mouse or rabbit IgG (Sigma) per milligram of total protein and 30 µL of protein A or protein G beads for one hour at 4ºC on a rotating wheel. After centrifugation at 3,000 rpm for 2 minutes, pre-cleared lysates were transferred to new pre-chilled eppendorf tubes and incubated with 1-3 µg of primary antibody or random IgG per milligram of protein and incubated overnight on a rotating wheel at 4ºC. The following day immunoprecipitates were collected by adding 30 µL of protein A or protein G agarose beads and incubating for 1 hour at 4ºC on a rotating wheel. Beads were washed five times with 1 mL of RIPA lysis buffer, with incubation on the rotating wheel for 3-5 minutes at 4ºC, during each wash. After the final wash, samples were either acid eluted (2.2.5) or denatured in 3X Laemmli buffer at 95ºC for 5 minutes. After centrifugation at 13,000 rpm for five minutes, samples were analyzed by SDS-PAGE and western blotting.

2.2.5 Co-Immunoprecipitation

Cells were lysed in Co-IP buffer [50 mM HEPES pH 7.5, 150 mM NaCl, 10% glycerol, 1% w/v Triton X-100, 1 mM EGTA, 1.5 mM $MgCl_2$, ETDA-free protease inhibitor cocktail, 1.5 mM Pefabloc SC Plus (Roche), phosphatase inhibitor complex II (Sigma P5726) and complex III (Sigma P0044)]. Typically 1-5 mg of total protein was used for co-immunoprecipitation. Protein volumes were equalized using Co-IP lysis buffer

so that each co-immunoprecipitation was performed in 1 mL of final volume. After preclearing, proteins of interest were immunoprecipitated as described above, using 1-3 µg of primary antibody or random IgG per milligram of protein. After incubating overnight on a rotating wheel at 4°C, immunoprecipitates were collected by adding 30 µL of protein A or protein G agarose beads and incubating for 1 hour at 4°C on the rotating wheel. Beads were washed five times with 1 mL of Co-IP wash lysis buffer [50 mM HEPES pH 7.5, 300 mM NaCl, 10% glycerol, 1% w/v Triton X-100, 1 mM EGTA, 1.5 mM $MgCl_2$, EDTA-free protease inhibitor cocktail, 1.5 mM Pefabloc SC Plus (Roche)]. Between each wash, co-immunoprecipitates were incubated on the rotating wheel for 3-5 minutes at 4°C. After the final wash, samples were either acid eluted for analysis by mass spectrometry (**as in section 2.2.6**) or denatured in 3X Laemmli buffer at 95°C for 5 minutes for analysis by SDS-PAGE and western blotting (**as in section 2.2.3**).

2.2.6 Acid Elution of Immunoprecipitates

Immunoprecipitated proteins were washed as described above. Following final wash, proteins were eluted by incubating beads with 50 µL of 125 mM glycine solution (pH 2.5) for 10 minutes at 4°C. The beads were centrifuged at 3,000 rpm for 2 minutes and the supernatant was transfered to a new pre-chilled eppendorf tube. This was repeated twice more for a total of three elutions and eluted proteins were pooled in a pre-chilled eppendorf tube. Acid was neutralized by adding an equal volume of 10 mM Tris-Cl (pH 8.0). Proteins were concentrated using an Amicon Ultra-0.5 mL centrifugal 10 kDa filter (Millipore) according to the manufacture's protocol. Briefly, supernatant was transferred to a 10 kDa filter fitted to a 1.5 mL eppendorf and centrifuged at 14,000 rpm for 15 minutes at 4°C. Proteins were washed with 100 µL of 10 mM Tris-Cl (pH 7.5) and centrifuged at 14,000 rpm for 15 minutes at 4°C. After two washes, proteins were recovered by inverting the filter into

a fresh 1.5 mL eppendorf tube which was centrifuged at 5,000 rpm for 5 minutes at 4ºC. The final volume of supernatant in each sample was brought to 50 µL using 10 mM Tris-Cl (pH 7.5). Immunoprecipitated proteins were either denatured in 3X Laemmli buffer at 95ºC for 5 minutes and analysed by western blotting or analysed by Mass spectrometry (**as in section 2.5.3**)

2.3 Procedures for DNA work

2.3.1 General Techniques

All solutions used Milli-Q grade water and all tubes were autoclaved prior to use. Tips fitted with a filter were used for pipetting solutions and DNA. DNA was suspended in TE buffer or water, aliquoted and stored at -20ºC.

2.3.2 Quantification of nucleic acids

DNA concentration was determined using a ND-1000 spectrophotometer (Nanodrop Technologies, Wilmington, DE, USA), measuring absorbance at 260 nm.

2.3.3 Preparation of plasmids

Plasmids encoding human FLAG-His6 ATM wild type (wt) or kinase dead (kd) in pcDNA3.1 were kindly provided by Dr. MB Kastan (St. Jude Children's Research Hospital, Memphis, TN, USA). Previously prepared glycerol stocks were streaked onto Luria Bertini (LB)-agar plates with ampicillin and incubated at 37ºC overnight. The following day individual colonies were picked and incubated in 5 mL LB medium with 5 µL of 100 mg/mL ampicillin (final concentration 100 µg/mL) and grown overnight at 37ºC in a shaking incubator. Preparation of plasmids used the QIAGEN plasmid mini kit. To prepare miniprep DNA, 5 mL of culture was collected by centrifugation at 8000 rpm for one minute. Cells were resuspended in 250 µL of P1 buffer with RNase, followed by lysis and denaturation by adding 250 µL of P2 buffer.

Following 2-3 minute incubation at room temperature, 350 µL of buffer N3 was added for neutralization and mixed by gently inverting the tubes 4-6 times. After centrifugation at 13000 rpm for 10 minutes, the supernatant was transferred to a silica-gel containing column which provided a surface for plasmid binding. Columns containing DNA were washed twice with 1 mL of PE buffer and eluted in 50 µL of Milli-Q water. ATM expression plasmids were verified by restriction enzyme digest.

2.3.4 Digestion of DNA with restriction endonucleases

Plasmid DNA was digested using NcoI restriction enzyme using the manufacture's protocol (Fermentas). For this, 1 µg of DNA was diluted with 10X Tango buffer in nuclease-free water. Digestion was carried out with 1 µL (3 units) of NcoI restriction enzyme for 2 hours at 37^{o}C in a volume of 20 µL and analyzed by agarose gel electrophoresis.

2.3.5 Gel electrophoresis of DNA

Following digestion, DNA was analysed on 1% agarose gels, which were prepared by melting 1 g agarose (Gibco-BRL) in 100 mL 1XTris-acetate-EDTA (TAE) buffer (40 mM Tris, 20 mM Acetic acid, 1 mM EDTA, pH 8.0). After cooling to approximately 55^{o}C, 0.5 µg/mL of ethidium bromide was added and the gel was poured into a flat bed apparatus (Gibco-BRL Model H5) and allowed to set. The gel was submerged in 1X TAE buffer and DNA was mixed with one sixth volume of 6X Orange DNA loading dye (Fermentas) and loaded into the wells. DNA was separated by electrophoresis at 100 volts, in parallel with 1 kb DNA ladder (New England Biolabs). DNA was visualized using UV light and gels were photographed using a Multimage II camera and AlphaView software (Alpha-Innotech, USA).

2.4 Procedure for RNA Extraction and Quantitative real-time PCR (qRT-PCR)

2.4.1 General Techniques

All solutions used Milli-Q grade water and all tubes were autoclaved prior to use. Filter tips were used for pipetting solutions and RNA. RNA was suspended in DEPC-Treated nuclease-free water (Invitrogen), and stored at -80^{o}C.

2.4.2 RNA Extraction from cultured cells

RNA was extracted from cultured cells using the RNeasy kit (Qiagen) according to the manufacturer's protocol. Cells were cultured in 10 cm dishes and when 50-70% confluent, cells were harvested by first washing the monolayer twice with cold PBS and scraping into 350 µL of RTL buffer containing 0.1 M β-mercaptoethanol (Sigma, St. Louis, MO, USA). Lysates were transferred to a pre-chilled eppendorf tube and homogenized by passing through a 19-gauge needle 8-10 times. One volume of 70% ethanol was added to homogenized lysates and mixed by pipetting. Lysates were transferred to a silica-membrane column and centrifuged for 15-30 seconds at 10,000 rpm. An optional DNase digestion was performed on column to reduce genomic DNA contamination. This was accomplished by first adding 350 µL of buffer RW1 to the column and centrifuging for 15-30 seconds at 10,000 rpm. DNase I stock solution was diluted one in eight in RDD buffer prior to use, and 80 µL of this solution was added directly onto the membrane, and incubated on the membrane for 15 minutes at room temperature. Then 350 µL of buffer RW1 was added and columns were centrifuged for 15-30 seconds at 10,000 rpm. A second wash with 700 µL of buffer RW1 was added to the columns and centrifuged for 15-30 seconds at 10,000 rpm. Following two washes in 500 µL of buffer RPE, RNA was eluted in 30 µL of DEPC-treated nuclease-free water (Invitrogen) by centrifugation at 10,000 rpm for 1

minute. The concentration of RNA was assessed by spectrophotometry and purity was assessed by judging the ratio of absorbance at 260 nm versus 280 nm.

2.4.3 Reverse Transcription (RT)

Total RNA was reverse-transcribed into complementary DNA (cDNA) using the High Capacity cDNA Archive Kit (Applied Biosystems) according to the manufacturer's instructions. Briefly, 2 µg of total RNA was added to PCR tubes and DEPC-treated water was added to a final volume of 10 µL. A 2X reverse transcription master mix was prepared, containing (per reaction) 2 µL of 10X RT buffer, 0.8 µL 25X dNTPs, 2 µL of 10X RT random primers, and 4.2 µL of DEPC treated water. To each PCR tube, 10 µL of 2 X RT master mix was added. Reaction tubes were placed in a Peltier Thermo Cycler (MJ Research, Waltham, MA, USA) and incubated at 25°C for 10 minutes, 37°C for 120 minutes, 85°C for 5 minutes and 4°C for 10-15 minutes. The cDNAs were stored at -20°C and subjected to quantitative real-time PCR (qRT-PCR).

2.4.4 qRT-PCR

2.4.4.1 Primer design

Primer-BLAST (http://www.ncbi.nlm.nih.gov/tools/primer-blast/) was used to generate primers for qRT-PCR. Forward and reserve primers were designed to generate products less than 150 base pairs and were ordered from Invitrogen Life Sciences Technologies. The primers used for qRT-PCR are listed in **table 5**.

Target Gene	Exon	RefSeq	Forward primer (5'→ 3')	Reverse primer (5'→3')
Human BRCA2	1	NM_000059.3	GCTGCGCCTCGGGTGTCTTT	ACCGCGCCGGTCACAAATCT
Human BRCA2	11	NM_000059.3	GGTCAGGTAGACAGCAGCAAGCA	TCAACAGGCCAGCAAACTTCCGT
Human BRCA2	17	NM_000059.3	GGAAACTGGCAGCTATGGAATGTGC	TGAAGAAGCACCCTTTCTCGGCT
Human α-Tubulin	3	NM_032704.3	CCCCTTCAAGTTCTAGTCATGC	ATTGCCAATCTGGACACCA

Table 5: PCR Primers for qRT-PCR

2.4.4.2 qRT-PCR

All qRT-PCR reactions were performed in triplicate per sample/per primer and prepared by a robot in the RotoGene 3000 qPCR system (Corbett Research, Sydney, Australia). The SensiMix SYBR kit (Bioline Reagents Ltd., UK) was used according to the manufacturer's protocol for qRT-PCR analysis. Briefly, each sample contained: 20 ng of total cDNA, 10 pmole of forward and reverse primers (Table 3), 10 µL of 2X SYBR mixture consisting of Heat-activated DNA polymerase, ultra-pure dNTPs, $MgCl_2$ (6 mM) and SYBR Green I. DNA polymerase was activated by first heating samples to 95^{o}C for 15 minutes, followed by amplification of cDNA for 40 cycles of 95^{o}C for 10 seconds and 60^{o}C for 40 seconds.

2.4 Cell Based Assays

2.4.1 Growth Assays

2.4.1.1 Clonogenic Survival Assay

Cell survival was assessed by clonogenic assay. Cells were disaggregated using 3 mM EDTA and counted using trypan blue dye (Sigma) and a hemocytometer. For DU145 cells, 3000 cells were seeded in a 10 cm dish or 1000 per well of a 6 well plate, in triplicate. The following day, cells were pre-treated with inhibitor in complete growth medium for 1-4 hours and then irradiated (0-10 Gy). Dishes were incubated for 10-14 days at 37^{o}C and 5% CO_2. Once colonies reached approximately 50

cells,they were fixed and stained for 30 minutes with 0.1% Coomassie, 7% acetic acid and 50% methanol at room temperature. Dishes were washed in water and air-dried. Colonies were counted on a Colcount automated colony counter (Oxford Optronix) and results were expressed as a percentage of survival in untreated control dishes.

2.4.1.2 Cell Proliferation Assay

Cells were seeded or reverse transfected with siRNAs into triplicate wells of u-clear 96-well plates (**section 2.1.4.2**). The cells were treated with inhibitors or solvent control 48 hours after transfection. For treatment of untransfected cells, chemical inhibitors were added 24 hours after seeding. Plates were incubated for 5 days at 37ºC and 5%CO_2. Cell viability was measured using CellTiter-Glo (CTG) Luminescent Assay (Promega). The assay reagent measures ATP-induced luminescence and was added directly to the wells in a 1:1 ratio with the medium in the wells. Plates were incubated for 30 minutes at room temperature in the dark, read in a luminometer (Fluorstar Optima, BMG Labtech) and values were normalized to solvent-treated cells. Using data from three independent experiments, curves were fitted using GraphPad Prism v5 to extrapolate the concentration of drug required to inhibit 50% of growth (GI_{50}).

2.4.2 Immunofluorescence Microscopy

Cells were seeded on glass coverslips 24 hour prior to treatment with chemical inhibitors and/or ionizing irradiation (**as in section 2.1**). Following treatment, cells were washed three times with 1 mL of PBS at room temperature before fixation in 4% paraformaldehyde (VWR) in PBS for 15 minutes at room temperature. After fixation, cells could be stored in 0.1% sodium azide in PBS at 4ºC for future staining. Cells

were washed three times for 5 minutes at room temperature with Tris-buffered saline (TBS) and blocked and permeabilized in 10% FCS, 0.3% Triton X-100 in TBS, for 1 hour at room temperature. Cells were incubated overnight at 4°C with primary antibody (**Table 6**) made up in blocking buffer. The next day, cells were washed three times for 5 minutes at room temperature with TBS and incubated with 1:2000 anti-rabbit or anti-mouse secondary antibody conjugated to Alexa Fluor 488 (Molecular Probes) or Alexa Fluor 555 (Molecular Probes) in blocking buffer for 30 minutes at room temperature. Following four washes for five minutes with TBS with 0.05% Tween 20, and one wash with distilled water for five minutes to reduce salt crystals, coverslips were mounted with Fluoromount-G with DAPI (SouthernBiotech). Slides were analyzed using a Zeiss Axioplus-2 microscope and images were captured using a AxioCam colour camera (Zeiss). Each experiment included a negative control stained without primary antibody.

Name	Source	Species	Dilution	Catalogue Number
RAD51 [14B4]	Abcam	Mouse	1:300	ab213
γ-H2AX	Millipore	Mouse	1:2000	05-636
γ-H2AX	Millipore	Rabbit	1:2000	04-817

Table 6: Primary Antibodies for Immunofluorescence

2.4.3 Cell Cycle Analysis by Flow Cytometry

2.4.3.1. Propidium Iodide

Treated cells were harvested with 3 mM EDTA in PBSA and pelleted by centrifugation at 1200 rpm for 5 minutes at 4°C. Cells were fixed by adding 1 mL of chilled 70% ethanol while vortexing, and incubated at -20°C overnight. The following day, cells were pelleted by centrifugation at 1200 rpm for 5 minutes at 4°C, resuspended in 200 µL of PBSA containing 10 µg/mL Propidium Iodide (PI) (stock 1 mg/mL, Molecular Probes) and 100 µg/mL RNase A (stock 10 mg/mL, Fermentas)

and incubated at room temperature for 30 minutes. Prior to analysis, samples were transferred to 5 mL Polypropylene Round-bottom tubes (BD Falcon) and brought to a final volume of 500 µL with PBSA. Samples were analysed by flow cytometry using a Beckman CyAn ADp Color flow cytometer and further analysis was carried out using FlowJo software (USA).

2.4.3.2 Bromodeoxyuridine (BrdU) Incorporation Assay

Treated cells were pulse labelled with 10 µM of 10 mM BrdU stock (Sigma) in complete medium for 15 minutes at 37°C. Cells were harvested with 3 mM EDTA in PBSA and pelleted by centrifugation at 1200 rpm for 5 minutes at 4°C. Cells were fixed by adding 1 mL of chilled 70% ethanol while vortexing and incubated at -20°C overnight. The following day, cells were pelleted by centrifugation at 1200 rpm for 5 minutes at 4°C and acid permeabilized by resuspending cells in 1 mL of acid solution (2 M HCl, 0.5% Triton X-100) for 30 minutes at room temperature. The acid was neutralized for 5 minutes with 1 mL of 0.1M $Na_2B_4O_7 \cdot 10H_2O$. Cells were incubated overnight at 4°C in 200 µL of 0.5 ng/µL anti-BrdU primary antibody (Abcam) made up in 1% BSA with 0.5% Tween in PBS. The following day, cells were incubated with 50 µL of Alexa-488 conjugated anti-rat secondary antibody (Invitrogen) diluted 1:250 in 1% BSA with 0.5% Tween in PBS for 30 minutes at room temperature. After incubation, cells were pelleted by centrifugation at 2000 rpm for 5 minutes at 4°C, resuspended in 200 µL of PBSA containing 10 µg/mL propidium iodide (PI) and 100 µg/mL RNAse A and incubated at room temperature for 30 minutes. Prior to analysis, samples were transferred to 5 mL Polypropylene Round-bottom tubes (BD Falcon) and brought to final volume of 500 µL with PBSA. Samples were analysed by flow cytometry using a Beckman CyAn ADp Color flow cytometer.

2.5 Mass Spectrometry (MS) Analysis

2.5.1. General techniques

All reagents used to prepare and analyse samples were MS/HPLC grade, and were opened only in sterile fume hoods. All solutions were prepared fresh and filter-sterilized through 0.22 μM filters. To minimize keratin contamination, electrophoresis was carried out in a fume hood, as were all subsequent in-gel or in-solution digest steps.

2.5.2. In Gel Digest

In gel digest was adapted from a protocol kindly supplied by Dr. Benedikt Kessler (Nuffield Department of Clinical Medicine, University of Oxford). Immunoprecipitates were separated by electrophoretic mobility on a pre-cast 10% Bis-Tris gel (Invitrogen). The gel was fixed in 50% methanol with 10% acetic acid in MilliQ water for 10 minutes while shaking at room temperature. Following fixation, the gel was incubated in staining solution [20 mL methanol, 20 mL of stainer A (Invitrogen), with 55 mL of MilliQ water] for ten minutes at room temperature before adding 5 mL stainer B (colloidal blue, Invitrogen) to the staining solution. The gel was incubated for 3 hours at room temperature and then destained overnight in MilliQ water at room temperature with shaking. Using a clean scalpel for each sample, equal sized portions were cut out of the gel and cut into smaller pieces before transferring to a fresh eppendorf tube. Gel pieces were incubated overnight in 200 μL of wash solution [50% methanol and 5% acetic acid in MilliQ water]. The following day an additional 200 μL of wash solution was added and samples were further incubated for 3 hours at room temperature before centrifuging at 13,000 rpm for 30 seconds and removing excess wash solution. Gel pieces were dehydrated by adding 200 μL of acetonitrile (ACN), incubating for 5 minutes at room temperature, centrifugation at 13,000 rpm for 30 seconds and removal of ACN. Following two ACN dehydrations,

gel pieces were dried in a vacuum centrifuge for 5 minutes, 5,000 rpm at 50°C. Disulfide bonds were reduced by incubating gel fragments in 30 µL of dithiothreitol (DTT) solution [10 mM DTT with 100 mM ammonium bicarbonate] for 10 minutes at room temperature. Excess DTT solution was removed and 30 µL of 50 mM iodoacetamide buffer was added to gel fragments for 30 minutes at room temperature, to prevent reformation of disulfide bonds. Gel pieces were centrifuged at 13,000 rpm for 30 seconds, iodoacetamide was removed and gel pieces were dehydrated by adding 200 µL of ACN, and incubating for 5 minutes at room temperature. The ACN was removed and gel pieces were dried in a vacuum centrifuge for 5 minutes. After a second ACN wash, samples were dried under vacuum to remove acetonitrile. Tryptic digest was performed by incubating gel pieces with 30 µL of 20 ng/µL trypsin in 50 mM ammonium bicarbonate. Digestion was carried out overnight at 37°C, and the following day the supernatant was transferred to a fresh eppendorf tube. Gel fragments were washed three times with 50 µL of extraction buffer [5% ACN with 0.1% trifluoroacetic acid (TFA) in 50 mM ammonium bicarbonate]. Each wash was pooled with the supernatant from digestion. Finally, samples were dried down completely in a vacuum centrifuge and resuspended in 20 µL buffer A [2% acetic acid, 0.1% formic acid in MilliQ water]. Samples were further purified by ZipTip purification (**as in section 2.5.4**).

2.5.3. In Solution digest

In solution digest was performed according to a protocol supplied by Dr. Benedikt Kessler. Immunoprecipitated proteins were eluted and concentrated as described in section 2.2.6. Proteins were then completely dried down in a vacuum centrifuge at 50°C, 5000 rpm for 15 minutes and resuspended in 100 µL 6 M urea [in 100 mM Tris-Cl, final pH 7.8] and incubated with 5 µL DTT solution [200 mM DTT in 100 mM Tris-Cl, final pH 7.8], to reduce disulfide bonds, for 60 minutes at room temperature.

Following incubation, 20 µL of alkylating solution [200 mM iodoacetamide in 100 mM Tris-Cl, final pH 7.8] was added for 60 minutes at room temperature. Prior to digestion with trypsin, the sample was diluted by adding 775 µL of MilliQ water to bring the concentration of urea down to 667 mM. Digestion of samples was carried out overnight at 37^{o}C by adding 20 µL of a 0.2 µg/µL trypsin solution [in 100 mM Tris-Cl, final pH 7.8]. The following day, digestion was stopped by adding 1 µL TFA to bring the final pH to below 6. Finally, samples were dried down completely in a vacuum centrifuge and resuspended in 20 µL buffer A [2% acetic acid, 0.1% formic acid in MilliQ water]. Samples were further purified by ZipTip purification (2.5.4).

2.5.4 ZipTip Purification

To remove residual ions ZipTip C_{18} (Millipore) pipette tips incorporate a resin bed that allows for peptide binding. First, ZipTips were prewet by drawing up and ejecting 10 µL of acetonitrile. Each 20 µL protein sample was drawn up into a ZipTip 10 times and washed three times in 0.1% TFA with 5% methanol by repeatedly aspirating and dispensing wash solution. After the final wash, proteins were eluted in 30 µL 50% ACN in 0.1% TFA and stored at -20˚C.

2.5.5. Mass Spectrometry

Samples were analysed by Dr. Garth Hamilton (Department of Oncology, Oxford) on a Liquid chromatography (LC)-MS/MS tandem mass spectrometer (HCTplus, Bruker) as described in **Chapter 5**.

2.6 Statistical Analysis

The graphing and statistical analysis software Prism v.5.0 (GraphPad, USA) and Excel (Microsoft, USA) were used to plot and analyze data. Graphs were plotted to show mean values and standard error of the mean (SEM). Data were compared

using the student’s t-test for two groups, one way ANOVA for more than two groups, and two way ANOVA to compare set of data.

Chapter 3: Investigation of the hypothesis that ATM function is influenced by IGF signalling in human prostate cancer cells

3.1 The Role of IGF-1R in DNA Repair

The first link between IGF-1R and DNA damage came from a breast cancer study showing that patients over-expressing IGF-1R were more likely to experience an early recurrence within the irradiated site (Turner *et al.*, 1997). Since this early indication of clinical radio-resistance, several studies have investigated the mechanism by which IGF-1R signalling can influence DNA damage repair. Torjanek et al. (2003) showed that IGF signalling supports homologous recombination mediated DNA repair via a direct interaction between IRS-1 and RAD51, the recombinase required for the strand invasion step of homologous recombination. The absence of IGF-1R activation causes IRS-1 to directly bind to and retain RAD51 in the cytoplasm, inhibiting homologous recombination (Trojanek *et al.*, 2003). This finding has been supported by other studies from the same group (Reiss *et al.*, 2006; Trojanek *et al.*, 2006).

Previous work from our laboratory showed that IGF-1R down-regulation enhanced the radio-sensitivity of B16 murine melanoma cells (Macaulay *et al.*, 2001). Depletion of IGF-1R reduced the levels of ATM protein, apparently at a post-transcriptional level, and impaired ATM kinase activity, suggesting that IGF-1R signalling can affect ATM function. Subsequent experiments using gene silencing

implicated IRS-1-AKT signalling in mediating a link between IGF-1R and ATM (**Figure 5**). Work investigating a possible interaction between IRS-1 and ATM was the focus of another student within our laboratory; results indicated that an IGF-regulated interaction is detectable in MCF-7 breast cancer cells and indeed this has been reported (Jeon *et al.*, 2008), but an interaction between IRS-1 and ATM was not detectable in prostate cancer cells (Chitnis, Macaulay unpublished). The focus of this work was to investigate the hypothesis that IGF-1R signalling can influence the function of ATM in prostate cancer cells.

3.2 Results

3.2.1 Inhibition of IGF-1R sensitises DU145 prostate cancer cells to Ionizing Radiation

Previous work from our lab demonstrated that IGF-1R depletion sensitizes prostate cancer cells to ionizing radiation (Turney *et al.*). While siRNA-mediated protein depletion is a very effective method in the laboratory setting, small molecule inhibitors are a more appropriate option for clinical use. A small molecule IGF-1R inhibitor was kindly provided by Elizabeth Anderson (AstraZeneca, United Kingdom). AZ12253801, is an ATP-competitive IGF-1R tyrosine kinase inhibitor that shows ~10-fold selectivity over the insulin receptor (in-house data from AstraZeneca). The IC_{50} values for inhibition of IGF-1R and insulin receptor phosphorylation *in vitro* are 2.1 and 19 nmol/L, respectively. The IC_{50} for inhibition of IGF-1R–driven proliferation in 3T3 mouse fibroblasts transfected with human IGF-1R is 17 nmol/L, whereas the IC_{50} for epidermal growth factor receptor (EGFR)–driven proliferation is 440 nmol/L. AZ12253801 has been tested against a wide range of other relevant kinases, where IC_{50}s are generally >1 μmol/L or the compound has little or no inhibitory activity at 10

μmol/L (in-house data from AstraZeneca). In previous work from our group, this agent has been shown to inhibit IGF-1R phosphorylation in intact cells (IC_{50}= 2 nM) and proliferation (GI_{50}= 120 nM) in DU145 cells (Aleksic *et al.*, 2010). The large difference observed between the IC_{50} and GI_{50} might be attributable to several factors. Firstly, the assays were performed over different durations, one hour and seven days respectively, and it is possible that the inhibitor was not active throughout the growth assays. This could have been checked by performing analyses as in Figure 6A below at different time points. Additionally, half maximal inhibition of IGF-1R autophosphorylation was achieved by 2 nM, but the downstream AKT and ERK pathways required higher concentrations of AZ12253801 to be inhibited. Finally it is possible that growth inhibition at relatively high AZ12253801 concentrations could be due to off target effects of the compound.

Initial experiments investigated the activity of AZ12253801 *in vitro*. DU145 prostate cancer cells were serum starved overnight, and following pre-treatment with increasing concentrations of AZ12253801 (0-100 nM), cells were stimulated with 0 or 50 nM IGF-1 in the final 15 minutes. Cells were collected and lysates were separated by SDS-PAGE and analysed by immunoblotting. The effectiveness of AZ12253801 was determined by assessing the levels of phosphorylated IGF-1R, as well as its downstream effectors AKT and ERK 1/2. Treatment with AZ12253801 led to a dose dependent decrease in the levels of phospho-IGF-1R (Tyr1135/1136), with apparently complete inhibition of receptor autophosphorylation being achieved by 30 nM (**Figure 6A**). AZ12253801 at 30 nM also inhibited phosphorylation of AKT (S473) (**Figure 6A**). Phosphorylation of ERK1 (Thr202) and ERK2 (Tyr 204) was not completely suppressed even at 30-100 nM AZ12253801, although did return to basal levels at 30 nM. Therefore, a concentration of 30 nM was chosen for further experiments.

To test effects of IGF-1R inhibition on radiosensitivity of prostate cancer cells, DU145 cells were seeded in 10 cm dishes for clonogenic assay. The following day, cells were pre-treated with solvent (0.0003% DMSO) or 30 nM AZ12253801 and after 1 hour treated with 0 – 10 Gy irradiation. Results of the clonogenic assay are shown in **Figure 6B** and similar results were obtained in a second independent experiment. Control-treated DU145 cells were relatively resistant to 2-5 Gy irradiation, with reduction in clonogenic survival only at 5 Gy (Figure 2B). Cells pre-treated with 30 nM AZ12253801 were more radiosensitive, with an SF_{50} (dose required to reduce cell survival to 50%) of 2 Gy, compared with 5.5 Gy in control-treated cells (2.75 fold sensitization, $p < 0.0001$, by two way ANOVA). Following 5 Gy irradiation cell survival was 63.3% in control cells and 3.74% in AZ12253801 treated cells (17 fold sensitization).

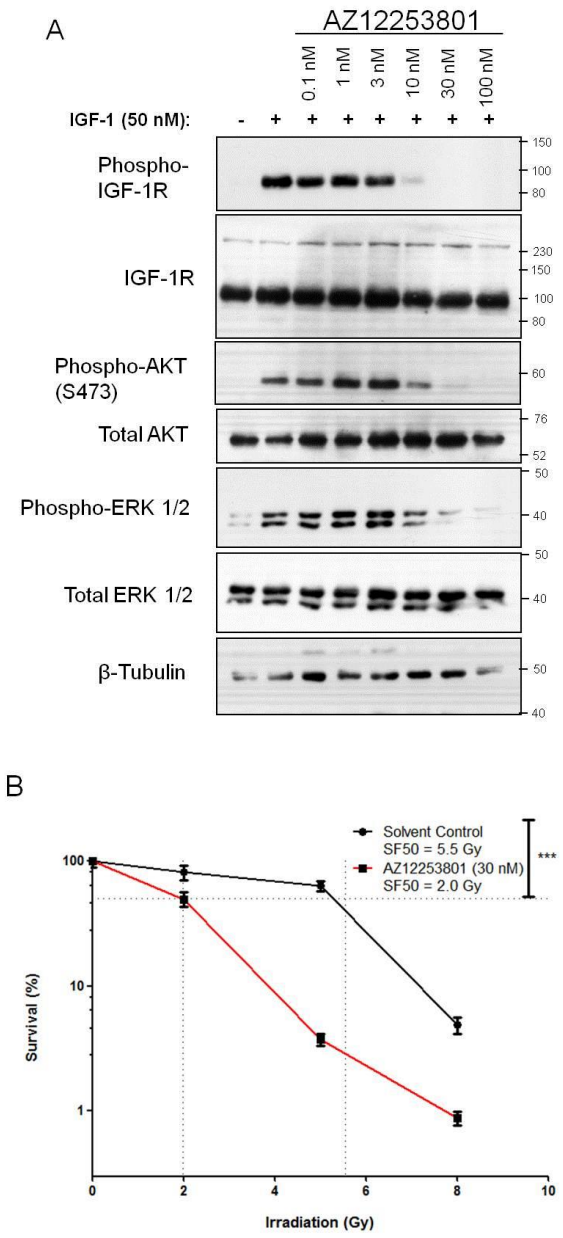


Figure 6: Effects of IGF-1R inhibition on IGF signalling and radiosensitivity of DU145

A) DU145 cells prostate cancer cells were serum starved and pre-treated for one hour with increasing concentrations of AZ12253801 before being treated with 50 nM IGF-1 for 15 minutes. Cell lysates were analyzed by SDS-PAGE and immunoblotted for phospho-IGF-1R and downstream proteins (p-AKT and p-ERK 1/2). B) DU145 cells were seeded at 3000 cells per 10 cm^2 dish, and the following day pre-treated with IGF-1R inhibitor for 1 hour and irradiated. After 10 days visible colonies were stained and counted. Graph shows clonogenic survival (% unirradiated), mean ± SEM of triplicate wells, *** $p< 0.0001$ by 2 way ANOVA. Similar results were obtained in a second independent experiment.

3.2.2 Detection of a 350 kDa protein that is phosphorylated on a motif recognized by AKT in response to IGF-I

The initial focus of this project has been investigation of the hypothesis that IGF signalling via AKT can influence the function of ATM. AKT is a serine/threonine kinase with diverse cellular functions, which include cell survival, growth, proliferation, angiogenesis, metabolism, and migration (Manning and Cantley, 2007). AKT accomplishes this wide range of activity by phosphorylating proteins on the motif RXRXXS*/T*. Scansite (http://scansite.mit.edu/) motif search was used in order to determine whether ATM contained any putative AKT phosphorylation sites. Motif search showed ATM to have two candidate motifs for phosphorylation by AKT (**Figure 7A**), the first located in the FAT domain on serine 2141 (RDREF*S) and the second on threonine 2751 in the PI3K domain (RKRKL*T).

A commercially available antibody was used for western blotting to detect AKT substrates phosphorylated on the motif RXRXXS*/T* (Cell Signaling #10001). Initially, human prostate cancer cells (DU145) or breast cancer cells (MCF7) were serum-starved overnight and treated with 50 nM IGF-1 for 30 minutes. IGF-1 treatment resulted in the appearance or increased intensity of multiple bands representing putative AKT substrates, including a prominent band that migrated at approximately 350 kDa, this is equivalent to the electrophoretic mobility of ATM, and indeed re-blotting for ATM confirmed that the 350 kDa phopho-product had the same electrophoretic mobility (**Figure 7B-7C**). In both cells lines, particularly MCF7, the change of intensity of this band was the largest difference between the IGF-1 treated and serum starved lanes (indicated by arrows **Figure 7B-7C**). Investigation of the time dependence of this putative phosphorylation indicated that there was no further increase in band intensity after 30 minutes (**Figure 7D**).

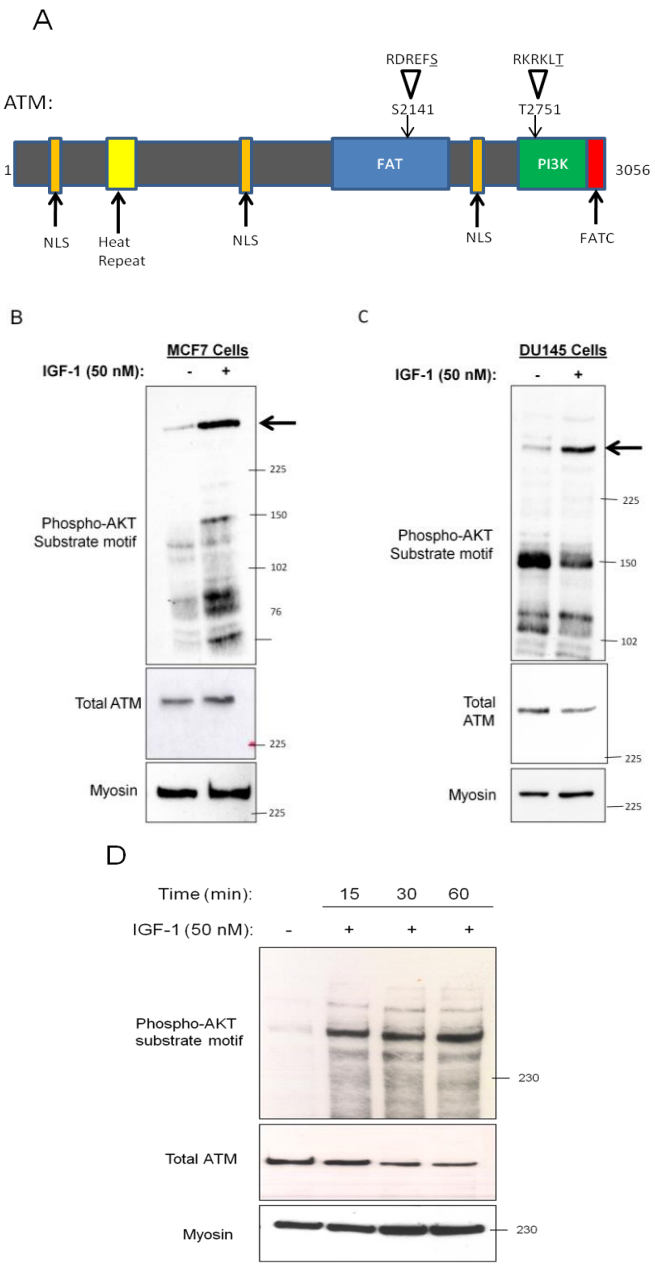


Figure 7: Investigation of possible IGF-induced phosphorylation by AKT on ATM

A) ATM is a large protein that belongs to the phosphatidylinositol 3-kinase-related kinase (PI3K) family. Closest to the N-terminus is Heat Repeat domain which can directly bind to the C-terminus of NBS1. The FRAP-ATM-TRAP (FAT) domain interacts with ATM kinase domain to stabilize the C-terminus region of ATM. Also within the FAT domain is the auto-phosphorylation site on serine 1981 that is phosphorylated in response to DNA damage and is important for its monomerization (Lavin, 2008). Located at the C-terminus is the FATC domain containing a binding site for acetyltransferase TIP60, which acetylates ATM on Lysine 3016 and this post-translational modification is important for ATM activation (Lavin, 2008). B) Human MCF7 breast cancer and C) human DU145 prostate cancer cells were serum-starved and treated with solvent (-) or 50 nM IGF-1 (+) for 30 minutes. Cell lysates were analysed by SDS-PAGE and western blotting for proteins phosphorylated on AKT substrate motif and total ATM. Myosin (230 kDa) was used as a high molecular weight loading control. Arrow indicates a protein of ~350 kDa, the same electrophoretic mobility as ATM, that is phosphorylated on RXRXXS*/T* motif in response to IGF-1. D) Human DU145 prostate cancer cells were serum-starved and treated with solvent (-) or 50 nM IGF-1 (+) for 15, 30 or 60 minutes. Cell lysates were analysed by SDS-PAGE. Immunblotting with phospho-AKT substrate motif antibody showed the level of phosphorylation plateaued by 30 minutes.

3.2.2 Use of siRNA and short hairpin approaches to investigate the IGF-induced 350kDa phospho-product

The next experiments used gene silencing to determine whether the appearance of the 350 kDa phospho-product was dependent on AKT and on the presence of ATM. DU145 cells were transfected with siRNAs to ATM, AKT1 or AKT2 before being serum starved for 24 hours. Cells were either left untreated or treated with IGF-1 for 30 minutes and lysates were analysed by western blotting (**Figure 8A**). All cells showed IGF-induced phosphorylation of the receptor, confirming the bioactivity of the ligand (**Figure 8A**). Immunoblotting also confirmed depletion of the individual AKT isoforms. Knocking down either isoform of AKT led to an overall reduction in the detection of products phosphorylated on AKT substrate motifs upon IGF stimulation (**Figure 8A**). The intensity of the 350 kDa phospho-product was markedly reduced, although not abolished, by both AKT1 and AKT2 knockdown. This implicates both AKT isoforms, either directly or indirectly, in the phosphorylation of this protein. In an attempt to assess whether the 350 kDa phospho-product was ATM, parallel cultures were transfected with ATM siRNA. However, it did not prove possible to deplete ATM below levels present in control-transfected DU145 cells, and there was no reduction in the IGF response detected by the AKT phospho-motif antibody (**Figure 8A**).

An alternative approach used Hela cells that had been stably transfected with LacZ (control) or ATM shRNAs. In these cells, levels of ATM were reduced to almost undetectable levels compared to control LacZ transfectants (**Figure 8B**). HeLa shLacZ and shATM cells were serum starved for 24 hours and treated with IGF-1 for 30 minutes before analysis by western blotting. Both cell lines showed a triplet of

phospho-AKT substrate motif immunoreactivity at approximately 350 kDa in untreated cells (**Figure 8B**). Re-blotting for total ATM indicated that ATM had the same electrophoretic mobility as the middle band of the triplet (indicated by the arrow in **Figure 8B**). Upon IGF-1 treatment, HeLa shLacZ cells showed a modest increase in phosphorylation of the 350 kDa band (**Figure 8B**). HeLa shATM cells showed the same triplet pattern on blotting with the p-RXRXXS/T antibody but there was no detectable change in the 350 kDa phospho-protein on IGF-1 treatment. Therefore this experiment did not clarify whether the 350 kDa phospho-protein was ATM.

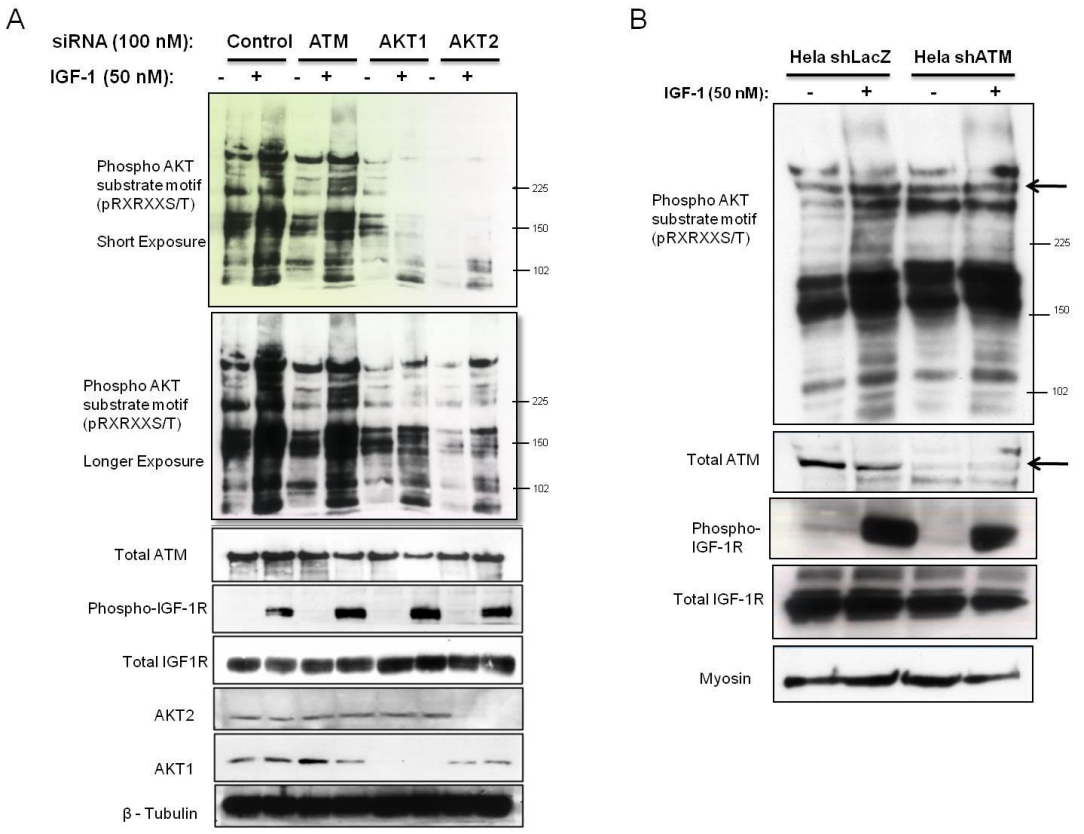


Figure 8: Effects of depletion of AKT or ATM on IGF-induced 350 kDa phospho-protein

a) DU145 prostate cancer cells were transfected with siRNAs to deplete ATM, AKT1, AKT2 or a non-silencing control siRNA. After 24hr the cells were serum-starved and the following day were IGF-treated for 30 min prior to lysis for SDS PAGE and immunoblotting. Knockdown of AKT1 or AKT2 suppressed phosphorylation of the 350kDa protein, using an antibody that recognises proteins phosphorylated on AKT substrate motif RXRXXS/T. b) HeLa cells stably transfected with control shRNA or ATM shRNA were serum-starved overnight and IGF-treated as in a). Immunoblotting for phospho-AKT substrate motif

produced 3 bands in the region of ~350kDa; the middle band (arrowed) overlay total ATM. IGF-induced IGF-1R phosphorylation confirmed that the ligand was bioactive.

3.2.3 Probing for Phospho-AKT substrate motif immunoreactivity in ATM immunoprecipitates

Thus far, western blotting had detected an IGF-induced phospho-product of 350 kDa, but it was unclear whether this was indeed ATM. Consequently, immunoprecipitation (IP) was used in order to clarify whether ATM was the target of this phosphorylation. The next series of experiments used immunoprecipitation with the antibody that recognises proteins phosphorylated on the motif RXRXXS*/T*, and an antibody to total ATM (**Figure 9A**).

Initially, RXRXXS*/T* immunoprecipitates from serum-starved or IGF-treated cells were blotted for total ATM, and a very faint band was detectable in immunoprecipitates from IGF-stimulated cell lysates, but not from serum-starved cells, or control-antibody precipitates (**Figure 9A**). Despite further repeated attempts ATM could not be more confidently detected in phospho-AKT motif immunoprecipitates**.** Furthermore, ATM immunoprecipitates did not appear to contain phospho-AKT substrate motif immunoreactivity (**Figure 9B**). This situation did not change, despite further scale-up and optimisation of conditions for IP.

Two further strategies were used to investigate this hypothesis. The first was an ATM overexpression system, and the second was to investigate the consequence of AKT inhibition on ATM function. These investigations were carried out in parallel, but will be presented sequentially for clarity.

A FLAG-tagged ATM plasmid was obtained from Dr. Michael Kastan, Saint Jude Hospital, Memphis Tennessee (**Figure 10A**) (Canman *et al.*, 1998). Use of this

plasmid allowed for the option of FLAG tag IP, for which very effective antibodies are available. However, this strategy also presented two challenges: the first was the possibility that the plasmid could undergo rearrangement and the second was to find effective methods of transfecting the plasmid into cells.

Due to the size of the plasmid (14.2 kb, **Figure 10B**), rearrangements could occur during growth of bacterial cultures, and this was checked by restriction enzyme digest of each plasmid preparation. In the absence of rearrangement, Nco-I digestion of wild type plasmid would produce fragments of 0.4, 0.8, 1.8 and 3.5 kB, while digestion with Nco-I of kinase dead (kd) plasmid would produce fragments of 0.4, 0.8, 1.4 and 3.5 kB. This was the pattern that was observed in restriction digest of each plasmid preparation (**Figure 10B**).

Secondly, a plasmid of this size was very difficult to transfect into cells. Therefore, before performing large scale IP, a simple transfection test was performed. HEK293T cells were transfected using the calcium phosphate method, in which the incubation of plasmid with calcium phosphate causes precipitation of calcium-plasmid complexes that are taken up by endocytosis (Canman *et al.*, 1998). Compared to pcDNA3.1 empty vector transfectants, cells transfected with ATM plasmid showed higher levels of ATM (**Figure 10C**). Using the same transfection conditions, HEK293T cells were transfected with ATM plasmid, and FLAG tag immunoprecipitates were analysed by western blotting for FLAG or ATM (**Figure 10D**). However, compared with mock transfectants, cells transfected with the ATM plasmid did not appear to overexpress ATM. Despite multiple attempts, further optimization of the transfection method did not improve ATM expression levels and therefore this line of investigation could not be pursued further.

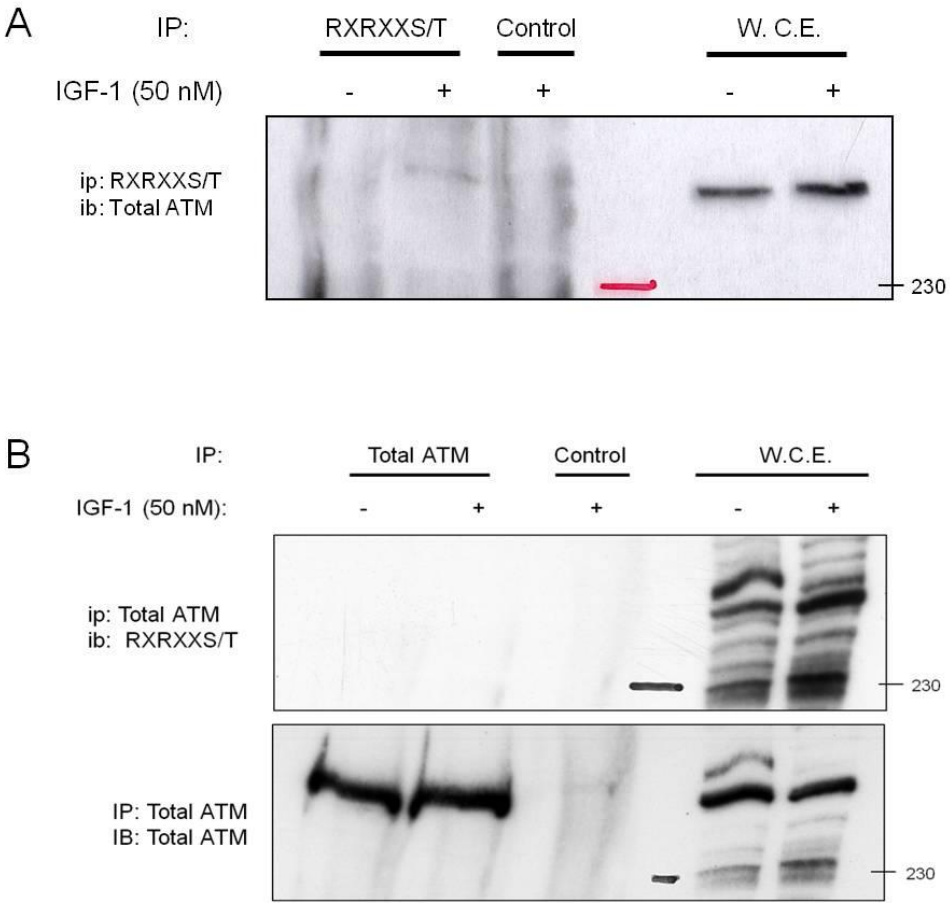


Figure 9: Immunoprecipitation of endogenous ATM

DU145 cells were serum-starved and treated with solvent (-) or 50 nM IGF-1 (+) for 30 minutes and lysates were immunoprecipitated with A) phospho-AKT substrate motif antibody (RXRXXS/T), B) Total ATM antibody or control irrelevant antibody (rabbit IgG). Immunoprecipitates and whole cell extracts (WCE) were analysed by SDS-PAGE and immunoblotted for phospho-AKT substrate motif antibody and total ATM.

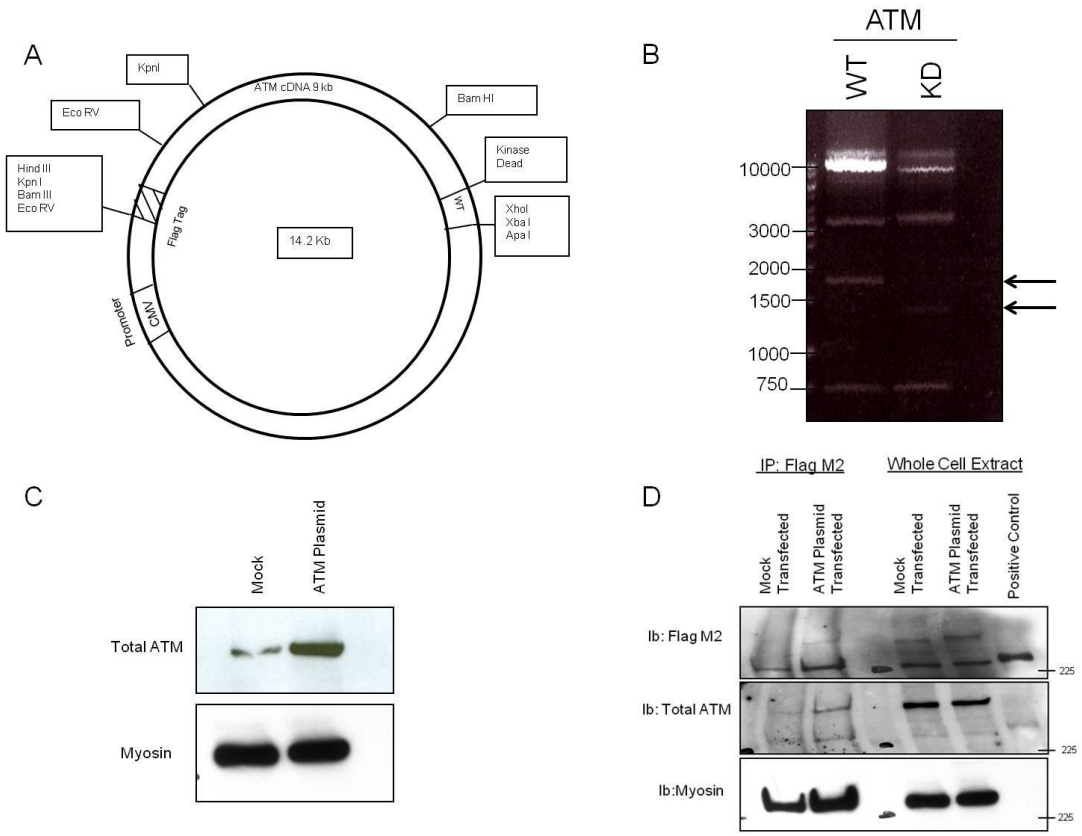


Figure 10: Immunoprecipitation of overexpressed ATM

A) FLAG-tagged ATM construct (Canman *et al.*, 1998) B) Due to the size of the plasmid, rearrangements could occur during growth of bacterial cultures, and this was tested by restriction enzyme digest of each plasmid preparation. Nco-I digest of wild type plasmid produced fragments of 0.8, 1.8 and 3.5 kB, while digestion with Nco1 of kinase dead (kd) plasmid produced fragments of 0.8, 1.4 and 3.5 kB. The expected 0.4 kB product of each digestion was probably run off the gel. C) HEK 293T cells were transfected with ATM plasmid and after 48 hours lysates were analysed by SDS-PAGE and immunoblotted for total ATM and myosin as a loading control. D) HEK 293T cells were transfected as above and lysates were immunoprecipitated with FLAG-M2 antibody and analysed by SDS-PAGE before immunoblotting for FLAG M2, total ATM and Myosin. Lysate from chicken DT40 cells transfected with FLAG tag Fanconi anemia group M protein was obtained from Dr. Rebekka Schwab (University of Oxford, Oxford, UK) and was used as a positive control for FLAG western blot.

3.2.4 Functional significance of AKT inhibition on radiosensitivity of DU145

In parallel with the above approaches, experiments were conducted to assess whether IGF-1R, acting via AKT, is indeed required for ATM function. If that were the case, it was predicted that inhibition of AKT should influence radiosensitivity of prostate cancer cells, and should induce phenotypes consistent with impaired function of ATM. These experiments used a commercially available AKT inhibitor (AKT X, Calbiochem, (Thimmaiah *et al.*, 2005)), and an inhibitor of ATM as a positive control for radiosensitisation. First, it was necessary to establish concentrations of the AKT inhibitor (AKTi) (Thimmaiah *et al.*, 2005) and ATM inhibitor KU-55933 (ATMi) (Hickson *et al.*, 2004) that would inhibit target protein function. DU145 cells were serum starved overnight and pre-treated with 0-10 μM AKTi for 4 hours, and in the final 30 minutes were treated with 0 or 50 nM IGF-1. Levels of phosphorylated AKT (serine 473) and glycogen synthase kinase 3 α/β (GSK3 α/β), a downstream target of AKT signalling, were measured by western blotting. Treatment with the AKTi led to a reduction in IGF-induced phosphorylation of AKT S473 and GSK3 α/β, which was dose dependent for GSK3 α/β, but not clearly so for AKT phosphorylation (**Figure 11A**). Inhibition of AKT phosphorylation was achieved using 5 μM of the inhibitor, while GSK3 α/β was significantly reduced but not suppressed even at 10 μM (**Figure 11A**). A concentration of 5 μM was chosen for further experiments, as used in previous reports (Thimmaiah *et al.*, 2005).

Similarly, a dose titration was performed using the ATM inhibitor KU-66933. DU145 cells were grown in complete medium and pre-treated with 0 - 20 μM ATMi before irradiation. Radiation-induced phosphorylation of ATM on serine 1981 and ATM-dependent phosphorylation of Chk2 were measured by western blotting. The ATM

inhibitor reduced ATM autophosphorylation on S1981 at 5-20 μM, and suppressed Chk2 phosphorylation at 10-20 μM (**Figure 11B**), and so 10 μM was the concentration chosen for further experiments as had been used in published reports (Hickson *et al.*, 2004). These experiments also used the IGF-1R inhibitor, AZ12253801 that had been shown to radio sensitize DU145 cells (**Figure 11C).**

To test effects on radiosensitivity, DU145 cells were seeded in 10 cm dishes for clonogenic assay. The following day, cells were pre-treated with inhibitors of AKT, IGF-1R or ATM, and after 1 hour treated with 0 – 10 Gy irradiation. After 10 days visible colonies were stained and counted, and results of the clonogenic assay are shown in **Figure 11C**. As predicted, ATM inhibition caused significant radiosensitization compared to solvent control-treated cells. There was also detectable radiosensitisation of cells pre-treated with IGF-1R or AKT inhibitors, and the effect was intermediate between solvent-treated and ATM inhibitor-treated cells (**Figure 11C**). While pre-treatment with the IGF-1R inhibitor AZ12253801 enhanced radiosensitivity following 8 Gy irradiation ($p < 0.006$, by one way ANOVA), the response at 2-6 Gy were not different from controls, and 2 way ANOVA indicated no significant difference in survival between controls and AZ12253801-treated cells. This was in contrast to the previous result shown in **Figure 6B**, where the same concentration (30 nM) of AZ12253801 had induced more marked radiosensitization. This may be a result of the change in dishes and seeding density between **Figure 6B** (10 cm 3000 cells per dish) and **Figure 11C** (6 cm with 1,000 cells per well). Subsequent work by others in the laboratory does support AZ12253801-induced radiosensitisation of DU145 cells (Chitnis *et al.*, in preparation). Therefore, if time had permitted it would have been preferable to repeat the clonogenic survival assay in 10 cm dishes in triplicate.

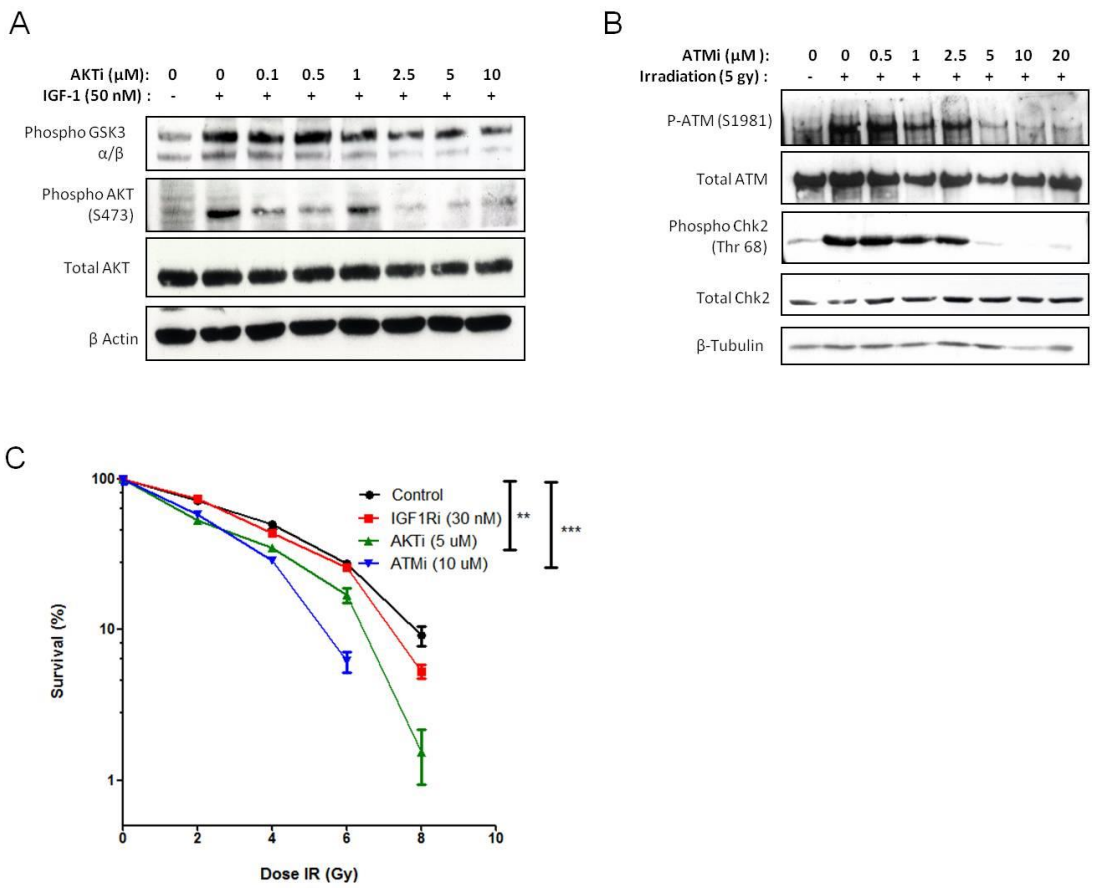


Figure 11: Effects of IGF-1R and AKT inhibition on radiosensitivity of DU145 cells

A) DU145 cells were serum starved for 24 hours and the following day were pre-treated with AKT inhibitor (AKTi) for 4 hours. In the final 30 minutes, cells were treated with IGF-1 (50 nM) and lysates were analysed by SDS-PAGE and immunoblotting. B) DU145 cells were pre-treated with inhibitor of ATM (ATMi) for 4 hours and in the final hour of pre-treatment irradiated (5 Gy). Phospho-ATM S1981 and phospho-Chk2 were suppressed at 5-20 μM. C) DU145 cells were pre-treated with inhibitors of ATM (ATMi), IGF-1R (IGF-1Ri) or AKT (AKTi) for 1hr, irradiated and after 10 days visible colonies were stained and counted. Graph shows clonogenic survival (% unirradiated), mean ± SEM of triplicate dishes. Similar results were obtained in a second independent experiment. Both AKTi and ATMi induced significant radiosensitisation compared with controls (** $p<0.01$, *** $p<0.001$ by 2 way ANOVA).

3.2.5 Assay for radio-resistant DNA synthesis

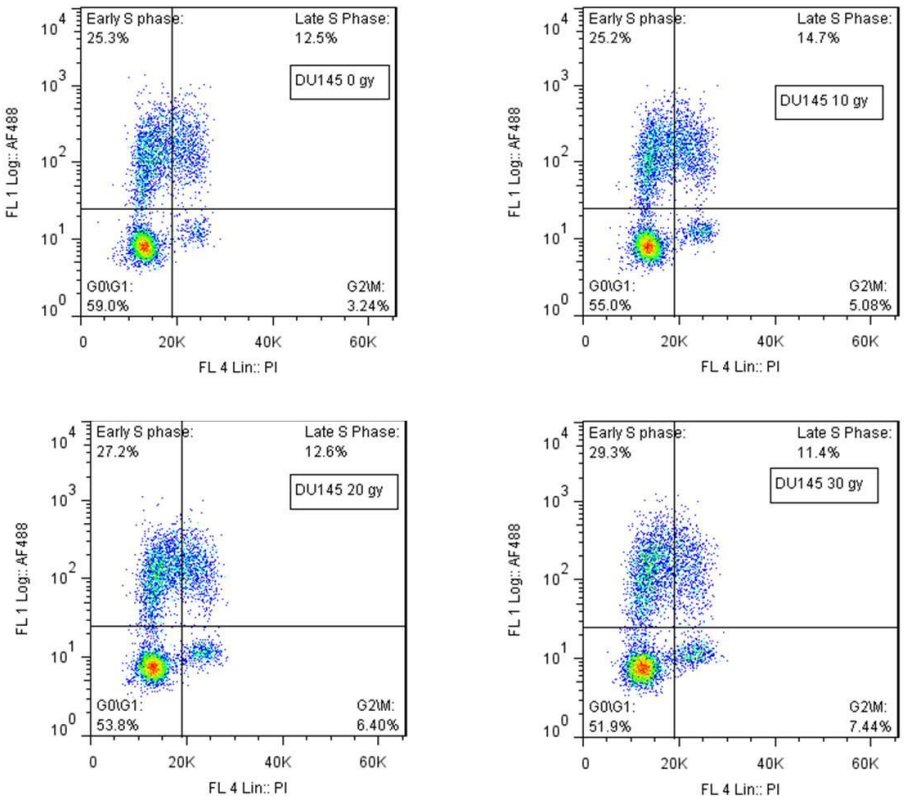
The demonstration of radiosensitisation following AKT inhibition does not imply an effect on damage sensing or core DNA repair processes, and could simply be a result of enhanced apoptosis. Therefore, assays that are more specific for ATM function were utilized, including effects on cell cycle progression and ATM-dependent phosphorylation of downstream effectors. After DNA damage, normal cells show a delay in cell cycle progression, allowing for either repair of damage or triggering programmed cell death (apoptosis). Failure of the intra-S-checkpoint is manifest by the inability of cells in S phase to prevent further DNA synthesis in response to ionising irradiation, a phenotype known as radio-resistant DNA synthesis (RDS) (Luo *et al.*, 2008). Activation of the intra-S-checkpoint is dependent on the proper function of ATM to activate many downstream mediators central to the DNA damage response (Lavin, 2008). Indeed the presence of RDS is a hallmark of cells harbouring defective ATM, and has also been observed in cells that lack functional NBS-1 (Luo *et al.*, 2008). In previous work from our group, radiosensitisation and RDS have been observed in murine melanoma cells in which IGF-1R was downregulated (Macaulay *et al.*, 2001).

The Bromodeoxyuridine (BrdU) incorporation assay was used to study cell cycle progression. BrdU is a synthetic thymidine analogue that can be incorporated into the DNA of dividing cells, and is detectable by flow cytometry using fluorescent antibodies. Before assessing the effect of IGF-1R or AKT inhibitors, assays were conducted to test for the predicted radiation-induced suppression of cells in late S phase (**Figure 12A**). However, cell cycle analysis revealed no change in the proportion of DU145 prostate cancer cells entering late S or G_2/M phase following IR

(**Figure 12B**). Compared to control unirradiated cells, increasing doses of IR appeared to cause little change in the cell cycle profile, with only modest reduction in G_1 and increase in G_2/M.

Repeated attempts were made to optimize the BrdU incorporation assay using conditions exactly as previously described, where the BrdU assay had been used to study ATM function in MCF7 breast cancer and LNCaP prostate cancer cells. In that report, control cells had shown reduction in S-phase fraction 1-1.5 hours after 10 Gy irradiation (Tsai *et al.*, 2008). However, in this project inhibition of cell cycle progression from early to late S phase was not observed one hour after irradiation of DU145 (**Figure 12**) or irradiated MCF7 cells (not shown). Experiments were also conducted by post-doctoral scientist Dr. Martin Kerr to assess whether evidence of the intra S-phase checkpoint was apparent 4 hours after irradiation of DU145 cells, but as here, there was no dose-dependent reduction in the S-phase fraction. Therefore, it did not prove possible to use this assay to study effects of IGF-1R or AKT inhibitors on ATM function.

A



B

Treatment	Proportion in Phase of Cell Cycle (%)				
Dose IR (gy)	G_0/G_1	Early S	Late S	Total S	G2/M
0	59.0	25.3	12.5	37.8	3.24
10	55.0	25.2	14.7	39.9	5.08
20	53.8	27.2	12.6	39.8	6.40
30	51.9	29.3	11.4	40.7	7.44

Figure 12: Cell Cycle distribution following irradiation of DU45 cells

A) DU145 cells were seeded at $1X10^6$ per 10 cm dish and the following day treated with 0-30 Gy of IR. Cells were incubated for 1 hour post IR and in the final 30 minutes were labelled with BrdU, before fixing and staining with anti-BrdU antibody for cell cycle analysis by FACS (according to 2.4.3.2). B) The table summarizes the cell cycle profile, shown as a percent of total cells in each phase.

3.2.5 Use of siRNA and inhibitors to study ATM dependent phosphorylation of downstream mediators

ATM plays a central role in the DSB response by phosphorylating many downstream proteins, and these events can be exploited to study ATM function. KRAB-associated protein 1 (KAP-1) is a nuclear protein that is phosphorylated in an ATM-dependent manner on serine 824. Following phosphorylation by ATM, KAP-1 is inhibited, leading to global chromatin decondensation (Goodarzi *et al.*, 2008). The phosphorylation of KAP-1 was assessed by western blotting following depletion of IGF-1R, AKT1, ATK2 or IRS-1. Cells transfected with control siRNA showed irradiation-induced phosphorylation of KAP-1 compared with unirradiated cells (**Figure 13A**). Both isoforms of *AKT* were effectively silenced, but irradiated cells showed no reduction in phosphorylation of KAP-1 compared with control cells. Similarly, silencing *IGF-1R* or *IRS-1* did not lead to any suppression of KAP-1 phosphorylation, although depletion of IRS-1 was suboptimal (**Figure 13A**).

In order to verify that KAP-1 phosphorylation was ATM dependent, the experiment was repeated using chemical inhibitors. DU145 cells were pre-treated with 5 μM AKTi, 10 μM ATMi, or 120 nM AZ12253801 for 1 hour, followed by irradiation. Solvent control-treated cells showed IR-induced phosphorylation of KAP-1 compared to unirradiated cells (**Figure 13B**). In cells pre-treated with ATM inhibitor there was clear attenuation of KAP-1 phosphorylation and also of ATM autophosphorylation on S1981. As in the gene silencing experiments (**Figure 13A**), pre-treatment with IGF-1R or AKT inhibitors did not result attenuate IR-induced phosphorylation of KAP-1 (**Figure 13B**).

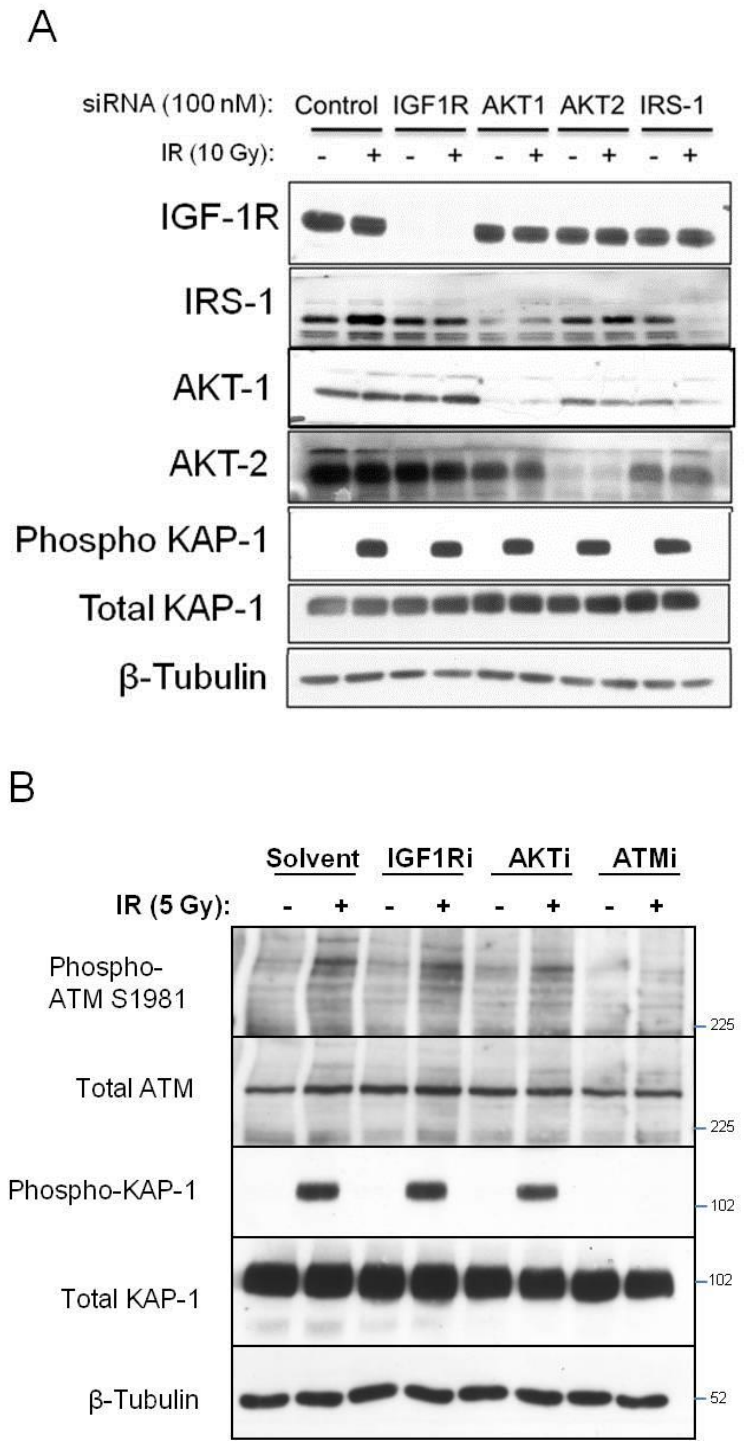


Figure 13: Effect of AKT and IGF-1R depletion or inhibition on downstream effectors of ATM

A) DU145 cells were siRNA-transfected and two days later were irradiated (10 Gy). After 1 hour lysates were analysed by SDS-PAGE and immunoblotted to asses KAP-1 phosphorylation on S824, and to check the efficiency of gene silencing. ATM dependent phosphorylation of KAP-1 was not inhibited in cells depleted of IGF-1R, IRS-1 or AKT1/2. b) DU145 cells were pre-treated with inhibitors of IGF-1R (IGF-1Ri = 120 nM), AKT (AKTi = 5 μM), or ATMi (10 μM) for 4 hours and in the final 1 hour were irradiated (5 Gy). One hour later, lysates were analysed by SDS-PAGE and immunoblotted for phosphorylation of KAP-1 on S824 and ATM on S1981.

3.3 Discussion

Previous work from our laboratory showed that IGF-1R downregulation is associated with enhanced radiosensitivity in B16 mouse melanoma cells (Macaulay *et al.*, 2001). In this report, IGF-1R downregulation demonstrated a reduced radiation-induced p53 accumulation and serine 18 phosphorylated p53; these effects were associated with impaired ATM kinase activity (Macaulay *et al.*, 2001). Subsequent work from our laboratory used pulsed-field gel electrophoresis and ɣH2AX focus formation to show that IGF-1R depletion sensitized DU145 and PC3 prostate cancer cells to ionizing radiation (Turney *et al.*, 2012). These findings, and experiments in MCF7 cells depleted of IGF axis components (**Figure 5**) led to the hypothesis that IGF-1R signalling can influence ATM activation and function via AKT. However, at the conclusion of the experiments presented in **Figure 13**, it was clear that there was inadequate support for the hypothesis that AKT may be required for the previously reported functions function of ATM in human prostate cancer cells. Furthermore there was no evidence that ATM was the IGF-sensitive 350 kDa phospho-protein detected by the Phospho-AKT substrate motif antibody. Several factors may contribute to the findings in the original work, that showed evidence for IGF-1R mediated effects on ATM (Macaulay *et al.*, 2001), while studies using IGF-1R depletion or inhibition in DU145 prostate cancer cells did not show the same effect. B16 melanoma cells express wild-type p53, and may be more readily prone to apoptosis upon IGF-1R downregulation. It is possible that ATM could have been a target of apoptotic cleavage, which generates a kinase-inactive ATM protein product (Smith *et al.*, 1999). In contrast, DU145 prostate cancer cells might be more resistant to apoptosis, as a result of their mutated p53 status (Isaacs *et al.*, 1991), and thus do not show this effect.

Several reports, including some from our group, indicate that IGF-1R depletion or inhibition radiosensitizes tumour cells (Isebaert *et al.*, 2011; Rochester *et al.*, 2005; Turney *et al.*, 2012; Yavari *et al.*, 2010). Similarly, published reports show that PI3K-AKT inhibition sensitizes human carcinomas to ionizing radiation (Fujiwara *et al.*, 2007; Kim *et al.*, 2005; Prevo *et al.*, 2008). However, the work presented here suggests that the effects of IGF-1R depletion or inhibition on radiosensitisation are not via effects on ATM in human prostate cancer cells. As a result, further work on this project has been stopped, and work on two new projects was taken on to reduce the risk should one of them fail. The work was completed in parallel however will be presented sequentially for clarity.

Chapter 4: Investigating the binding partners of nuclear IGF-1R

4.1 Introduction

In addition to being expressed on the cell membrane, many membrane RTKs have been shown to translocate to the nucleus, including fibroblast growth factor receptor (FGFR), insulin receptor and the epidermal growth factor receptor (EGFR) family (Massie and Mills, 2006; Wang *et al.*, 2010). Amongst these, nuclear translocation of EGFR is the most well characterised (Lin *et al.*, 2001). Functional studies of nuclear EGFR reveal a role in the transcription of genes involved in proliferation and cell cycle regulation (Lo and Hung, 2007). Nuclear EGFR has also been shown to interact directly with DNA-PK, involved in DNA damage repair by NHEJ (Dittmann *et al.*, 2005).

Recent work in our laboratory has shown that the IGF-1R is able to translocate to the nucleus of renal, breast and prostate cancer cells. Moreover, in renal cancer patients, high levels of nuclear IGF-1R were associated with poor survival (Aleksic *et al.*, 2010). IGF-1R was also identified in the nucleus of melanoma cells by Larsson's group (Sehat *et al.*, 2010).

In light of the multiple roles of nuclear EGFR, our laboratory is taking two different approaches to investigate the functional significance of nuclear IGF-1R. The first is to perform ChIP sequencing to identify DNA sequences that are directly or indirectly bound to IGF-1R. This may identify a role for nuclear IGF-1R in direct regulation of transcription. This project is being carried out by Dr. Aleksic, Post-doctoral scientist

in our laboratory, in collaboration with Professor David Neal's group in Cambridge. The second approach is to study the function of nuclear IGF-1R using mass spectrometry to identify interacting protein complexes. This approach may lead to the identification of partners of IGF-1R that facilitate putative roles in transcription, DNA repair or other functions as yet unidentified. The mass spectrometry is being conducted in collaboration with Dr. Garth Hamilton and Dr. Eric O'Neill (Department of Oncology, Oxford University).

4.2 Results

4.2.1 Immunoprecipitation of nuclear IGF-1R

Prior to our group's publication of nuclear IGF-1R import (Aleksic *et al.*, 2010), work from our laboratory had tested multiple different fractionation methods before identification of reagents in the Nuclear Extraction Kit (Panomics) as providing the best separation of membrane, cytoplasmic and nuclear components. Briefly, this method involved disruption of the cell membrane in hypotonic buffer A, and release of nuclear proteins with detergent and high salt buffer B (Aleksic et al 2010). The composition of these buffers was unknown. For this project, to ensure proper lysis and preserve any potential nuclear interactions, buffer B from the Panomics kit was replaced on the advice of Dr. O'Neill by a nuclear lysis buffer (NLB) containing 1% NP-40, 20 mM Hepes pH 7.5, 0.5 mM EDTA, 300 mM NaCl, 100 mM NaF, 10 mM β-glycerophosphate and 1 mM sodium orthovanadate, protease inhibitor cocktail (Roche), Pefabloc (Roche), and phosphatase inhibitor cocktail I and II (Sigma). The high salt content (300 mM NaCl) was suggested by Dr. O'Neill to reduce nonspecific interactions, although it was recognized that this could also reduce the chances of detecting weaker specific interactions. It was also important to consider that IGF-1R protein localized to the plasma membrane, ER and Golgi, and the ER and Golgi networks are in close proximity to the nucleus; indeed, a reticular network, the so-called nucleoplasmic reticulum, is continuous with the ER and nuclear envelope (Adams *et al.*, 2000; Echevarria *et al.*, 2003). Given that the purpose of this work was to identify novel binding partners of nuclear IGF-1R, it was important to find a fractionation method that would preserve the integrity of the nucleus, while reducing the amount of contaminating plasma membrane, Golgi, and ER.

Initial experiments assessed the performance of the Panomics buffer A to generate a non-nuclear fraction, followed by nuclear lysis in NLB. Nuclear and cytoplasmic fractions were immunoblotted for IGF-1R and markers of different subcellular components: Golgi network (golgin-84), ER (calnexin), membrane marker (sodium/potassium ATPase) and nuclear envelope marker (Lamin A). There was clear enrichment of Lamin A, but detectable Golgi and ER components in these nuclear extracts (**Figure 14A**). To reduce ER and Golgi contamination, a washing step was added using NLB without detergent, to avoid premature lysis of nuclei, and washing nuclei once before lysis in NLB. Immunoblotting for Na^+/K^+ ATPase indicated that the nuclear washing step reduced membrane contamination to almost undetectable levels, and furthermore, there was a clear reduction in golgin-84 and a minor reduction in calnexin in washed nuclei (**Figure 14A**). The washing step did reduce the yield of IGF-1R protein, but given the clear evidence of reduced contamination by other subcellular fractions, this step was used to prepare nuclear extracts for optimization of IP prior to mass spectrometry.

To check the efficiency of IGF-1R immunoprecipitation (IP) from nuclear lysates, DU145 cells were fractionated by swelling in buffer A (Panomics), and nuclei were washed as above and lysed in NLB. Nuclear extracts were used to IP IGF-1R using Cell Signalling (#3027) antibody that recognizes the IGF-1R beta subunit (**Figure 14B**). In addition, whole cell extracts were prepared by lysing DU145 cells in NLB, serving as a positive control for IGF-1R IP (**Figure 14B**). The results showed that IGF-1R was successfully precipitated from both nuclear and whole cell extracts (**Figure 14B**). Supernatant from the IP was also analysed by western blotting to check IGF-1R immunodepletion. Immunoblotting of cell lysates detected 98 kDa IGF-1R β subunit in nuclear lysates and whole cell extracts, and also showed a series of small products in nuclear extracts that were not present in cytoplasmic

fractions or WCE. These products were also present in the IP supernatant of the nuclear fraction, and it appeared that only the 98 kDa band had been depleted by IP (**Figure 14B**). McElroy et al. suggested that IGF-1R may be a substrate for γ-secretase cleavage, generating products of approximately 52 kDa (McElroy *et al.*, 2007) which may account for the smaller products observed. However, experiments using siRNA mediated depletion of IGF-1R showed that IGF-1R knockdown depleted the 98 kDa product and not the smaller products (unpublished data, Dr. Tamara Aleksic, University of Oxford). This suggests that the bands detected at ~52-76 kDa on western blotting of nuclear extracts are unlikely to be products of the *IGF-1R* gene, and may be cross reacting proteins in nuclear extracts.

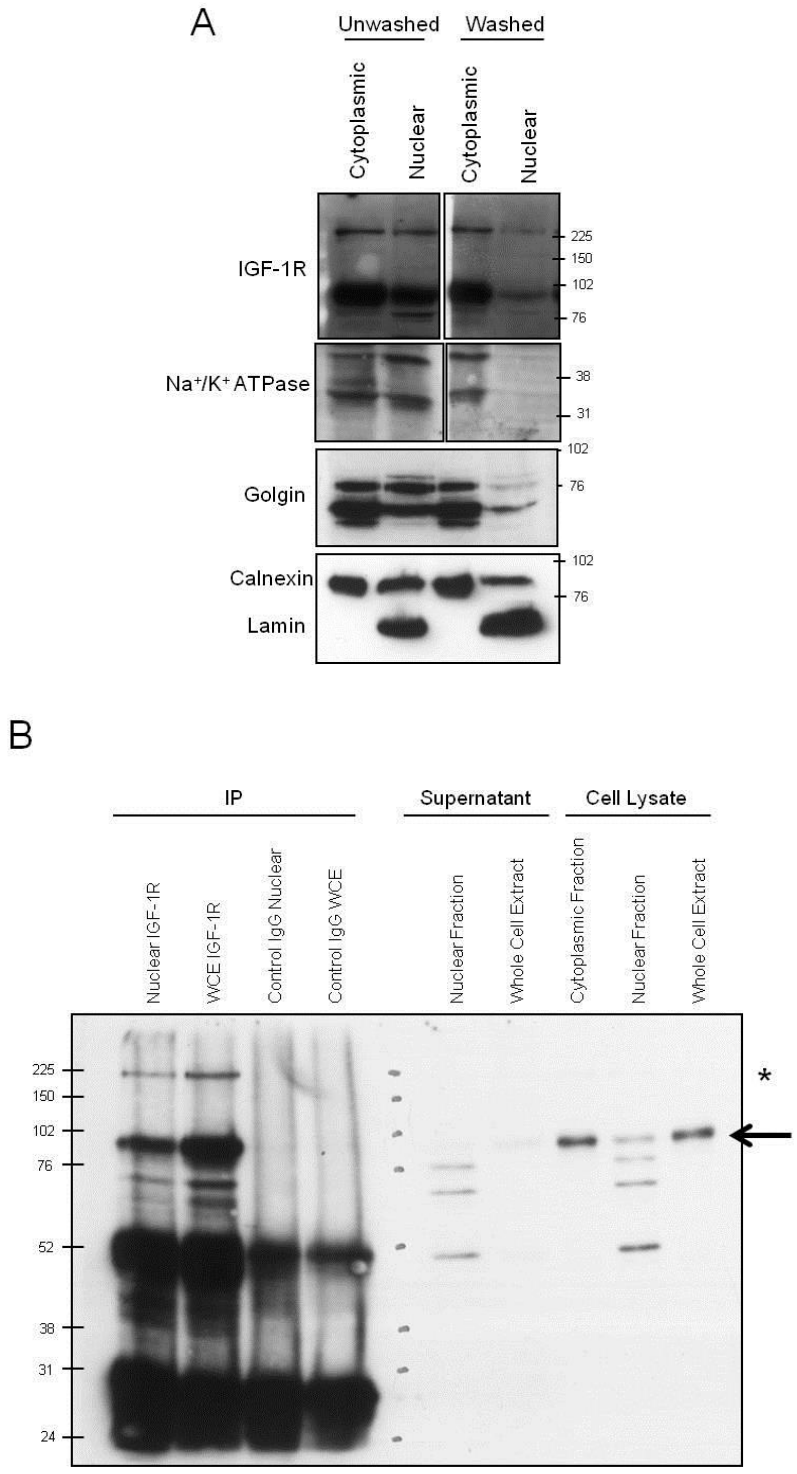


Figure 14: Immunoprecipitation of nuclear IGF-1R

A) DU145 nuclear extracts were prepared using Panomics buffer A, with the additional step of washing nuclei once in NLB without detergent. Lysates were analysed by SDS-PAGE and immunoblotted for IGF-1R, Golgin-84, Calnexin, Lamin A, and Sodium-Potassium ATPase (Na^+/K^+ ATPase). B) Washed DU145 nuclei were lysed and prepared as in A. Immunoprecipitates of nuclear IGF-1R or control irrelevant antibody (rabbit IgG) were analysed by SDS-PAGE and immunoblotted for IGF-1R. In parallel, whole cell extracts (WCE) were used as a positive control, and were immunoprecipitated with IGF-1R or control antibody as for nuclear extracts. Arrow indicates a 98 kDa protein that migrates at the same electrophoretic mobility as IGF-1R β subunit. *, 220 kDa IGF-1R proreceptor.

4.2.2 Initial MS analysis

Using the conditions optimized in 4.2.1, an initial large scale IP was performed to identify potential binding partners of nuclear IGF-1R in DU145 prostate cancer cells growing in complete medium. For this analysis, 25 milligrams of nuclear extracts were prepared using Panomics kit buffer A followed by a single wash using NLB buffer without detergent, and finally lysis in NLB. Following a pre-clearing step using 25 µg of random IgGs and protein A agarose beads, nuclear IGF-1R was immunoprecipitated using 10 µg of IGF-1R antibody or control irrelevant rabbit IgG. As a control for immunoprecipitation, IGF-1R was also immunoprecipitated from 11 milligrams of whole cell extract created by lysing DU145 cells in NLB directly.

Prior to MS analysis, 2% of each IP was western blotted to check that IGF-1R had been successfully immunoprecipitated (**Figure 15A**). The remaining IP samples were separated by electrophoretic mobility on a 10% Bis-Tris gel and stained with colloidal Coomassie blue according to the method described in section 2.5.2. **Figure 15B** shows a scanned image of the stained gel. There were many visible bands in both IGF-1R and control IPs. A band of ~98 kDa could not be detected in IGF-1R IPs, although there were several bands in the lower part of the gel (~40-50 kDa) that appeared to be enriched in IGF-1R compared to control IPs from nuclear extract. Boxes indicate regions of the gel that were excised for MS analysis. For each region that was removed from the nuclear IGF-1R IP, a corresponding region was excised from the control IP for comparison. Additionally, regions of the gel (bands 12-15) were excised from IGF-1R and control IPs at ~100 kDa, which corresponds to the predicted migration of the IGF-1R beta subunit. Gel pieces were prepared by in gel digest (according to 2.5.2) and ZipTip purification (2.5.4), and samples were analysed by Dr. Garth Hamilton (University of Oxford, Oxford) using an ultra performance liquid chromatography-mass spectrometry (UPLC-MS/MS) Nano-

UPLC-MS/MS tandem mass spectrometer (Nano-Acquity, QTOFpremier, Waters). To reduce contamination, samples from the nuclear control IP were analysed first, followed by a series of washing steps with serial dilutions of acetonitrile (100%, 50% and 30% ACN) prior to analysis of peptides derived from the nuclear IGF-1R IP.

Analysis of IPs from whole cell extracts showed that the IGF-1R beta subunit was detected at ~100kDa in the IGF-1R IP (band 14) but not the control IP (band 15) (**Figure 15B**). Although detectable in western blots of the same IPs (**Figure 15A**), the IGF-1R itself was not identified by MS in the IGF-1R IP from nuclear extract (band 12). This could be due to the low yield of immunoprecipitated IGF-1R, or possibly due to the abundance of other proteins in this region, including trypsin and keratin contaminants. In both nuclear IGF-1R and nuclear control IP, the IgG heavy and light chains were identified in bands 1, 10, 4 and 16 respectively. Although bands 2 and 3 appeared to have IGF specific bands, these proved to contain mainly cellular contaminants such as actin and extracellular contaminants such as cytokeratins.

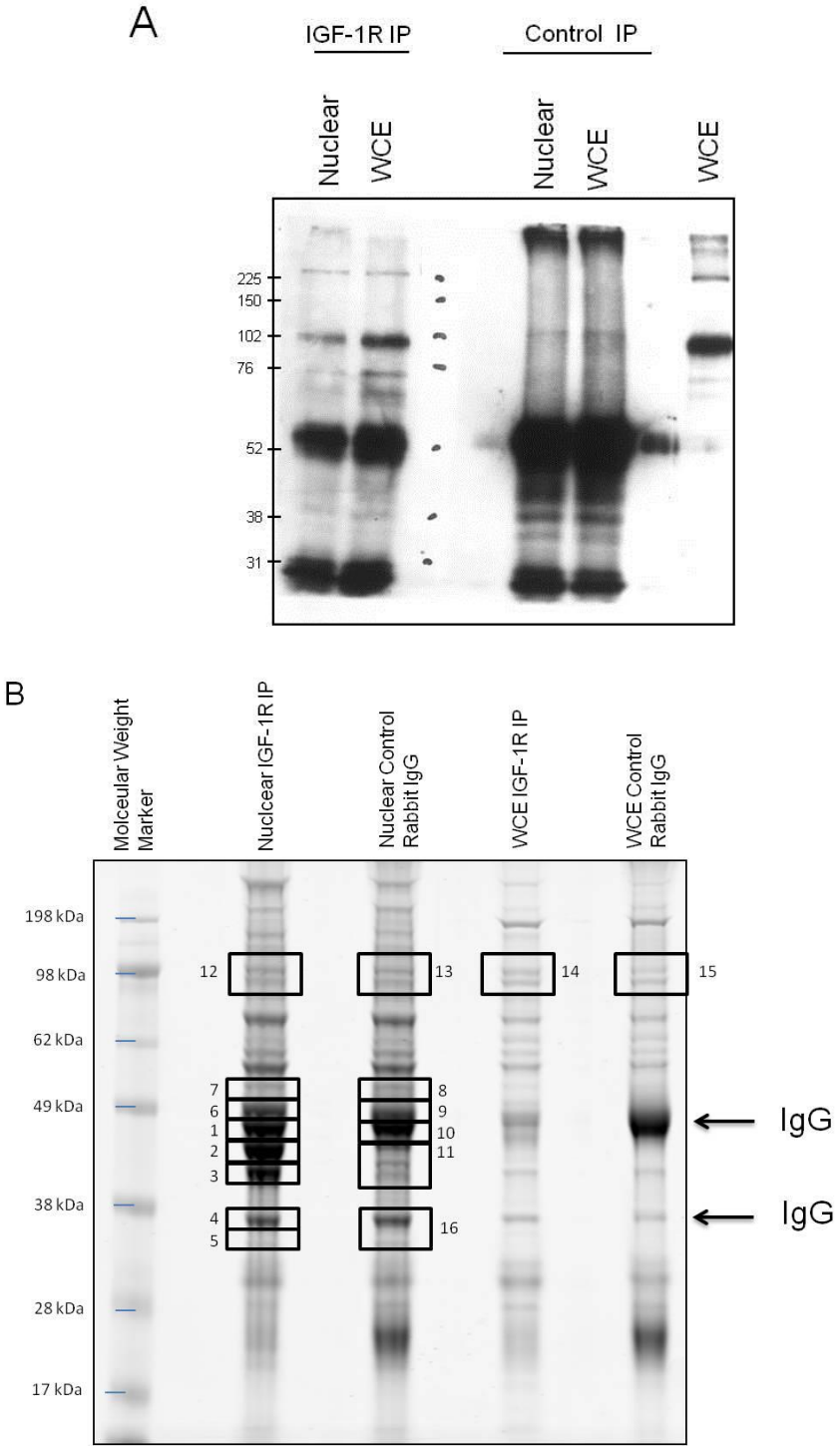


Figure 15: Analysis of large-scale IGF-1R IPs

A) DU145 nuclear extracts were prepared as described in section 4.2.2. Two percent of immunoprecipitates using IGF-1R or control antibodies were analysed by SDS-PAGE and immunoblotted for IGF-1R. IPs of whole cell extracts (WCE) were used as a positive control. B) Remaining IP samples were separated by SDS-PAGE. Boxes indicate regions of the gel that were excised for mass spectrometry analysis.

Table 7 shows proteins identified at approximately 100 kDa in IGF-1R and control IPs from DU145 nuclear extracts. Those highlighted in yellow were specific to IPs using the IGF-1R antibody. Of the top 14 isolates from band 12 of the nuclear IGF-1R IP, ten were also identified in the nuclear control IP (band 13) and were considered non-specific. The top hit in terms of peptide coverage was Bruton Tyrosine Kinase Associated Protein 135 (BAP-135), also known at General Transcription Factor II-I (TF II-I), from which 23 separate peptide sequences were detected by mass spectrometry as shown in **Figure 16**. Four TFII-I peptides were also detected in the control IP. However, these peptide sequences were shorter (7-15 amino acids) and overlapped with peptide sequences detected in the nuclear IGF-1R IP. This might be due to the fact that the same scalpel was used to excise bands 12 and 13. However, the relatively high peptide coverage identified in the IGF-1R IP, and the paucity of TF II-I peptides in the control IP, suggest that TF II-I may be a genuine IGF-1R interacting protein.

Another protein identified in band 12 was Rho Guanine Nucleotide Exchange Factor 12 (**Table 7)**. A previous report has linked a member of the Rho Guanine nucleotide exchange factor family to the IGF-1R beta subunit (Taya *et al.*, 2001). Leukaemia-associated Rho guanine nucleotide exchange factor (LARG) has been shown to bind directly to the carboxy terminus of the IGF-1R beta subunit, and plays a role in the IGF-induced activation of Rho/Rho-kinase pathway, thereby regulating cytoskeletal rearrangements (Taya *et al.*, 2001).

The identification of RNA Polymerase II Subunit B1 CTD Phosphatase, also known as RNA polymerase II-associated protein, (RPAP2) suggests that nuclear IGF-1R may have transcriptional role (**Table 7**). RPAP2 is a phosphatase that directly interacts with the carboxy-terminal domain (CTD) of RNA Pol II that is

phosphorylated on Ser7. This interaction leads to the dephosphorylation of Pol II on Ser5 (Egloff *et al.*, 2012). The phosphorylation of RNA Pol II on Ser5 is reported to play a role in promoter clearance (Buratowski, 2009). The identification of a RNA pol II interacting protein is of interest given the co-localization shown by immunofluorescence between nuclear IGF-1R and RNA pol II in the report from our group of nuclear IGF-1R translocation (Aleksic *et al.*, 2010).

Band 12 (# of peptides)	Band 13
Bruton Tyrosine Kinase Associated Protein 135 (23)	Leucine-rich PPR motif-containing protein
Keratin Type II Cytoskeletal - 7	Ig gamma chain C region
Keratin Type II Cytoskeletal - 1	Keratin Type II Cytoskeletal - 1
Rho Guanine Nucleotide Exchange Factor 12 (3)	Keratin Type 1 Cytoskeletal - 10
AT-rich interactive domain-contatining protein (1)	Ig kappa-b4 chain C region
Keratin Type II Cytoskeletal - 8	Transcription elongation regulator 1
SWI/SNF complex subunit SMARCC2	SWI/SNF complex subunit SMARCC2
Keratin Type 1 Cytoskeletal - 9	Keratin Type 1 Cytoskeletal - 9
Trypsin	Trypsin
Serum Albumin	Serum Albumin
Keratin Type 1 Cytoskeletal - 18	General transcription factor II-I
Keratin Type 1 Cytoskeletal - 75	
Plectin	
RNA Polymerase II Subunit B1 CTD Phosphatase Rpap2 (1)	

Table 7: Proteins identified in IGF-1R (Band 12) and control (Band 13) immunoprecipitates.

Table shows proteins identified by MS analysis of band 12 from Figure 15. Proteins highlighted in yellow are specific to nuclear IGF-1R immunoprecipitation. Numbers in parentheses indicate number of peptides identified..



Figure 16: Amino acid sequence of Bruton tyrosine kinase associated protein 135 (BAP-135)

Sequences in red indicate peptide fragments identified by mass spectrometry from band 12 (IGF-1R IP). Sequences underlined indicate peptide fragments identified from band 13 (control IP).

4.2.3 Further optimization of nuclear IGF-1R extraction and immunoprecipitation

The first MS analysis had been performed on nuclear proteins extracted using commercial reagents (Panomics). Despite using 25 mg of nuclear extract, the IGF-1R beta subunit had not been detected by MS analysis (**Figure 15, Table 7**). The composition of the Panomics buffers was unknown, although it was suspected that the hypotonic buffer A contained detergent, because of frothing on pipetting. Therefore, it was decided to use an alternative buffer of known composition. The next experiments used in-house hypotonic buffer [10 mM Tris-Cl (pH 7.5), 10 mM KCl, 1 mM EDTA, 1 mM EGTA, 2 mM $MgCl_2$, supplemented with 1 mM DTT, EDTA-free protease inhibitor cocktail, 1.5 mM Pefabloc SC Plus]. The aim was to further optimize nuclear fractionation, in order to increase the nuclear IGF-1R yield and the chance of identifying the IGF-1R beta subunit by MS. Fractionation using the hypotonic buffer was performed as described in section 2.2.2. Briefly, cells were

allowed to swell in hypotonic lysis buffer for 10 minutes before douncing 20 times in a pre-chilled tight fitting Dounce tissue homogenizer. A sample was then checked with trypan blue, and if necessary the douncing was repeated until greater than 99% of cell membranes were disrupted. Nuclei were pelleted, 1 mL of the non-nuclear fraction was saved for immunoblotting and nuclei were lysed in NLB.

As before (**Figure 14A**), the efficiency of fractionation was assessed by immublotting for components of different subcellular fractions. **Figure 17** compares the fractionation using the Panomics buffer A with in-house hypotonic lysis buffer. Immunoblotting for the plasma membrane marker Na^+/K^+ ATPase indicated that membrane proteins were present in the non-nuclear fraction extracted by both the hypotonic lysis buffer and the Panomics. In the nuclear extracts the level of Na+/K+ ATPase was reduced to a greater extent with the Panomics kit fractionation method and to a lesser extent with the hypotonic lysis buffer (**Figure 17**). There were detectable Golgi and ER components in nuclear extracts from both the Panomics and hypotonic lysis buffer. However, similar to the membrane marker, the levels of Golgi and ER were reduced to a greater extent by the Panomics method compared with to the in-house hypotonic lysis buffer (**Figure 17**). In addition, the different fractionation methods showed different levels of nuclear IGF-1R. Fractionations using the Panomics kit buffer A produced equal levels of IGF-1R between the WCE and the non-nuclear fraction, with low levels detectable in the nuclear fraction (**Figure 17**). Using the hypotonic lysis buffer there was little IGF-1R detectable in the 'non-nuclear' fraction, but this might be due to absence of detergent in the hypotonic lysis buffer. It was notable that extraction using in-house hypotonic and NLB buffers generated nuclear extracts that contained higher levels of IGF-1R than extracts created after hypotonic swelling in Panomics buffer A (**Figure 17**). The retained amounts of IGF-1R in the non-nuclear and nuclear extracts prepared with in-house buffers was

comparable to the relative distribution of IGF-1R in the DU145 cells previously shown by immunofluorescence (Aleksic *et al.*, 2010). This led to the speculation that detergent in Panomics buffer A might be causing premature nuclear lysis.

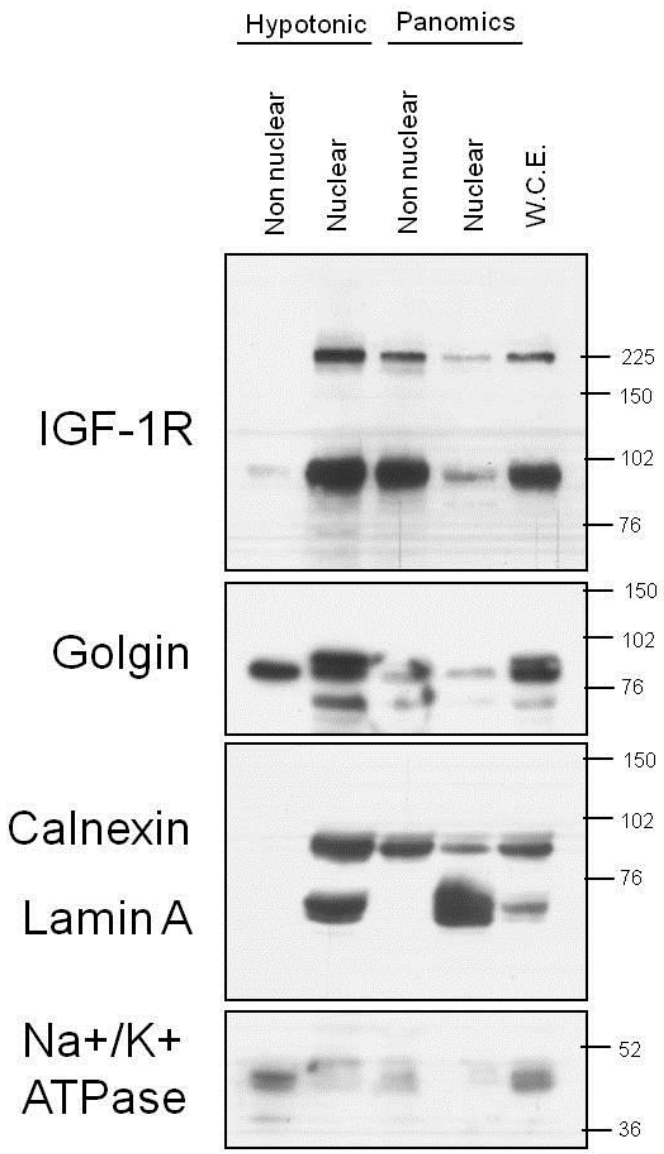


Figure 17: Nuclear fractionation

DU145 were cells were fractionated using either hypotonic lysis buffer or Panomics buffer A followed by final lysis of nuclei in NLB Equivalent amounts of protein were subjected to western blotting to assess fractionation, in parallel with a sample of whole cell extract (WCE).

In an attempt to reduce ER and Golgi contamination of nuclear extracts prepared using in-house buffers, a washing step was added prior to nuclear lysis. This step used NLB replacing the 1% NP-40 with 0.1% Tween-20, to minimize premature nuclear lysis. In addition to the markers of fractionation previously used, further markers of cytoplasm (MEK1/2) and nucleoplasm (KAP-1) were added. KAP-1 is a nuclear protein that upon phosphorylation by ATM leads to global chromatin decondensation (Goodarzi *et al.*, 2008). Therefore, KAP-1 was used as a fractionation marker, to identify whether either Buffer A of the Panomics kit or the in-house hypotonic method was prematurely lysing nuclei.

Figure 18 shows western blotting results comparing different methods of washing nuclei following disruption of the cell membrane with either the Panomics kit Buffer A or hypotonic lysis buffer. Two different methods of washing and purifying nuclei were used following in-house hypotonic lysis buffer: the first involved washing the nuclei three times with NLB replacing the 1% NP-40 with 0.1% Tween-20. The second method used a sucrose gradient, performed as described in section 2.2.2, and involved centrifugation of nuclei through increasing concentrations of sucrose (0.25 M, 0.35 M and finally 0.88 M) (Desjardins *et al.*, 1963).

The original method using Panomics buffer A, with three washes of the nuclear pellet, generated a nuclear extract with good enrichment of the nuclear envelope marker Lamin A, and the lowest level of contaminating plasma membrane, Golgi, and ER contaminants. However, there was negligible IGF-1R remaining in nuclear extracts, and blotting for KAP-1 supported speculation that nucleoplasmic proteins were being extracted by hypotonic (and detergent-containing) Panomics buffer A.

Nuclear pellets generated after swelling and douncing in in-house hypotonic buffer were purified by sucrose gradient or washing in 0.1% Tween 20. The sucrose gradient method, despite have been used for many years to prepare nuclei (Desjardins *et al.*, 1963; Vaseva and Moll, 2012), generated 'nuclear' extracts with slight reduction in cytosolic (MEK 1/2) and Golgi (Golgin-84) content, but was otherwise very similar to whole cell extract. The presence of significant plasma membrane contaminants suggests that this would not be a suitable method for identification of nuclear IGF-1R binding partners.

The in-house hypotonic buffer did not contain detergent, and did not extract nucleoplasmic contaminants (KAP-1) into the 'non-nuclear' fraction. After three washes in 0.1% Tween-20, the resultant nuclear extracts contained negligible Na^+/K^+ ATPase, and reduced levels of MEK 1/2 and Golgin. Given the close relationship of the ER and nucleus (Echevarria *et al.*, 2003) it was not unexpected to see ER contamination, but this cellular compartment contains uncleaved IGF-1R proreceptor, which can be differentiated by size from mature IGF-1R subunits.

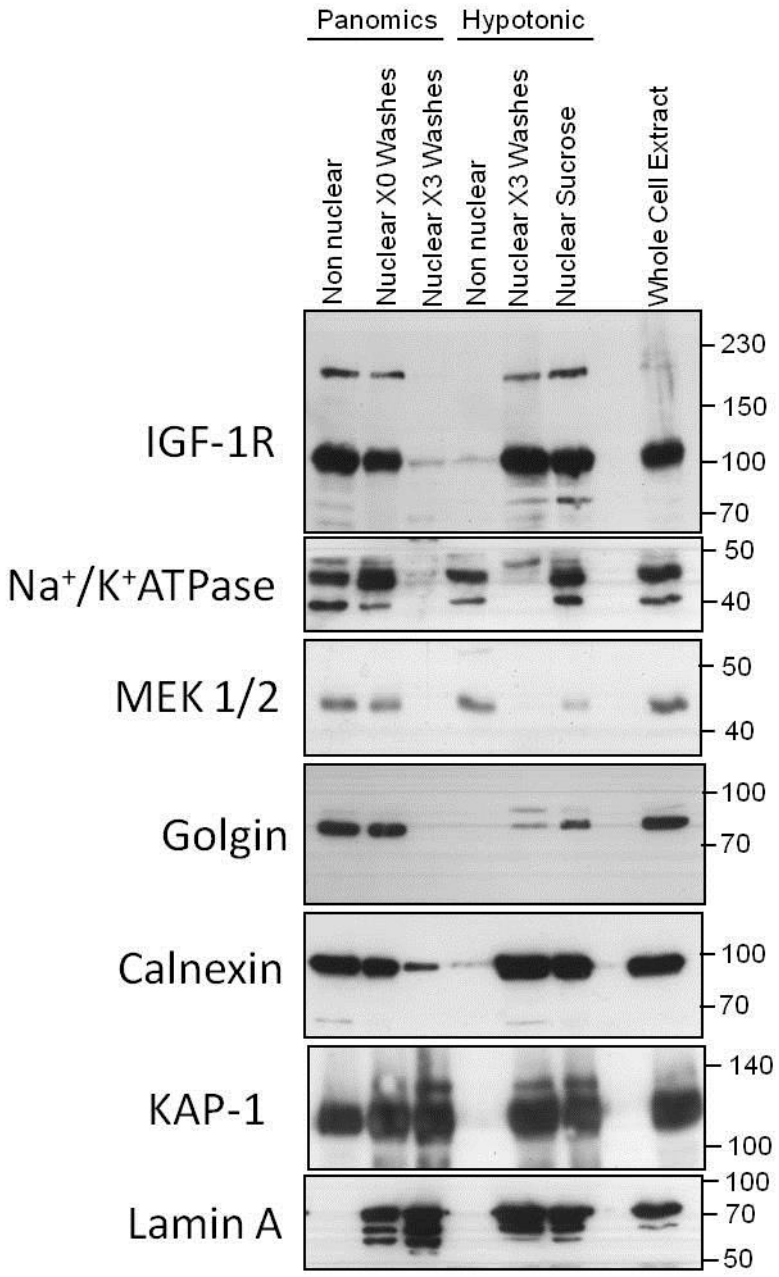


Figure 18: Optimisation of nuclear extraction by different washing methods
DU145 cells were fractionated by i) swelling in Panomics buffer A (hypotonic buffer with detergent), pelleted nuclei were either unwashed or washed three times with NLB buffer containing 150 mM NaCl and 0.1% Tween-20 and lysed in NLB; ii) swelling in detergent free hypotonic buffer, douncing, and pelleted nuclei were washed 3 times with NLB containing 150 mM NaCl and 0.1% Tween 20 or centrifuged through a sucrose gradient (0.25, 0.33, 0.8 M sucrose), finally nuclei were lysed in NLB. Extracts were separated by SDS-PAGE and immunoblotted for IGF-1R, Golgin (Golgi marker), calnexin (ER), Lamin A (nuclear envelope), KAP-1 (nucleoplasm), MEK1/2 (cytosol), and Na+/K+ ATPase (plasma membrane). Similar results were obtained from independently prepared extracts using the Panomics reagents (n = 3), hypotonic with washes (n = 4) and sucrose gradient (n = 3).

Following this analysis, it was decided to repeat the MS using the selected extraction method using in-house hypotonic buffer, Tween-20 washes and lysis in NLB. In addition to producing the best separation of nuclear and non-nuclear components, this method was advantageous in that it was cheaper that commercial reagents to scale up. This second MS analysis had two main objectives: 1) to test whether the newly optimized conditions allowed for detection of the IGF-1R beta subunit by MS and 2) to reduce the number of nonspecific proteins in the control immunoprecipitation. With this second aim in mind, the conditions for washing co-immunoprecipitated proteins were changed at the suggestion of Dr. Garth Hamilton (Department of Oncology, Oxford). In the previous MS analysis, co-precipitated proteins were washed three times by adding 1 mL of NLB and gently inverting the tube 3-5 times. To provide a more stringent wash, 1 mL of NLB was added and immunoprecipitates were incubated on a rotating wheel for 5 minutes at 4^{o}C, and this was repeated for a total of five washes (as in 2.2.6).

DU145 prostate cancer cells were cultured in complete medium, and were fractionated to generate two aliquots of 5 mg nuclear extracts, for immunoprecipitation using IGF-1R or control antibodies. Co-immunoprecipitated proteins were washed 5 times as described above and were separated by electrophoretic mobility on a 10% Bis-Tris gel. **Figure 19A** shows a scanned image of the stained gel. **Figure 19B** shows the stain gel with boxes to indicate regions of the gel that were excised for MS analysis. As before, for each region removed from the nuclear IGF-1R lane, a corresponding region was excised from the control IP lane for analysis (**Figure 19B**). It was clear that the increasing duration of IP washes had reduced the number of non-specific proteins in the control IP, and perhaps the use of lower amount of input (5 mg vs 25 mg in the first MS **Figure 15**) had also contributed (**Figure 19**). Bands 1 and 13 contained the light chains and the heavy

chains were identified in bands 6 and 18 (**Figure 19**). Between the light and heavy chains of both the nuclear IGF-1R IP and Control IP, no bands were detected by colloidal Coomassie staining or by MS analysis.

The stained gel showed a band in box 9 that migrated at the predicted electrophoretic mobility of the IGF-1R beta subunit at approximately 98 kDa (**Figure 19B**), and this band was not present in control IP (box 21 of **Figure 19B**). By MS analysis this was confirmed to be the IGF-1R beta subunit. Nuclear IGF-1R immunoprecipitates also contained two bands at ~120-200 kDa (box 10) that were not present in the control IP (box 22, **Figure 19B**). The smaller of the two bands corresponds to the predicted electrophoretic mobility of IGF-1R alpha subunit at approximately 135 kDa (**Figure 14**), and this was confirmed by MS analysis. The band at approximately 170 kDa was identified by MS as cytokeratin contamination, most likely introduced after the band was excised from the gel. Boxed regions 7, 8, 12, 19, 20, 24 also contained keratin and trypsin contaminants (**Figure 19B**).

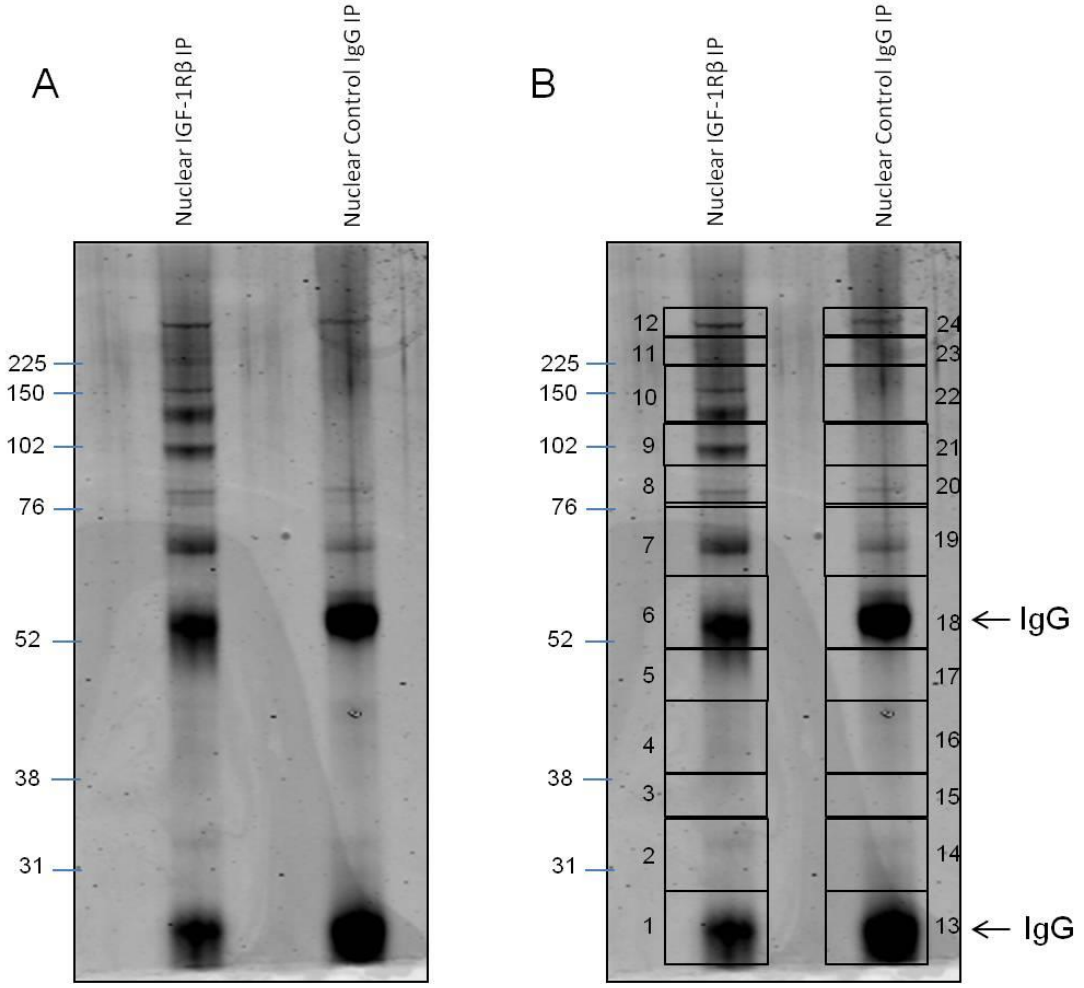


Figure 19: Nuclear IGF-1R IP using in-house washing and lysis buffers

DU145 cells were cultured in complete medium, disaggregated using 3 mM EDTA in PBS, pelleted and swelled in detergent free hypotonic lysis buffer. After douncing, nuclei were pelleted and washed three times with NLB with 0.1% Tween 20. IGF-1R and control immunoprecipitates were performed from 5 mg of nuclear extract and immunoprecipitated proteins were separated by electrophoretic mobility. Boxes indicate regions of the gel that were removed for mass spectrometry analysis.

4.2.4 Identification of potential IGF-1 ligand induced nuclear IGF-1R binding partners

The above described method allowed for immunoprecipitation of IGF-1R from extracts enriched for nuclear components while not prematurely lysing nuclei. Increasing the washes decreased the non-pecific co-precipitation of proteins in control IPs, as can be seen from a comparison of the control IP lanes of **Figure 15B** and **Figure 19A**. Furthermore, using these conditions, the IGF-1R beta and alpha subunits were detectable by MS analysis, suggesting that this method was appropriate for further analysis.

Previous work from our laboratory showing the presence of the IGF-1R in the nucleus had identified that prior to endocytosis, the recptor undergoes IGF-induced IGF-1R kinase activation and internalisation prior to nuclear IGF-1R translocation (Aleksic *et al.*, 2010). Specifically, it was shown that the IGF receptor translocated to the nucleus 15-60 minutes after stimulation with 30-50 nmol/L IGF-1 (Aleksic *et al.*, 2010). This relatively rapid time course of receptor internalization and nuclear import is in accord with the kinetics of EGFR nuclear translocation (Lin *et al.*, 2001). Sehat *et al.* also reported that IGF-1R localizes to the nucleus of melanoma cells although this was found to occur 6-8 hours following IGF-treatment and requiring IGF-1R SUMOylation (Sehat *et al.*, 2010).

Therefore, it appears that, as with other receptor tyrosine kinases (Wang *et al.*, 2010), receptor activation provides the physiological stimulus to nuclear translocation. To investigate the significance of IGF-1 induced translocation for IGF-1R binding partners, an MS analysis was performed comparing IGF-1R immunoprecipitated from IGF-1 treated cells to serum starved cells. Initially, DU145 prostate cancer cells were cultured in complete medium to approximately 60%

confluence. Cells were serum starved for 24 hours, before being treated with 50 nmol/L IGF-1 or solvent for one hour. Cells were collected and nuclear extracts were prepared using the optimized protocol developed as above (section 4.2.3). Fractionation was assessed by immunoblotting nuclear and non-nuclear extracts for markers of plasma membrane, Golgi, and ER (**Figure 20A**). In both starved and IGF-1 stimulated fractions, the level of plasma membrane marker Na+/K+ ATPase was clearly reduced in nuclear extracts compared with non-nuclear extracts, although both extracts contained detectable levels of ER and Golgi markers (**Figure 20A**). It was noted that immunoblotting for Golgin-84 showed a different pattern in extracts from control and IGF-treated cells, although the reason for this is unclear. IGF-1R or control IPs were performed from 12 milligrams of pre-cleared nuclear extract from starved or IGF-stimulated cells. Immunoprecipitates were collected with protein A agrose beads and washed five times for five minutes with NLB. On the advice of Dr. Eric O'Neill and Dr. Garth Hamilton, separation by SDS-PAGE was omitted, and precipitated proteins were subjected to in-solution digest, as a method of reducing contamination by keratin and cytokeratin. Therefore, after completion of IP washes, co-precipitated proteins were acid eluted from the beads using 125 mM Glycine (pH 2.5), neutralized using 10 mM Tris-Cl (pH 7.5) and concentrated using Amicon 10 kDa filters (as in section 2.2.6).

Prior to MS analysis, 2% of each IP was western blotted to check that IGF-1R had been successfully immunoprecipitated from serum starved and IGF-1 treated nuclear extracts (**Figure 20B**). In solution digestion was performed as described in section 2.5.3. Briefly, this involved reducing and blocking disulfide bonds with 200 mM DTT and 200 mM iodoacetamide, respectively, before overnight digestion with 0.2 µg/µL trypsin at 37^{o}C. On the following day, digestion was stopped with 1 µL of TFA, samples were dried down in a vacuum centrifuge, reuspended in 20 µL of buffer A

[2% acetic acid and 0.1% formic acid], ZipTip purified (section 2.5.4) and MS analyzed by Dr. Garth Hamilton.

Results from the MS analysis are listed in **Table 8**. IGF-1R alpha and beta subunits were detected in IGF-1R immunoprecipitates from serum-starved and IGF-1 treated nuclear extracts. Despite omission of SDS-PAGE and the associated manipulation of gel fragments, cytokeratin, keratin, and trypsin were detected in both control (serum-starved) and IGF-1 treated immunoprecipitates. Specific to the nuclear IGF-1R immunoprecipitates from serum-starved cells were two proteins: PI3K subunit alpha and centrosomal protein KIAA1731 homolog (highlighted in yellow, **Table 8**). Specific to IGF-1 treated nuclear extracts were two transcription factors: plant homeodomain (phd) finger protein 14 and T box transcription factor TBX3 (**highlighted in yellow Table 8**).

The identification of Phosphatidylinositol 4,5-bisphosphate 3-kinase catalytic subunit alpha (PI3-kinase alpha subunit) and centrosomal protein KIAA1731 as potential binding partners of nuclear IGF-1R suggests possible roles in transcription, cell cycle regulation, and survival in the absence of IGF-1. Classically, PI3-kinase alpha subunit plays a key role at the cell membrane by recruiting PH domain-containing proteins including AKT and PDK1 to the cell membrane, leading to activation of signalling cascades involved in cell growth, survival, proliferation, and motility (Yamaguchi *et al.*, 2011). Recruitment of PI3K subunits to the IGF-1R typically occurs upon receptor activation, leading to recruitment of adaptor proteins and signaling effectors to phospho-motifs. Therefore, the detection of PI3Kα in nuclear extracts could reflect low level contamination with plasma membrane compartments. However, PI3-kinase alpha subunit has been detected in the nucleus, where it promotes cell survival via upstream regulator PIKE and its downstream activator

AKT, mediating the anti-apoptotic activity of nerve growth factor (NGF) in the nucleus (Ahn *et al.*, 2004). Centrosomal protein KIAA1731 homolog is not a well characterized protein but may be involved in centriole formation and stability (Knorz *et al.*, 2010).

IGF-1R immunoprecipitates of nuclear extracts from IGF-treated cells identified three proteins that are candidate IGF-1 induced nuclear IGF-1R binding partners: T-Box transcription factor TBX3, Plant homeodomain (PHD) finger protein 14, and Kinesin-like protein KLP6. T-box transcription factor TBX3 is a member of the T-box transcription factor family, and is a transcriptional repressor involved in developmental embryonic processes (He *et al.*, 1999). TBX3 is frequently unregulated in cancers of the breast, ovary, pancreas, liver, lung and melanoma (Lu *et al.*, 2010). Overexpression of TBX3 has been shown to regulate the p53 pathway, suppressing apoptosis by suppression of $P14^{ARF}$ expression, which leads to MDM2-dependent sequestration, degradation and inactivation of p53 in MEFs and breast cancer cells (Carlson *et al.*, 2002; Yarosh *et al.*, 2008). Furthermore, TBX3 was identified as a downstream target gene of the Wnt/beta-catenin pathway: TBX3 transcription is directly up-regulated by beta-catenin and is required for beta-catenin-mediated cell survival and resistance to doxorubicin-induced apoptosis (Renard *et al.*, 2007).

Plant homeodomain (PHD) finger protein 14 is a nuclear protein belonging to the PHD finger family of proteins that are histone code readers, chromatin targeting and transcriptional regulators (Musselman and Kutateladze, 2009). The role of specific family member proteins is poorly characterized and is the subject of ongoing research (Fortschegger and Shiekhattar, 2011; Mansfield *et al.*, 2011).

The identification of two transcriptional regulators as putative binding partners of nuclear IGF-1R suggests that nuclear IGF-1R could contribute to regulation of transcription upon IGF stimulation. The identification of Kinesin-like protein 6 (KLP6) suggests a role in cell cycle regulation. KLP6 belongs to the Kinesin family of proteins. KLP6 along with Kinesin-like protein 5 (KLP5) colocalize to the mitotic kinetochores and are essential for efficient capturing of the kinetochores by the spindles (Garcia *et al.*, 2002). Recently, KLP6 has been described to contribute to the maintenance of mitochondrial morphology (Tanaka *et al.*, 2011).

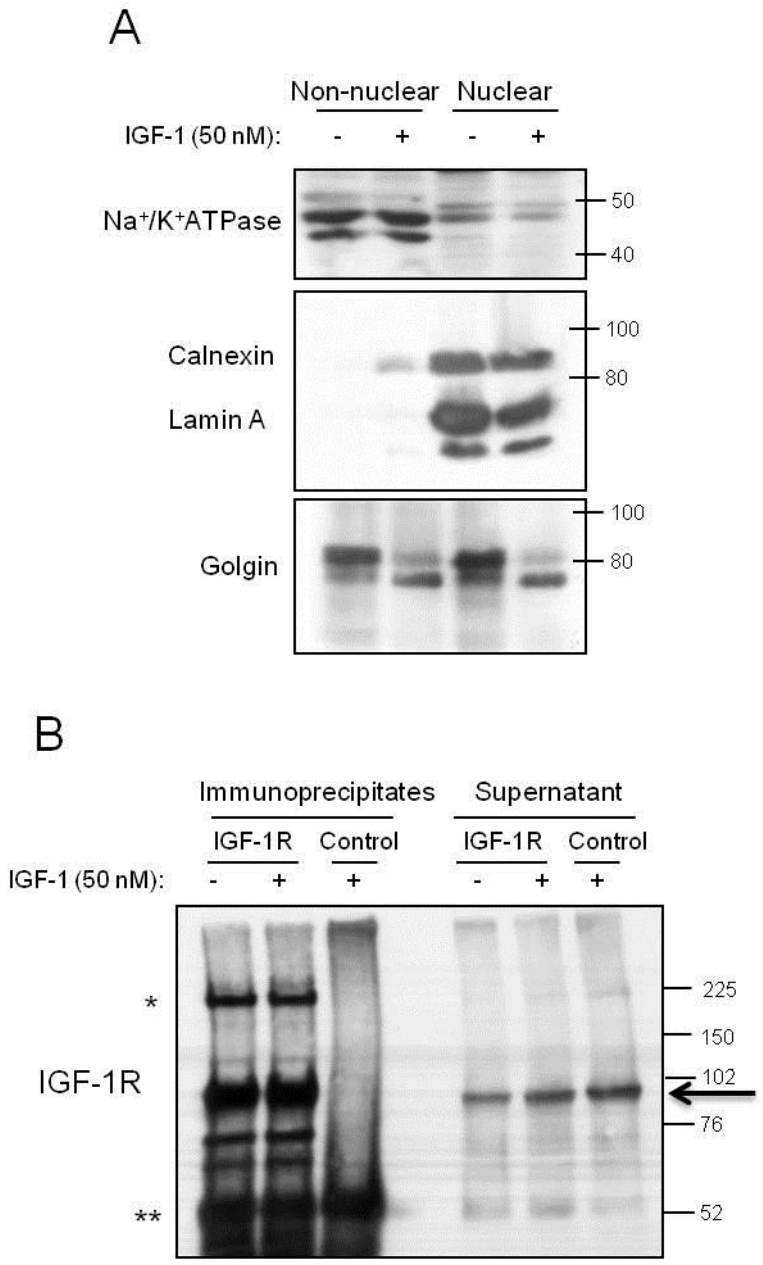


Figure 20: Testing fractionation and immunoprecipitation in IGF or solvent treated cells (A) DU145 cells were serum-starved and treated with 50 nM IGF-1. After 1 hour, cells were swelled in detergent-free hypotonic buffer, dounced, pelleted, washed 3 times with NLB containing 150 mM NaCl and 0.1% Tween 20 and nuclei were lysed in NLB. Extracts were separated by SDS-PAGE and immunoblotted for Golgin-84 (Golgi marker), calnexin (ER), Lamin A (nuclear envelope), and Na+/K+ ATPase (plasma membrane). (B) DU145 cells were serum-starved and treated with solvent (-) or 50 nM IGF-1 (+) for one hour and lysates were immunoprecipitated with IGF-1R beta subunit antibody (3027) or control irrelevant antibody (rabbit IgG). Immunoprecipitates and supernatants were analysed by SDS-PAGE and immunoblotted for IGF-1R β subunit (indicated by the arrow),* indicates IGF-1R proreceptor, ** indicates heavy chains.

IGF-1R IP (# of peptides)		Control IP
Serum-Starved	IGF-treated	IGF-treated
IgG Light Chains	IgG Light Chains	IgG Light Chains
IgG Heavy Chains	IgG Heavy Chains	IgG Heavy Chains
IGF-1R Beta Subunit (4)	IGF-1R Beta Subunit (9)	Cytoskeletal Keratin-1 Type II
IGF-1R Alpha Subunit (1)	IGF-1R Alpha Subunit (3)	Cytoskeletal Keratin-9 Type I
Trypsin	Trysin	Trysin
Cytoskeletal Keratin-1 Type II	Cationic-Trypsin	Cationic-Trypsin
Cytoskeletal Keratin-2b Type II	Cytoskeletal Keratin-1 Type II	Mitogen-activated protein kinase 15
Cytoskeletal Keratin-10 Type I	DNA Excision repair Protein ERCC-6-like	DNA Excision repair Protein ERCC-6-like
PI3-kinase subunit alpha (2) (2)	Kinesin-like protein KLP6 (2)	Bovine Serum Albumin
Centrosomal protein KIAA1731 homolog (3)	Plant Homeodomain (phd) finger protein 14 (3)	
	T box transcription factor TBX3 (5*)	

Table 8: Potential IGF-1 induced IGF-1R binding partners

Table shows proteins identified by MS analysis. Proteins highlighted in yellow are specific to nuclear IGF-1R immunoprecipitation. Numbers in parentheses indicate number of peptides identified, * includes one TBX3 peptide identified twice.

4.2.5 Identification of potential DNA damage induced nuclear IGF-1R binding partners

Thus far, MS had identified several transcription regulators as potential binding partners of nuclear IGF-1R. Our group is particularly interested in the role of IGF-1R in the DNA damage response (Macaulay *et al.*, 2001; Rochester *et al.*, 2005). In light of the recent report from our group that IGF-1R influences the rate of repair of radiation-induced DSBs (Turney *et al.*, 2012) and the known role of EGFR in binding to DNA-PK (Dittmann *et al.*, 2005), post-doctoral scientist Dr. Tamara Aleksic tested whether nuclear IGF-1R colocalizes with markers of DNA damage.

Figure 21 shows confocal images of DU145 prostate cancer cells co-stained for IGF-1R (green) and ɣH2AX (red). The staining protocol to visualize ɣH2AX foci combines fixation and permeabilization in one step using 4% paraformaldehyde and 0.3% Triton X-100, followed by an extraction step to remove nucleoplasmic proteins that are not bound to chromatin. Nuclear ɣH2AX was not detectable in undamaged cells, and showed the expected pattern of focus formation one hour following 10 Gy ionizing radiation (**Figure 21A**). Nuclear IGF-1R staining followed a similar pattern: in the absence of DNA damage there was no detectable IGF-1R bound to chromatin, but one hour after irradiation there was an increase in the amount of IGF-1R retained on chromatin. However, it was clear that there was negligible co-localization with ɣH2AX foci (**Figure 21**), suggesting that IGF-1R might not directly participate in DNA repair at sites of DSB However, IGF-1R did appear to undergo damage-induced interaction with chromatin, suggesting that IGF-1R may contribute indirectly to the damage response, perhaps by regulating transcription, cell cycle progression or susceptibility to apoptosis. As the focus of my work is to explore the role of IGF-1R in the response of prostate cancer cells to DNA damage, I decided to perform an additional MS analysis on nuclear extracts derived from irradiated cells. Therefore,

DU145 cells were either mock irradiated or irradiated with 10 Gy ionizing radiation, and were incubated for an hour at 37°C, based on the data from Dr. Tamara Aleksic showing the highest binding of IGF-1R to chromatin one hour following irradiation (**Figure 21B**). Nuclei were isolated using the optimized in-house method, and nuclear extracts were prepared in NLB. After immunoprecipitation and washing of nuclear IGF-1R and control IPs, co-precipitated proteins were eluted using 125 mM glycine, concentrated by centrifugation through a 10 kDa Amicon filters and in-solution trypsin digest was performed. As in the previous MS analysis, the control (IgG) immunoprecipitates from nuclear irradiated extracts were analysed first to minimize contamination of subsequent samples, followed by non-irradiated nuclear IGF-1R immunoprecipitates and finally the nuclear IGF-1R immunoprecipitates from irradiated samples. Samples were analyzed by Dr. Garth Hamilton as before.

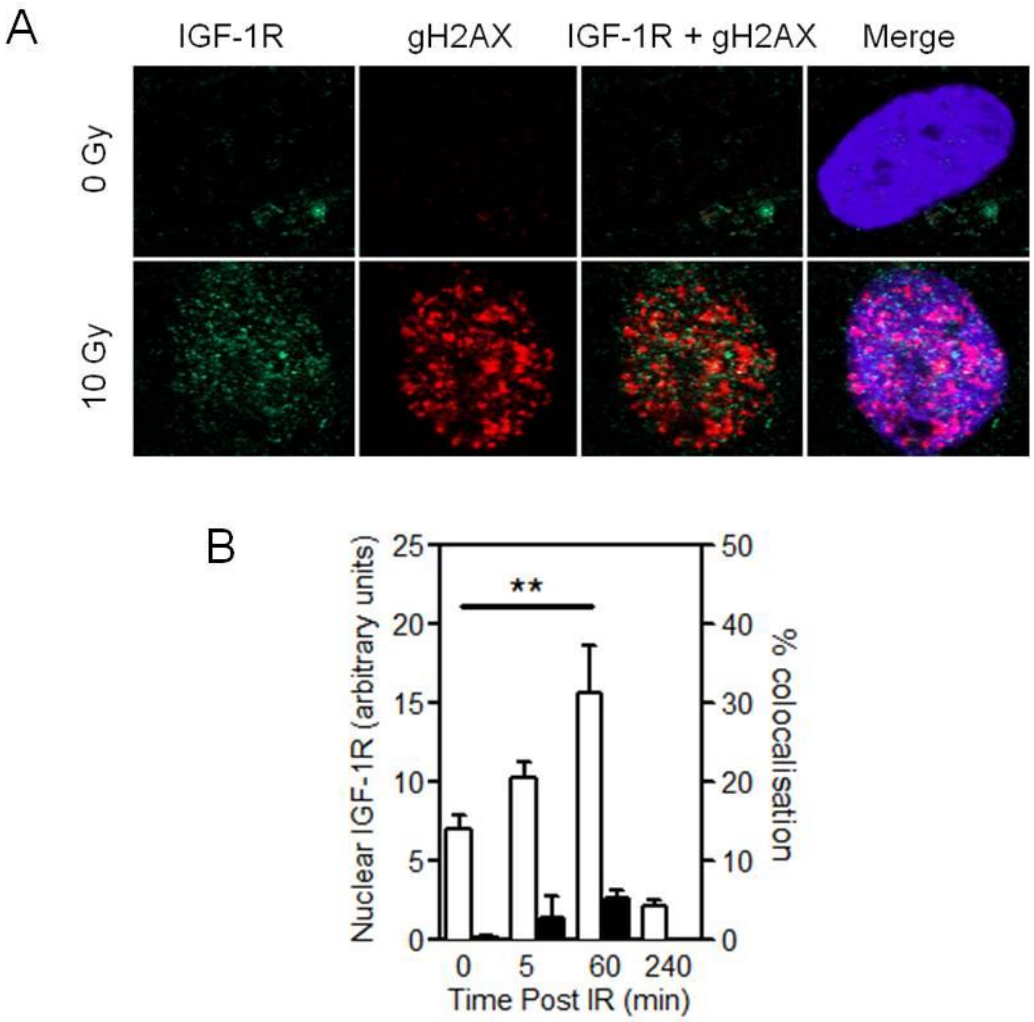


Figure 21: IGF-1R interacts with chromatin of irradiated cells

DU145 cells were irradiated at 0 or 10 Gy, and one hour following irradiation cells were fixed and permeabilized using 4% PFA with 0.3% Triton X-100 for 15 minutes, followed by a pre-extraction wash in solution containing 10 mM PIPE, 300 mM sucrose, 3 mM $MgCl_2$, 20 mM NaCL and 0.5% Triton X-100 (pH = 6.8). A) Shows the staining of DU145 cells with IGF-1R (green) and ɣH2AX (red). B) Images were analysed at different time points by ImageJ software with JACOP plug-in (Aleksic *et al.*, 2010), to quantify nuclear IGF-1R (white bars) and co-localization with ɣH2AX (black bars). ** $p<0.01$ for comparison of 0 and 60 minutes following irradiation by one-way ANOVA. The above work was completed by Dr. Tamara Aleksic.

Table 9 shows proteins identified by MS analysis of non-irradiated and irradiated nuclear IGF-1R immunoprecipitates and irradiated extract immunoprecipitated with control rabbit IgG. On this occasion, analysis of the control IP yielded only the IgG heavy and light chains and structural proteins including myosin, keratins and

cytokeratin. IGF-1R beta subunit was detected in IGF-1R immunoprecipitates from nuclear extracts of both non-irradiated and irradiated cells. Unlike the previous analysis, the IGF-1R alpha subunit was not detected. This could suggest a greater role of the beta subunit kinase domain in the radiation response, or could simply be an artefact of the analysis.

This analysis was influenced by the presence of polymer contaminants and therefore results are very preliminary. One peptide was identified from each of three separate proteins. TAX-1 binding protein 1 (TAX1BP1) was identified as a potential interacting protein of nuclear IGF-1R in undamaged cells (**Table 9**). TAX1BP1 is an 86 kDa protein that is a key regulator of the TNF-alpha mediated activation of NF-kappa B and JNK (De Valck *et al.*, 1999; Shembade *et al.*, 2007). Specifically, TAX1BP1 mediates the interaction of the deubiquitinating enzyme A20 with RIP1 to terminate NFκB and JNK signaling (Shembade *et al.*, 2007). The interaction with TAX1BP1 suggests that nuclear IGF-1R may play a role in regulating NF-kappa B mediated cell growth and survival.

In nuclear extract from irradiation DU145 cells, potential binding partners of nuclear IGF-1R included three proteins: Rho-GTPase-activating protein 44, EGFR substrate 15, and F-box only protein 18 (highlighted in yellow**, Table 9**). Rho-GTPase-activating protein 44 is a member of the Rho-GTPase-activating protein (RhoGAP) family that negatively regulates Rho-GTPase (Moon and Zheng, 2003). The conversion of Rho-GTPase to its inactive GDP-bound state is facilitated by RhoGAPs that increase the hydrolysis of GTP to GDP, accelerating the return of the Rho-GTP to the inactive state (Lamarche and Hall, 1994). The specific function of Rho-GTPase-activating protein 44 in this process or other interacting partners is yet to be identified. The conversion of Rho-GTPase from the inactive GDP bound state to the

active GTP bound state is regulated by Rho-guanine nucleotide exchange factors (Zheng, 2001). Rho proteins in the GTP bound state can interact with various downstream effectors to regulate gene transcription, cell polarity, cell cycle, and control of apoptosis (Van Aelst and D'Souza-Schorey, 1997). If validated, the interaction with Rho-GTPase-activating protein 44 in damaged cells might suggest a role for nuclear IGF-1R in regulating these processes.

The adaptor protein EGFR substrate 15 (EPS15) was also identified as a candidate interacting partner of nuclear IGF-1R in the presence of DNA damage. EPS15 is not a well characterized protein although it was found to be involved in the internalization of EGFR and c-Met receptors (Confalonieri *et al.*, 2000; Vecchi *et al.*, 2001). EPS15 had been identified in the nucleus, where it is reported to act as a positive regulator of transcription (Vecchi *et al.*, 2001). These data suggest that EPS15 could be involved in the internalization of the IGF-1R upon DNA damage, and/or involved in regulating gene transcription in damaged cells. This could be consistent with the finding that nuclear IGF-1R appeared to interact with the chromatin of irradiated cells, but did not co-localize with DSBs (**Figure 21A**).

The third potential IGF-1R binding partner in irradiated cells was F-box only protein 18, also known as F-box DNA helicase protein 1 (FBH1), a nuclear DNA-dependent ATPase (Kim *et al.*, 2002). FBH1 forms a complex with the hydrophobic scaffolding protein Cullin and Regulator of Cullins-1 (ROC1), an E3 ubiquitin ligase, and together this complex is involved in DNA unwinding in a 3' to 5' direction (Park *et al.*, 1997). FBH1 was also reported to be directly involved in repair, by influencing HR-mediated repair of DSB at stalled or collapsed replication forks (Osman *et al.*, 2005). In yeast, in the absence of RAD22 (ortholog of human RAD52), FBH1 can prevent RAD51-dependent recombination (Osman *et al.*, 2005). Recently, FBH1 was shown to be

involved in chromosome segregation during meiosis in yeast. In the absence of FBH1, chromosomes remain entangled or segregate unevenly during meiosis, and this results in part from a failure to efficiently dismantle Rad51 nucleofilaments that form during meiotic DSB repair (Sun *et al.*, 2011). This is interesting given preliminary data generated in our group, suggesting that IGF-1R inhibition sensitises melanoma cells to the methylating agent temozolomide, and this effect is associated with delayed resolution of RAD51 foci formed at replication-associated DSBs (Ramcharan and Macaulay, in preparation).

IGF-1R IP (# of peptides identified)		Control IP
Non-Irradiated (0 Gy)	Irradiated (10 Gy)	10 Gy
IgG Light Chains	IgG Light Chains	IgG Light Chains
IgG Heavy Chains	IgG Heavy Chains	IgG Heavy Chains
IGF-1R Beta Subunit (3)	IGF-1R Beta Subunit (5)	Cytoskeletal Keratin-1 Type II
Actin	Lamin subunit B	Cytoskeletal Keratin-9 Type I
Trypsin	Rho GTPase-activating Protein 44 (1)	Myosin
TAX1-binding protein (1)	F-box only protein 18 (1)	Calmodulin
Keratin Type I Cytoskeletal 19	Epidermal growth factor receptor substrate 15 (1)	Keratin type II cytoskeletal 1
Keratin Type II Cytoskeletal 1	Keratin type II cytoskeletal 7	Cytokeratin-19
Myosin	Homeobox protein Hox-B6	Keratin type II cytoskeletal 7
Tropomyosin Alpha-3	Actin	Keratin type I cytoskeletal 18
Calmodulin	Trypsin	

Table 9: Potential IGF-1R binding partners detected in non-irradiated and irradiated conditions

Table shows proteins identified by MS analysis. Proteins highlighted in yellow are specific to nuclear IGF-1R immunoprecipitation. Numbers in parentheses indicate number of peptides identified.

Thus after three independent MS analyses, several potential binding partners had been identified. It was notable, however, that none of the candidates was identified in more than one analysis. If time had permitted, it would have been preferable to perform MS on three independently derived sets of samples prepared under the same conditions of ligand stimulation or DNA damage.

Several of the candidate binding partners have known or putative roles in regulation of transcription. Therefore, in parallel with the investigations into the effects of ligand

stimulation and DNA damage, it was decided to attempt validation of the first candidate interacting protein, BAP-135/TF II-I.

4.2.5 General Transcription Factor II-I as a potential binding partner for nuclear IGF-1R

As discussed above, the top hit from the first MS analysis, performed on nuclear extract from cells cultured in full serum, was Bruton Tyrosine Kinase Associated Protein 135 (BAP-135), also known as General Transcription Factor II-I (TFII-I), from which 23 separate peptides sequences were detected by mass spectrometry as shown in **Figure 16**. The Bruton Tyrosine Kinase (BTK) is essential for B cell differentiation, and mutations in BTK result in the rare immunodeficiency disorder X-linked agammaglobulinemia (XLA) (Ng *et al.*, 2010). BTK is known to influence B cell calcium signalling and NF-κB activity, and may translocate to the nucleus to regulate Ig transcription (Ng *et al.*, 2010).

BAP-135/TFII-I exists as four isoforms alpha (α), beta (β), gamma (ɣ) and delta (Δ) that exist as monomers in the cytoplasm, however formation of stable hetero and homo dimers translocate to the nucleus (Cheriyath and Roy, 2000). Structurally, TFII-I contains a N-terminal leucine zipper (LZ) domain that is important for stabilizing homo- and hetero-dimers, a nuclear localization signal, and a basic repeat (BR) motif (**Figure 22**) (Cheriyath and Roy, 2001). The basic repeat domain is important for TFII-I binding to DNA, truncated TFII-I lacking the BR domain failed to bind DNA (Cheriyath and Roy, 2001). There is a series of 6 repeat domains (R1-6), which are 89 amino acids in length, each containing regions that are highly conserved across the four isoforms (Roy, 2012). In 1LN prostate cancer cells, TF II-I potentiates

cancer cell survival by enhancing the expression of the molecular chaperone GRP78 (Misra *et al.*, 2009).

To validate a possible interaction between TFII-I and nuclear IGF-1R, DU145 cells were serum-starved overnight and treated with solvent or 50 nM IGF-1 for 30 minutes, and TFII-I was immunoprecipitated from whole cell extracts. Immunoblotting suggested the presence of IGF-1R in IPs from IGF-1 treated cells (**Figure 23**). This suggests possible IGF-1 induced formation of a complex between TFII-I and IGF-1R. Although the IGF-1R band was of low intensity, it could possibly be enriched by immunoprecipitating TFII-I from nuclear extracts made from serum-starved and IGF-stimulated cells. This will need to be further validated by reciprocal immunoprecipitation for IGF-1R and immunoblotting for TFII-I, in DU145 cells and in other cell lines.

The membrane was then probed with phosphotyrosine antibody, revealing multiple products in IGF-treated cells. There was a clear band at ~100 kDa, consistent with phosphorylated and activated IGF-1R β subunit. There was also a tyrosine phosphorylated product at ~130 kDa, equivalent to the size of TFII-I. The most prominent product was at ~200 kDa and is of unknown significance.

The detection of a tyrosine-phosphorylated product of 130 kDa suggests the possibility that TFII-I might undergo phosphorylation in IGF-treated cells, perhaps induced directly by IGF-1R. Scansite (http://scansite.mit.edu/) motif search was used in order to determine whether TFII-I contained any putative growth factor receptor or downstream singaling phosphorylation sites. Motif search showed TFII-I to have three candidate motifs for phosphorylation by EGFR, Insulin Receptor and AKT1 (**Figure 22**), the first located in the first TF II-I repeat R1 on tyrosine 119 (Y119), the

second upstream of the NLS, an EGFR phosphorylation site on tyrosine 248 (Y248) and finally a possible AKT1 phosphorylation site on serine 722 (S722) in the fifth repeat (**Figure 22**). In response to growth factor signaling, TFII-I is known to be phosphorylated at Y248, triggering its translocation and enhancing transcription of *c-fos* (Kim and Cochran, 2000). Furthermore, this growth factor induced-phosphorylation at Y248 is required for cell cycle progression from G0 to G1 (Desgranges and Roy, 2006) and also the transition from G1 to S phase via transcriptional regulation of cyclin D1 (Desgranges *et al.*, 2005). TFII-I is removed from the condensed chromatin via phosphorylation by cyclin dependent kinase 1 (CDK1) at the G2/M boundary (Ashworth and Roy, 2009).

TFII-I was recently shown to undergo interaction with BRCA1, and to form foci following irradiation (Tanikawa *et al.*, 2011). BRCA1 has a molecular weight of ~220 kDa, can be tyrosine phosphorylated and is a candidate for the ~220 kDa phospho-product in **Figure 23**. This raises the intriguing possibility that via an interaction with the transcriptional regulator TFII-I, IGF-1R could influence the localization or function of BRCA1. This could be investigated by phospho-peptide MS analysis, and performing co-immunoprecipitation and immunofluorescent co-localization for IGF-1R, BRCA1 and TFII-I. Identification of any IGF-induced post-translational modification (PTMs) and their functional significance will need to be investigated by firstly identifying the site of phosphorylation and secondly by creating non-phosphorylatable or phosphomimetic mutant TFII-I and testing effects on TF II-I function.

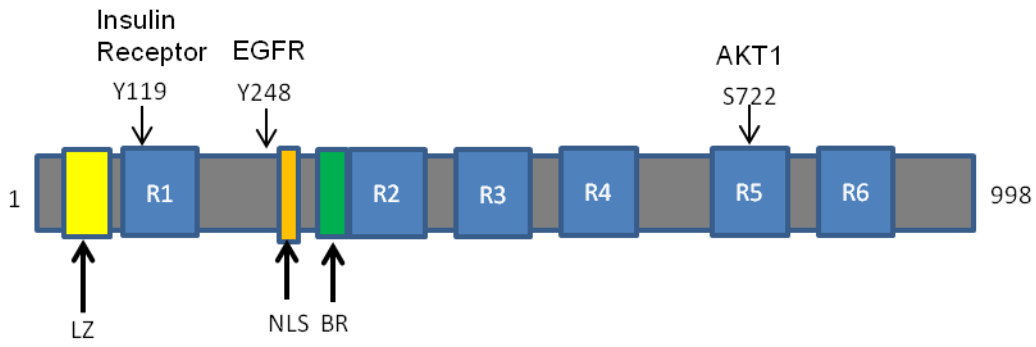


Figure 22: Diagram of General Transcription Factor II-I
TFII-I contains three candidate motifs for phosphorylation at tyrosine 248 (Y248) by EGFR, at tyrosine 119 (Y119) by Insulin Receptor and at serine 722 (S722) by AKT1. LZ = leucine Zipper, NLS = nuclear localization signal, BR = basic repeat, R1-R6 = repeat regions that are highly conserved across isoforms. Figure constructed using http://scansite.mit.edu/ and (Roy, 2007)

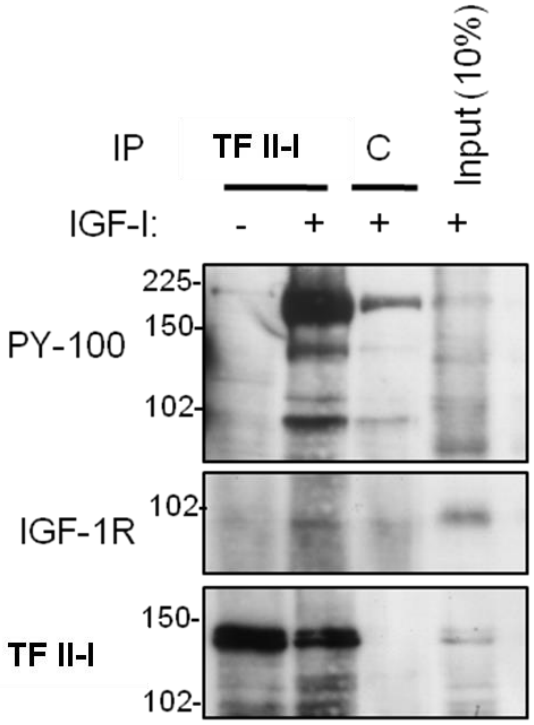


Figure 23: Investigating a potential interaction and post-translational modification on TFII-I by IGF-1R
DU145 cells were serum-starved and treated with solvent (-) or 50 nM IGF-1 (+) for 30 minutes and whole cell extracts were immunoprecipitated with TFII-I or control irrelevant antibody (rabbit IgG). Immunoprecipitates and supernatants were analysed by SDS-PAGE and immunoblotted with pan-phospho-tyrosine antibody, IGF-1R and TFII-I.

4.3 Discussion

Work published from our laboratory showed that the IGF-1R not only localizes to the plasma membrane but is also able to translocate to the nucleus of renal, breast, and prostate cancer cells, in an IGF-dependent manner (Aleksic *et al.*, 2010). Although the mechanism of nuclear translocation in prostate cancer cells was not reported by our group, work from Larrson's group described that IGF-1R nuclear translocation is dependent on SUMOylation, in melanoma cells (Sehat *et al.*, 2010). Clinically, we showed that high levels of nuclear IGF-1R were associated with poor survival in renal cancer (Aleksic *et al.*, 2010). This suggests both a biological and clinical relevance for the function of IGF-1R in the nucleus. In addition to the IGF-1R, VEGF and the EGFR family of RTKs have been shown to translocate to the nucleus, where they are known to regulate transcription (Massie and Mills, 2006; Wang *et al.*, 2010).

As this is the first time that IGF-1R has been shown in the nucleus, and the function has not yet been identified, it was very important to identify the optimal method for nuclear extraction while minimizing contamination from other subcellular compartments. Furthermore, to favour detection of specific interactions, the conditions for immunoprecipitation required optimization to ensure it was stringent enough to remove non-specific interactions while preserving nuclear IGF-1R interacting complexes. These optimized fractionation and immunoprecipitation conditions were applied to three independent MS analyses comparing three different conditions: cells grown in complete medium, serum-starved and IGF-1 treated or irradiated. The identification of several transcription factors suggests possible involvement of nuclear IGF-1R in the regulation of transcription. This is consistent with a report published showing that nuclear IGF-1R binds to the transcription factor

LEF1 in the nucleus and leads to enhanced promoter activity and up-regulation of cyclin D1 and axin2 (Warsito *et al.*, 2012). Given the importance of Cyclin D1 in the progression of cell cycle, specifically through G1 phase (Samani *et al.*, 2007), this could be an additional mechanism by which IGF-1R regulates cell cycle progression, to promote tumorigenesis. Recently, cyclin D1 was reported to directly interact with RAD51, a key protein in HR-mediated repair (Jirawatnotai *et al.*, 2011). Cyclin D1 is recruited to the site of damage in a BRCA2 dependent manner, and binds directly to RAD51. It is possible that nuclear IGF-1R is regulating levels of cell cycle or proliferation proteins such as cyclin D1 (Jirawatnotai *et al.*, 2011), CDK1 (Johnson *et al.*, 2011), or polo-like kinase 1 (PLK1) (Yata *et al.*, 2012), which also regulate the response to DNA damage. This raises the possibility that treatment with IGF-1R antibodies and inhibitors might provide a dual function: inhibiting tumour progression and also sensitizing cells to chemo and radio-therapy.

Chapter 5: Investigation of DNA repair hits identified in a synthetic lethality screen using IGF-1R inhibitor

5.1 Introduction

Synthetic lethality arises when mutations in two or more genes leads to cell death, whereas a mutation in any of these genes alone allows a cell to be viable (Kaelin, 2005). The concept was first identified in Drosophila, where genetic crosses between organisms harbouring mutations in certain non-allelic genes were lethal even though the homozygous parents were perfectly viable (Lucchesi, 1968). Subsequently, this concept was extended to describe the situation in which the combination of two defects impairs the fitness of an organism or cell, rather than inducing lethality, and this has been called synthetic sickness (Rehman *et al.*, 2012).

This concept has been extended to mammalian cells and the interaction between breast cancer susceptibility protein type 1 or 2 (BRCA1 or BRCA2) and poly (ADP—ribose) polymerase (PARP1) has become the paradigm for synthetic lethality in mammalian cells (Bryant *et al.*, 2005; Farmer *et al.*, 2005). In this model, a mutation in either PARP1, involved in the repair of single strand breaks, or BRCA1 or BRCA2, involved in homologous recombination, does not lead to cell death. However, inhibition of PARP1 in BRCA1 or BRCA2 deficient cells results in the accumulation of DNA lesions that cannot be repaired, and causes cell lethality (Bryant *et al.*, 2005; Farmer *et al.*, 2005).

Work in our laboratory is exploring this concept as a means of investigating factors that regulate sensitivity to IGF-1R inhibition. Another laboratory member recently completed a synthetic sickness/lethality screen, in collaboration with Professor Alan Ashworth at Breakthrough Breast Cancer (Dr. Shan Gao, 2012, University of Oxford, D.Phil. thesis July 2012). The aim of this screen is to identify kinase or DNA repair-related proteins that when depleted show synthetic sickness/lethality with IGF-1R inhibition in DU145 prostate cancer cells and MCF7 breast cancer cells. IGF-1R inhibition was achieved using AZ12253801, the IGF-1R kinase inhibitor that had been used in the first part of this project. DU145 and MCF7 cells had been transfected with siRNA libraries targeting 779 genes encoding kinases and kinase-associated proteins (SMARTpool, Dharmacon) and 230 DNA repair-related genes (Qiagen, UK) (**Figure 24A**). Each library was screened twice, and hits from the first screen were validated in a second round screen, which identified 6 potential DNA repair-related genes (**Figure 24B**) and 8 kinase genes. Ongoing work in the laboratory is pursuing several of these hits, including dishevelled 3 (DVL3).

5.2 Results

5.2.1 Screen for proteins that regulate sensitivity to IGF-1R inhibition

RAD51 was selected for further studies based on the fact that it was one of the strongest hits in DU145 prostate cancer cells (**Figure 24B**). Homologous recombination (HR) is a complex process that begins with resection of DNA end by MRN complex, BRCA1, CtIP, to create a 3' overhang, which is coated by replication protein A (RPA) (Sung and Klein, 2006). Subsequently, RPA is replaced with RAD51 with the assistance of assistance of mediator proteins including RAD52 and BRCA2

(Esashi *et al.*, 2007; Feng *et al.*, 2011). RAD51 is capable of searching the genome for homologous sister chromatid sequence and catalyzing the strand invasion step of HR (Kass and Jasin, 2010; Sung and Klein, 2006). The identification of RAD51 as a screen hit is interesting given previous work, including from our group, that IGF-1R can influence the homologous recombination pathway. Firstly, it was shown that RAD51 can interact with the IGF-1R docking molecule IRS-1 (Trojanek *et al.*, 2003). This interaction was shown in serum-starved cells, holding RAD51 in a cytoplasmic localisation. IGF-1 stimulation was show to attenuate this interaction, allowing RAD51 to traffic to the nucleus and form foci in response to DNA damage. In the absence of IGF-1, or failure of the IGF-1R to properly tyrosine phosphorylate IRS-1, localisation of RAD51 to the site of DNA damage was diminished (Trojanek *et al.*, 2003). Previous work from our laboratory has investigated the influence of IGF-1R depletion on the response of prostate cancer cells to DNA damage (Rochester *et al.*, 2005; Turney *et al.*, 2012). Using γH2AX focus counting and pulse field gel electrophoresis, IGF-1R depleted cells were shown to contain 30-40% more unrepaired DNA breaks than control cells (Turney *et al.*, 2012). Using a reporter assay for HR (Pierce *et al.*, 1999), depletion of IGF-1R was shown to induce modest but statistically significant reduction in HR in DU145 cells. Interaction between RAD51 and IRS-1 was not detectable in DU145 cells, and we speculate that the HR defect in IGF-1R depleted cells may be at least in part attributable to effects on cell cycle distribution (Turney *et al.*, 2012).

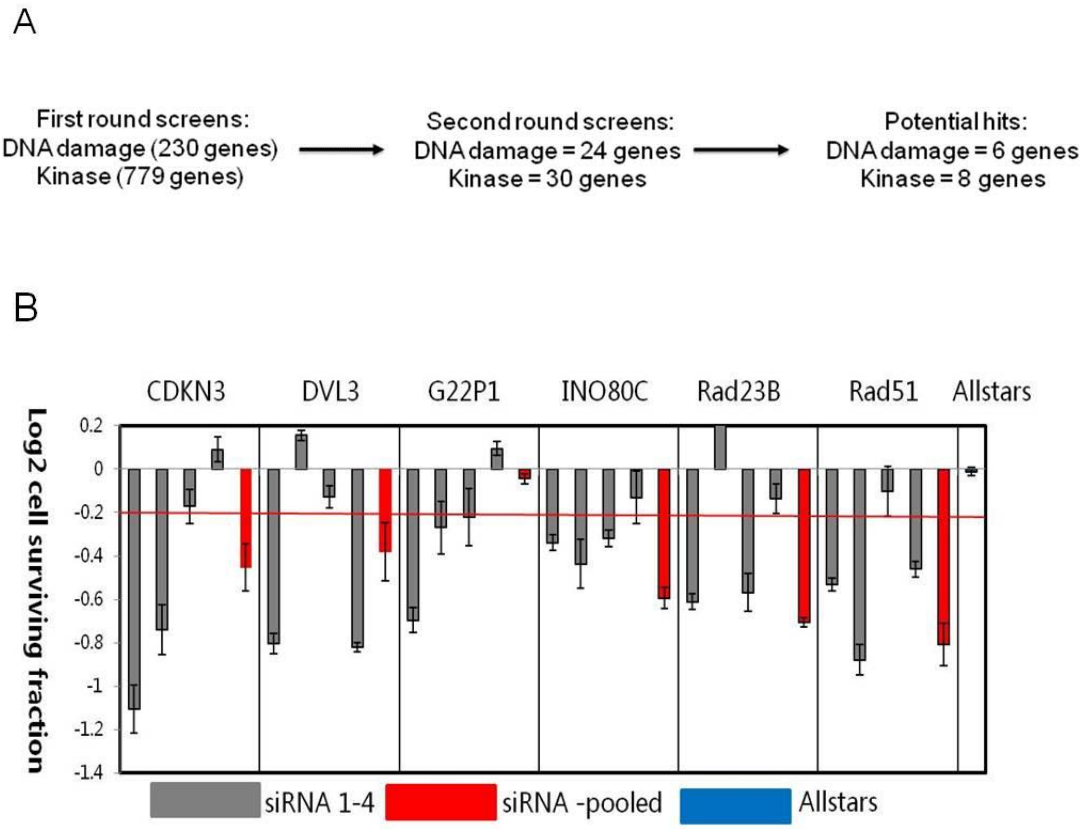


Figure 24: siRNA screen for synthetic/sickness lethality with IGF-1R inhibition

A) IGF-1R inhibited cells were screened against a DNA Damage library of 230 genes and a Kinome library of 779 known kinase and kinase associated genes by another member of the laboratory (Shan Gao). Second round screens were performed with 4 individual siRNAs and pooled Dharmacon siRNA to increase confidence that observed effects were not off-target effects of siRNA. B) Results of second round screen of DNA repair-related hits. Surviving fractions following IGF-1R inhibitor treatment are shown as mean ± SEM. Grey columns represent individual siRNAs, red columns represent pool of the four siRNAs. Potential hits were identified as those genes in which at least 2 individual siRNA and pooled siRNAs achieved log2 cell survival fraction < -0.2. This work was done by Dr. Shan Gao (D.Phil. thesis, Oxford University, July 2012)

5.2.2 Validation of RAD51 as a screen hit in DU145 prostate cancer cells

In order to validate RAD51 as a screen hit, it was first necessary to confirm that the screen siRNAs did effectively deplete RAD51. The large screen used reverse transfection, and so an initial assessment was made of the ability of RAD51 siRNA to deplete its target after reverse or forward transfection. Forward transfection typically involves seeding cells 24 hours prior to the addition of transfection reagent and siRNA complex, while reverse transfection involves incubation of transfection reagent and siRNA complex with cells in suspension, prior to adherence. As a positive control, this experiment used Qiagen IGF-1R siRNA, which has previously been shown to induce effective IGF-1R depletion (Aleksic *et al.*, 2010; Turney *et al.*, 2012). Forward transfection showed greater depletion of IGF-1R compared to reverse transfection, (**Figure 25A**) while immunoblotting for RAD51 showed comparable levels of depletion following forward and reserve transfection (**Figure 25A**). This confirmed that one of the screen siRNAs did deplete RAD51. The next step used forward transfection to test the efficacy of the two RAD51 siRNAs for use in subsequent assays (**Figure 25B**).

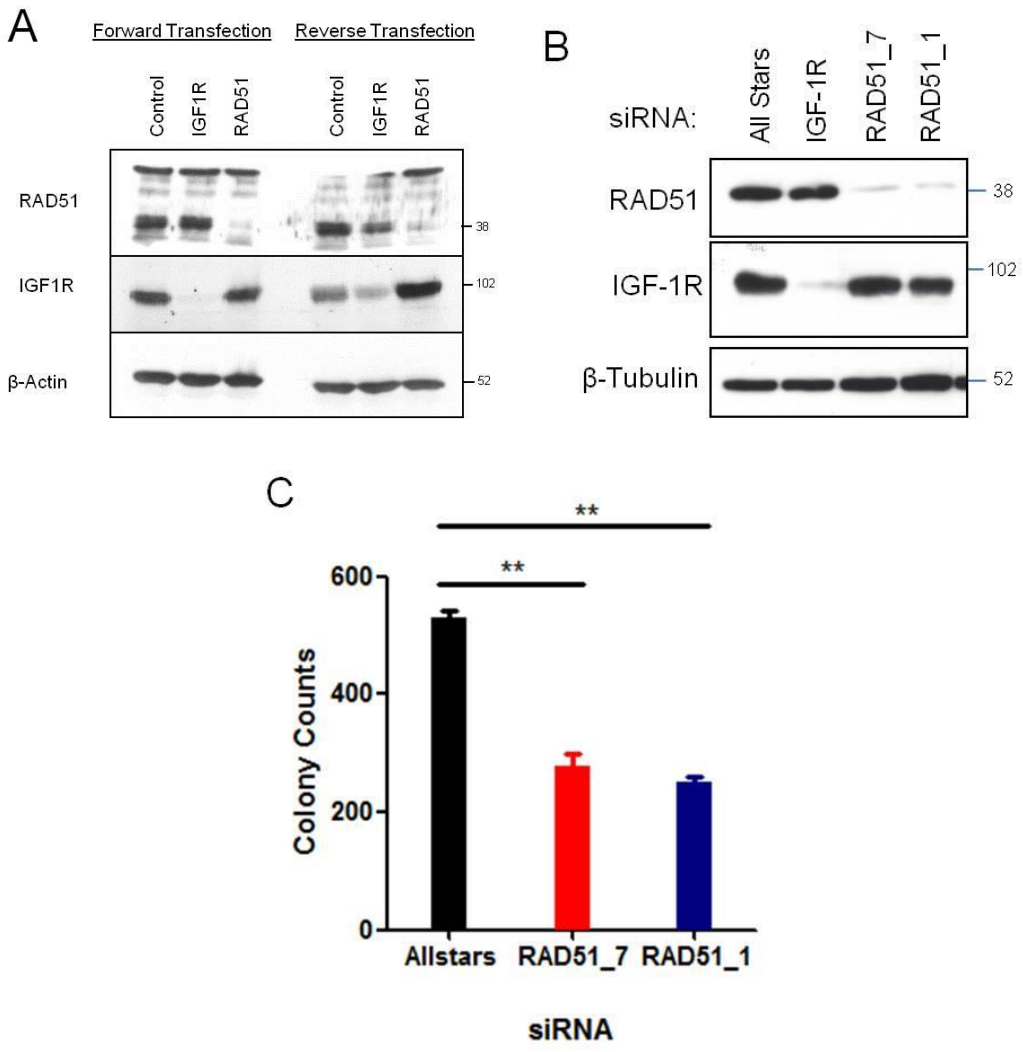


Figure 25: Validating RAD51 screen siRNA

A) DU145 cells were siRNA-transfected either by forward or reverse transfection and after 48 hours, lysates were analysed by SDS-PAGE. Depletion of target protein was assessed by immunoblotting for RAD51 and IGF-1R. Allstars was used as negative control and IGF-1R siRNA was used as a positive control. B) DU145 cells were forward transfected with two different siRNA for RAD51 and IGF-1R as a control for transfection and immunoblotted for RAD51 and IGF-1R as in A-C) DU145 cells were transfected with Allstars or RAD51 siRNA and the following day reseeded at 3,000 cells per 10 cm dish. Graph shows colony counts for cells transfected with Allstars or RAD51 siRNA. **p = 0.0023 for comparison of AllStars with RAD51_7 or p = 0.0056 by for comparison of AllStars with RAD51_7 paired t-test.

To investigate whether RAD51 depletion sensitized DU145 prostate cancer cells to IGF-1R inhibition, two independent assays were used: colony forming assay and Celltiter Glo cell viability assay (Promega). For the colony formation assay, DU145 cells were forward transfected with RAD51 siRNA or control siRNA, reseeded 24 hours later, and treated with AZ12253801 IGF-1R inhibitor 48 hours following

transfection. It was clear that depletion of RAD51 had a significant effect on the survival of DU145 cells even in the absence of AZ12253801 treatment. RAD51 depleted DU145 showed a 47% reduction in survival compared to control transfected cells (**Figure 25C**). Similar results have been reported previously, showing that RAD51 depletion leads to cell cycle arrest in G_2/M phase (Du *et al.*, 2010).

To assess effects on sensitivity to AZ12253801, control or RAD51 depleted cells were treated with AZ12253801 and colony formation was shown as percent survival in the absence of drug. The data were fitted to a curve, enabling extrapolation of the concentration of AZ12253801 that allowed survival of 50% of DU145 cells (survival factor 50%, SF_{50}). Control transfected cells treated with IGF-1R inhibitor showed a decrease in survival with increasing concentration of IGF-1R inhibitor (SF_{50} = 95 nM) (**Figure 26A**). RAD51 depletion, by either of two independent siRNAs, sensitised cells to the IGF-1R inhibitor, as calculated by the shift in SF_{50} values of 2.2 fold with siRNA RAD51_1 and 2.5 fold using RAD51_7 (**Figure 26A and Table 10**).

Celltiter Glo (CTG), an ATP dependent cell viability assay, was used as a second independent method to assess the effects of RAD51 depletion on sensitivity to IGF-1R inhibition in DU145 prostate cancer cells. The cells were reverse transfected with RAD51 or control siRNAs, and 48 hours later were treated with increasing concentrations of AZ12253801. Cell viability was measured by luminescence 5 days later, and was expressed as percent survival in the absence of drug. This enabled calculation of the concentration of AZ12253801 required to inhibit growth by 50% (Growth Inhibitory 50%, GI_{50}). AZ12253801 induced dose dependent inhibition of the viability of control transfected cells with GI_{50} value of 128 nM (**Figure 26B**), equivalent to the GI_{50} of 120 nM found by my colleague Shan Gao in the screen (Dr. Shan Gao, 2012, University of Oxford, D.Phil. thesis July 2012). RAD51 depletion

induced a shift in the dose-response curve to the IGF-1R inhibitor with a shift GI_{50} values (**Figure 26 and Table 10**), amounting to a 2.3 and 1.8 fold sensitisation using the two different siRNAs. Thus RAD51 depletion caused a 2.2-2.5 fold shift in SF_{50}, and a 1.8-2.3 fold shift in the GI_{50}, validating RAD51 as a screen hit in DU145 cells. This is a relatively modest effect, but is comparable to the magnitude of sensitisation to PARP depletion (rather than inhibition) in BRCA2 null cells (Farmer *et al.*, 2005).

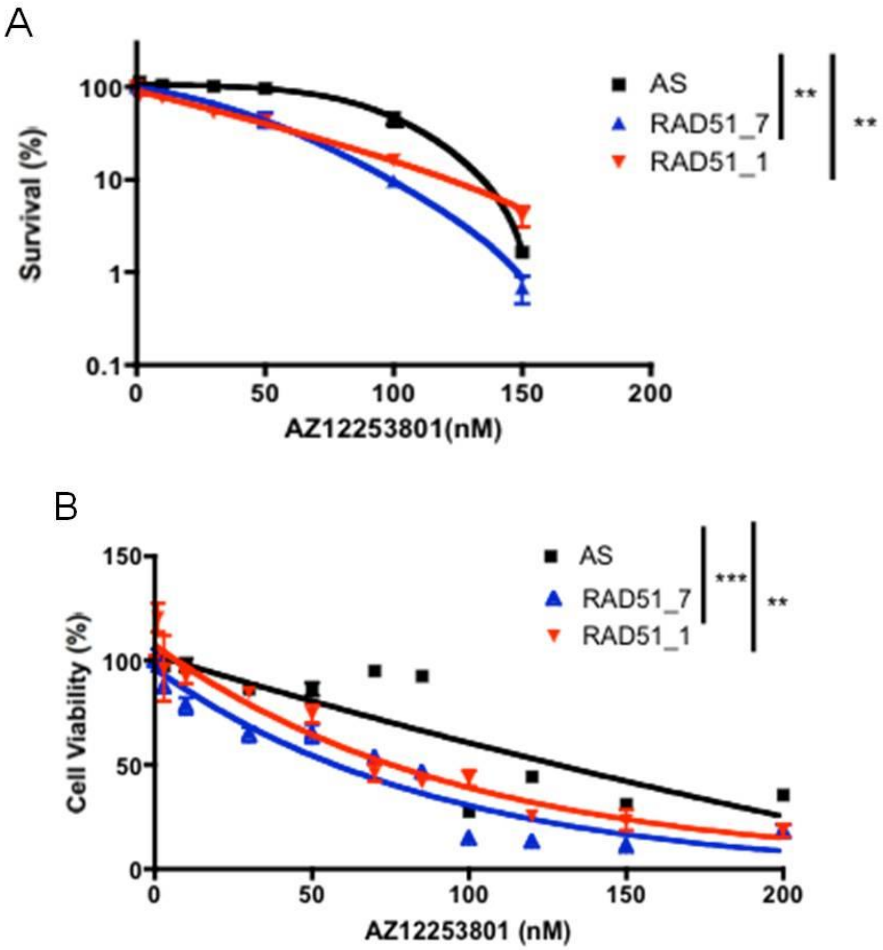


Figure 26: Effects of RAD51 depletion on sensitivity to IGF-1R inhibition in DU145 cells
A) DU145 cells were control or RAD51 siRNA transfected and the following day seeded at 3000 cells per 10 cm dish. Cells were treated with 0-200 nM IGF-1R inhibitor and after 10 days visible colonies were stained and counted. Graph shows clonogenic survival (% untreated), and shows two independent experiments pooled together. B) DU145 cells were control or RAD51 siRNA reverse transfected and 48 hours post transfection cells were treated with 0-200 nM IGF-1R inhibitor. After 5 days cell viability was measured by luminescence. Graph shows cell viability as a percent of the untreated cells, and represents three independent experiments pooled together.

Assay Type	SF_{50} / GI_{50} (nM)			SF_{50}/GI_{50} Control
	AS	RAD51_7	RAD51_1	SF_{50}/GI_{50} RAD51
Clonogenic Survival	95	44	-	2.2
Clonogenic Survival	95	-	37	2.5
CellTiter Glo	128	56	-	2.3
CellTiter Glo	128	-	74	1.8

Table 10: Effects of RAD51 depletion on sensitivity to IGF-1R inhibition

DU145 cells were control or RAD51 siRNA transfected and sensitivity to IGF-1R inhibition was measured by colony forming assay (clonogenic survival) or CellTiter Glo (cell viability) assay. Table shows SF_{50} and GI_{50} values extrapolated from pooled data from three independent experiments. Fold sensitization is reported as a ratio of the control transfected SF_{50} or GI_{50} to the SF_{50} or GI_{50} of the RAD51 depleted cells.

5.2.3 Investigating the effects of RAD51 depletion on sensitivity of IGF-1R inhibition in a panel of prostate cancer cell lines

The screen was performed using DU145 prostate cancer cells that are androgen receptor (AR) null due to promoter methylation preventing expression of the receptor (Chlenski *et al.*, 2001). Additionally, DU145 cells express mutant p53 with two amino acid mutations (Isaacs *et al.*, 1991). For this reason, it was important to understand whether RAD51 could influence sensitivity to IGF-1R inhibition in other prostate cancer cells lines. **Table 11** shows characterises status of DU145, PC3, LNCaP, and 22Rv1 prostate cancer cells. Like DU145, PC3 are AR null despite having a normal AR gene (Tilley *et al.*, 1995), while LNCaP and 22Rv1 prostate cancer cells express AR (Skjoth and Issinger, 2006). LNCaP and 22Rv1 cells also express wild-type p53, while DU145 and PC3 cells harbour mutant p53 (Bajgelman and Strauss, 2006; Skjoth and Issinger, 2006). These cell lines are also well-characterized for

phosphatase and tensin homolog deleted on chromosome 10 (PTEN) status: DU145 and 22Rv1 express wild-type PTEN, while PC3 cells are PTEN null and LNCaPs have a deletion of one PTEN allele and a mutation of the other, consistent with advanced clinical prostate cancer where PTEN loss is common (McMenamin *et al.*, 1999). LNCaP prostate cancer cells are known to lack IRS-1 (Reiss *et al.*, 2000).

The identity of each cell line was verified by short tandem repeat (STR) assay preformed at Cancer Research UK Laboratories, Clare Hall Hertfordshire. Prior to testing effects of RAD51 depletion, western blotting was carried out to check that the cell lines had the predicted phenotype, including basal phosphorylation and expression of components of the IGF-AKT axis including PTEN, and also AR and RAD51 (**Figure 27**). Immunblotting for AR and PTEN confirmed the known status in these cell lines, showing that LNCaP and 22Rv1 express AR while DU145 and PC3 are AR negative (**Figure 27**). Moreover, DU145 and 22Rv1 cells contain detectable PTEN, while PC3 and LNCaPs are PTEN deficient. Consistent with this, serine 473 phosphorylated AKT was detectable in the PTEN deficient PC3 and LNCaP, while PTEN wild type DU145 and 22Rv1 contained no detectable levels of phospho-AKT when cultured in complete medium (**Figure 27**). The PTEN wild-type cells DU145 and 22Rv1 also contained detectable levels of phospho-ERK1 and 2 (**Figure 27**). This is consistent with a report that re-expression of PTEN in prostate cancer cells not only suppresses AKT activation but also activates ERKs (Wu *et al.*, 2008). All four prostate cancer cell lines contained detectable levels of IGF-1R and RAD51 protein, with relative IGF-1R levels consistent with previous reports (**Figure 27**) (Rochester *et al.*, 2005; Turney *et al.*, 2012).

	DU145	PC3	LNCaP	22Rv1
Androgen Receptor	Null	Null	Present	Present
p53	Mutant	Null	WT	WT
PTEN	WT	Null	Mutant	WT
IRS-1	Present	Present	Null	Present

Table 11: Characterization of Prostate Cancer Cell Lines

Table summarizing the Androgen Receptor, p53, PTEN and IRS-1 status of DU145, PC3, LNCaP and 22Rv1 prostate cancer cells. Data from: (Bajgelman and Strauss, 2006; Litvinov *et al.*, 2006; Skjoth and Issinger, 2006)

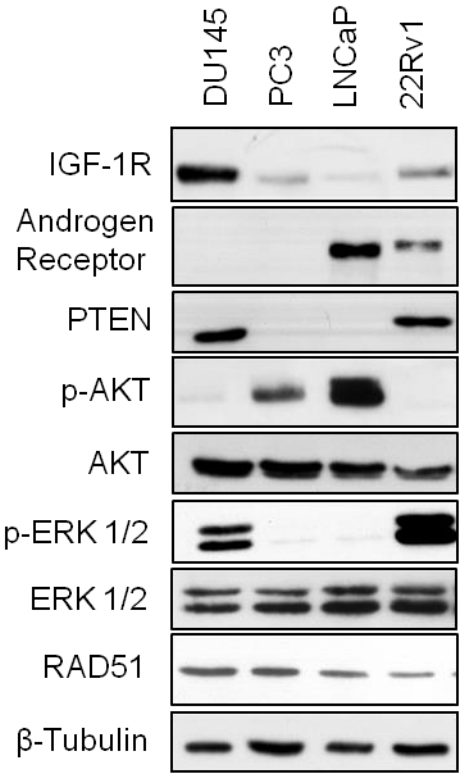


Figure 27: Characterisation of a panel of prostate cancer cell lines

DU145, PC3, LNCaP and 22Rv1 cells were lysed and equal amounts of soluble proteins were separated by SDS-PAGE and immunoblotted for components of the IGF-1R axis: IGF-1R, phospho-AKT (serine 473), total AKT, phospho-ERK 1 and 2, total ERK, PTEN, and also for AR and RAD51.

To screen the four prostate cancer cell lines, CTG cell viability assays were used, requiring reverse transfection to deplete RAD51. The recommended transfection reagent was different for the four prostate cancer cell lines (**Table 3**). For DU145

and 22Rv1 cells DharmaFECT transfection reagent 1 was recommended, and for PC3 and LNCaP cells DharmaFECT transfection reagent 2 was recommended (**Table 3**). To test the ability of the RAD51 siRNAs to deplete the target protein using these transfection reagents, a reverse transfection was performed. Effective RAD51 depletion was induced by two different siRNAs compared to control transfected cells (**Figure 28**). In DU145, PC3 and LNCaP prostate cancer cells, the RAD51_7 and RAD51_1 siRNAs depleted RAD51 to the same extent; in 22Rv1 cells RAD51_7 appeared marginally more effective than RAD51_1 (**Figure 28**). Thus, RAD51_7 was used to investigate RAD51 mediated resistance to IGF-1R inhibition in the panel of prostate cancer cell lines.

The recommended Dharmafect reagents tested in **Figure 28** were used to assess effects of RAD51 depletion in 22Rv1, PC3 and LNCaP cells. For these assays, RAD51-depleted and control transfected cells were treated with increasing concentrations of AZ12253801 48 hours following transfection, and cell viability was measured by luminescence 5 days later. **Figure 29** shows the results of CTG cell viability assays in LNCaP, PC3 and 22Rv1 cells. Control transfected cells treated with IGF-1R inhibitor showed a decrease in survival with increasing concentration of IGF-1R inhibitor (**Figure 29A-C**). RAD51 depletion did not sensitize LNCaP and PC3 cells to AZ12253801, but did enhance the sensitivity of 22Rv1 cells to IGF-1R inhibitor, seen by the shift in dose-response curves (**Figure 29A-C**). **Table 12** summarizes the calculated GI_{50} values for LNCaP, PC3 and 22Rv1 cells transfected with control or RAD51 siRNAs. Similar to results in DU145 prostate cancer cells, 22Rv1 cells showed a 1.9 fold sensitisation to IGF-1R inhibition following RAD51 depletion (**Figure 29C and Table 12**).

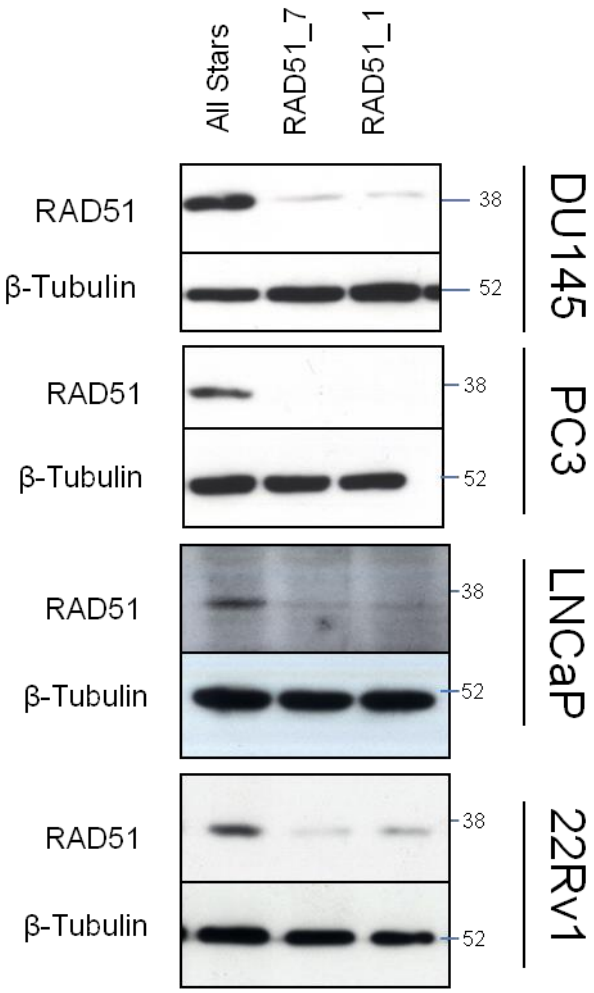


Figure 28: RAD51 depletion by reverse transfection in prostate cancer cells

DU145 and 22Rv1 cells were reverse transfected with DharmaFECT 1 while LNCaP and PC3 were reverse transfected with DharmaFECT 2. Reverse transfection was performed using 250,000 cells in a 6 well plate with control or 2 different RAD51 siRNA and after 48 hours, lysates were analysed by SDS-PAGE. Depletion of target protein was assessed by immunoblotting for RAD51. AllStars siRNA was used as negative control.

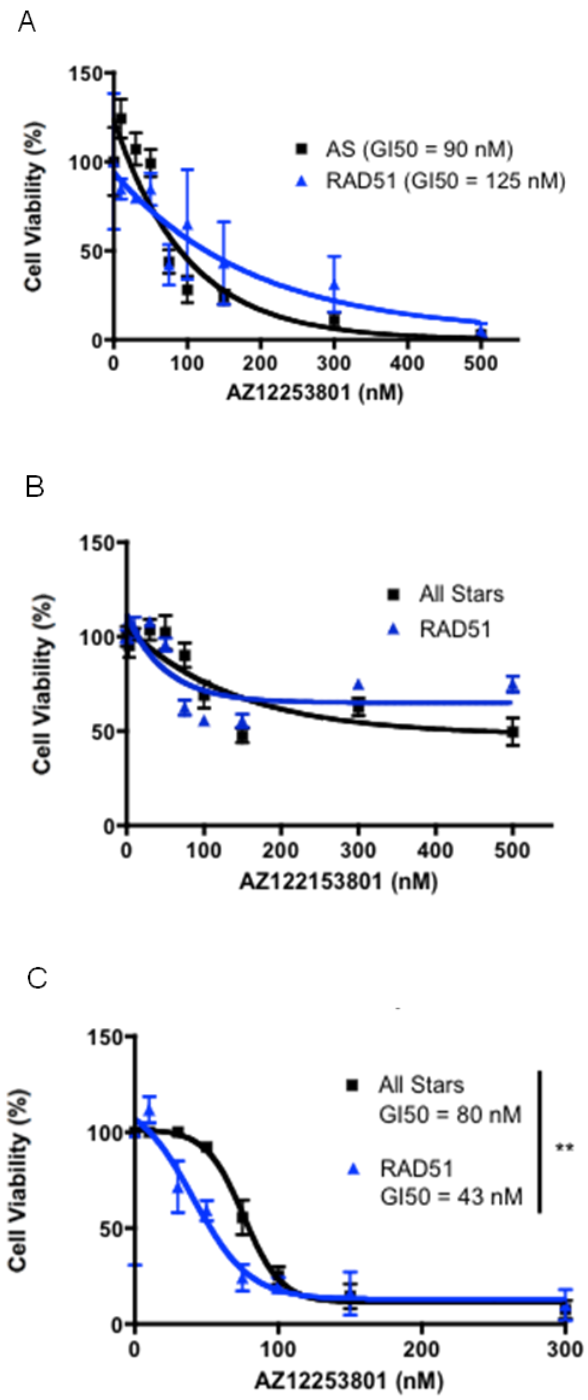


Figure 29: Effects of RAD51 depletion on sensitivity to IGF-1R inhibition in prostate cancer cell lines

CTG cell viability assay was performed for (**A**) LNCaP, (**B**) PC3, (**C**) 22Rv1 by reverse transfecting cells into a 96 well clear bottom plate, 48 hours later treating with containing AZ12253801 and 5 days later cell viability was measured by luminescence. Viability was expressed as a percentage of control or RAD51_7 transfected cells without inhibitor. Results represents the mean ±SEM of three independent experiments. Two way ANOVA was used to compare the sensitivity of control or RAD51_7 transfected cells to IGF-1R inhibition. ** p< 0.01, by 2-way ANOVA.

Cell Type	GI_{50} (nM)		GI_{50} Control / GI_{50} RAD51
	AS	RAD51_7	
DU145	128	56	2.3
PC3	NA	NA	1.0
LNCaP	90	125	0.7
22Rv1	80	43	1.9

Table 12: GI_{50} values and fold sensitization to IGF-1R inhibition in prostate cancer cell lines

Table shows GI_{50} concentration of IGF-1R inhibitor in control or RAD51_7 siRNA-transfected cells. The final column shows the fold sensitization of prostate cancer cells to IGF-1R inhibition, calculated as a ratio of GI_{50} value for control AllStars (AS) transfectants to RAD51 depleted cells. NA = not achieved.

Thus, DU145 and 22Rv1 prostate cancer cells showed sensitization to IGF-1R inhibition following RAD51 depletion. Both of these prostate cancer cell lines are PTEN wild type (**Figure 27**). This suggests a possible link between PTEN status and the ability of RAD51 depletion to affect sensitivity to IGF-1R inhibition. Given that at least 50% of prostate cancers retain wild-type PTEN, these findings suggest relevance to the majority of clinical cases of prostate cancer (Hollander *et al.*, 2011). An association between PTEN status and the ability of a screen hit to regulate AZ12253801 sensitivity was also found by another member of our laboratory, Dr. Shan Gao. In that case, sensitivity to AZ12253801 was enhanced in PTEN wild-type cells by depletion of DVL3, a WNT component that was found to regulate IGF signaling via the RAS-MEK-ERK pathway. This raised the possibility that RAD51 way also have a novel role in influencing IGF-1R signaling.

5.2.4 Investigating the effects of RAD51 depletion on IGF-1 signalling

Signalling via IGF-1R involves multiple adaptors and kinases including IRS-1-PI3K–AKT and RAS-RAF-ERK1 (Chitnis *et al.*, 2008). PTEN is an important regulator of the PI3K–AKT pathway, dephosphorylating phosphotidylinositol -3,4,5-triphosphate (PIP_3), and thus suppressing activation of PDK and subsequently AKT that acts to regulate cell growth and survival (Maehama and Dixon, 1998). DU145 and 22Rv1 cells, both PTEN wild-type, showed sensitization to IGF-1R inhibition following RAD51 depletion (**Figure 26 and 29**). Both DU145 and 22Rv1 also showed low basal levels of phosphorylated AKT and detectable basal levels of phosphorylated ERK 1/2 (**Figure 27**). It is possible that RAD51 depletion might alter the expression or phosphorylation of key components of the IGF-1R signalling pathways, thus providing a potential explanation for the observed sensitization to IGF-1R inhibition.

To investigate whether RAD51 depletion was affecting the activation status of components of the IGF axis, DU145 cells were transfected with control or RAD51_7 siRNA and 24 hours later were serum starved. The following day, cells were treated with solvent or 50 nM IGF-1 for 15 minutes, and lysates were analysed by immunoblotting for phosphorylated IGF-1R, AKT and ERK1/2 (**Figure 30**). Control transfected cells showed IGF-1 induced IGF-1R autophosphorylation on tyrosines 1135 and 1136 of the IGF-1R beta subunit. Downstream of IGF-1R activation, control transfected cells showed IGF-1 induced phosphorylation of Ser473 of AKT and Thr202/Tyr204 of ERK 1/2 (**Figure 30**). IGF-1R depleted cells showed markedly reduced phosphorylation of IGF-1R and AKT, although no change in phospho-ERK1/2 (**Figure 30**). Cells that were depleted of RAD51 showed a similar pattern of IGF-1 induced activation of phospho-IGF-1R, phospho-AKT and phospho-ERK 1/2 to

that observed in control cells (**Figure 30**). Furthermore, the level of expression of IGF-1R, AKT and ERK 1/2 did not change following RAD51 depletion when compared to control transfected cells (**Figure 30**). This suggests that RAD51 depletion did not affect IGF-1R activation and downstream signalling via the IRS-1-PI3K-AKT or RAS-RAF-MAPK-ERK pathways.

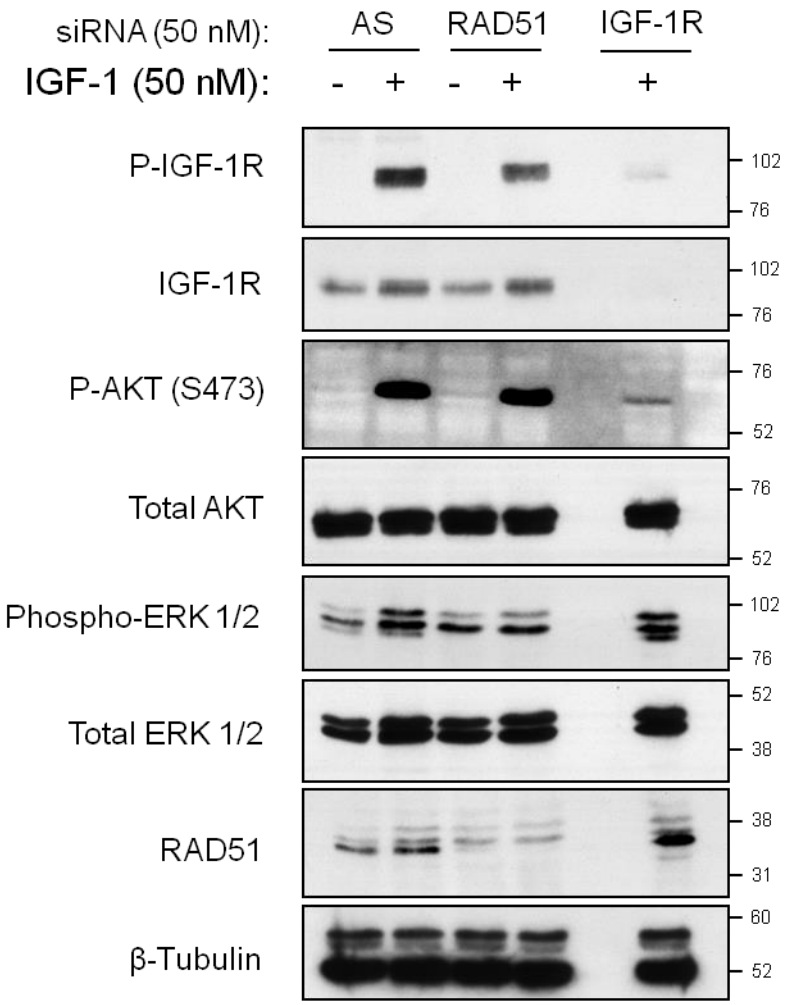


Figure 30: Investigating RAD51 depletion affects on IGF-induced signalling

DU145 cells were seeded at one million cells in a 10 cm dish, the following day forward transfected with AllStars (AS) non-silencing control or RAD51_7 siRNA and 24 hours following transfection cells were serum starved. Cells were treated with solvent control or 50 nM IGF-1 for 15 minutes. Lysates were separated by SDS-PAGE and immunoblotted for phospho-IGF-1R, phospho-AKT, phospho-ERK 1/2, RAD51 (to confirm depletion of target protein) and β-tubulin. IGF-1R depleted lysates, treated with IGF-1 served as a control. Similar results were obtained in two additional independent experiments.

5.2.6 Investigating the effects of BRCA2 depletion or deficiency on sensitivity to IGF-1R inhibition

Homologous recombination (HR) mediated repair of a double strand break occurs before the cell enters mitosis, in late S and G2 phase, when templates are available in the form of sister chromatids (Kass and Jasin, 2010). HR is initiated by the resection of the 5' ends by the CtIP and MNR complex which creates a 3' overhang that is coated by RPA with the help of RAD52, to prevent the formation of secondary structure (Kass and Jasin, 2010; Sung and Klein, 2006). BRCA1 is believed to play a role in the initial stages of the DNA resection process, via an interaction with CtIP regulated by CDK phosphorylation is thought to be important for resection (Kass and Jasin, 2010). RPA is displaced by RAD51 nucleofilaments that are loaded on to the 3' overhang, search the genome for homologous sequence and catalyzes the strand invasion step of HR (Esashi *et al.*, 2005; Sung and Klein, 2006). Formation of the RAD51 nucleofilament is facilitated by BRCA2, which is itself phosphorylated by CDKs in a cell cycle dependent manner (Esashi *et al.*, 2005; Sung and Klein, 2006). BRCA2 contains a series of 8 BRC motifs; within the C-terminus is the T2 domain that is capable of binding to the RAD51 nucleofilament and regulating its loading onto the DNA (Esashi *et al.*, 2007). Recently, it was shown that recruitment of RAD51 to sites of damage is also facilitated by Polo-like kinase 1 (Plk1) dependent phosphorylation of RAD51 on serine residue , which primes RAD51 for phosphorylation by casein kinase 2 (CK2), necessary for RAD51 binding to NBS1 (Yata *et al.*, 2012). **Figure 31** summarizes the initial steps of homologous recombination.

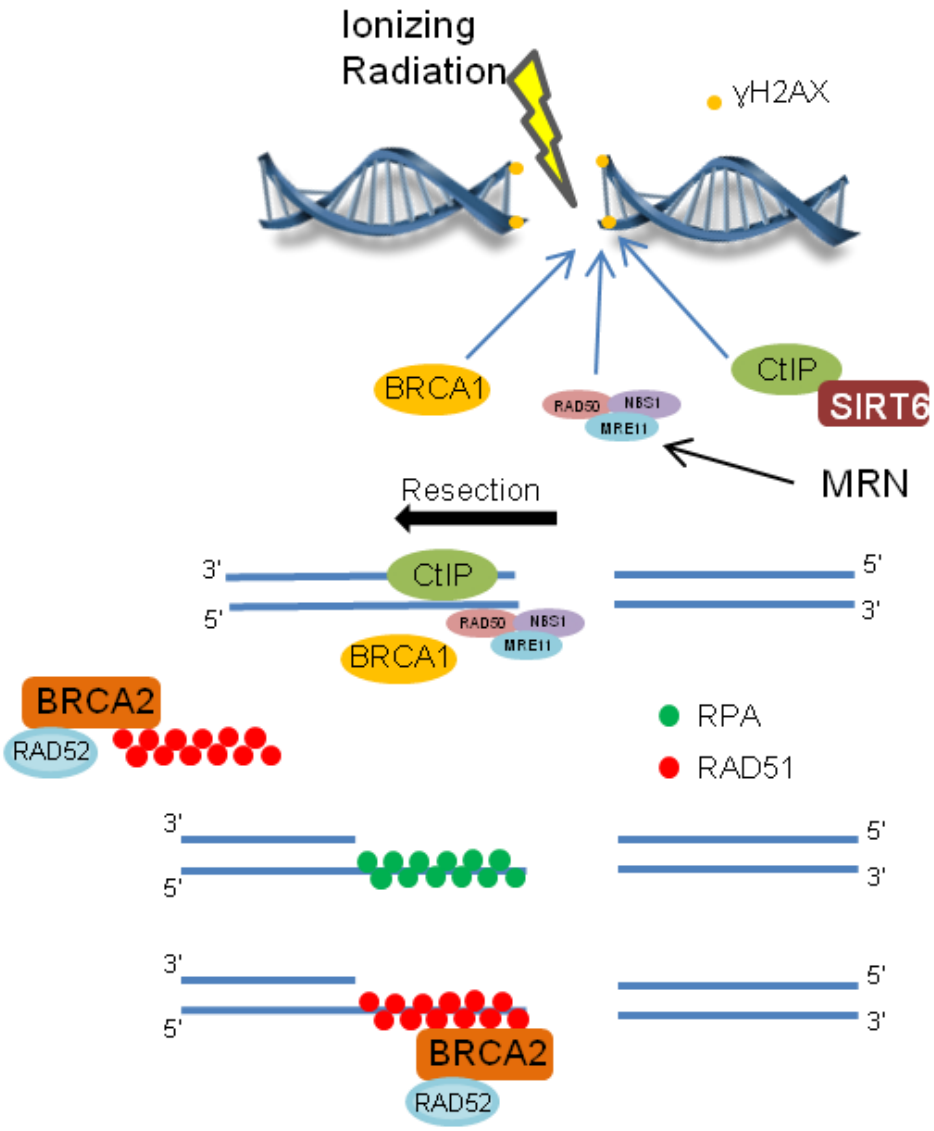


Figure 31: Initial stages of Homologous Recombination Repair

Diagram assembled from information in references cited in text.

The link between homologous recombination and IGF-1R has been reported previously by our laboratory as well as others. *Trojanek et al.*, showed that in the absence of IGF-1R activation, IRS-1 directly binds to and retains RAD51 in the cytoplasm, inhibiting homologous recombination (Trojanek *et al.*, 2003). Previous work in our laboratory used a repair assay to measure HR (Pierce *et al.*, 1999) and

found that IGF-1R depleted cells showed a modest reduction in HR (Turney *et al.*, 2012). The observed sensitization to IGF-1R inhibition in RAD51 depleted cells was surprising, because hits in synthetic sickness/lethality (SSL) screens typically reflect disruption of two separate pathways that each have the potential to compensate for defects in the other, the classic example being PARP and BRCA1/2 (Bryant *et al.*, 2005; Farmer *et al.*, 2005). However, SSL has also been described for proteins in the same pathway (Brough *et al.*, 2011; Hartman *et al.*, 2001).

If RAD51 was genuinely affecting sensitivity to IGF-1R inhibition, it would be predicted that alternative approaches to disrupt HR might have similar effect. Within the 230 proteins screened in the DNA repair library was the breast cancer susceptibility gene BRCA2, which was not identified as a hit in the screen. If RAD51 was a genuine hit, then it could be argued that BRCA2 should by also, unless BRCA2 was a false negative, ie the screen siRNAs did not deplete BRCA2 effectively. To test this possibility, two screen siRNAs were selected for further investigation, BRCA2_6, targeting the 3' end and BRCA2_7 targeting the 5' end of the BRCA2 transcript. DU145 cells were transfected using these BRCA2 siRNAs or a control siRNA, and 48 hours later RNA was isolated, reverse transcribed and analysed by real time PCR (**Figure 32**). The results showed that two of the BRCA2 siRNAs used in the screen caused depletion of BRAC2 only by 30% compared to control transfected cells. This modest effect might have been insufficient to cause any functional impairment. This did not help to clarify whether the observed effects of RAD51 depletion on AZ12253801 sensitivity was a result of impaired homologous recombination, or a new unidentified role of RAD51 independent of HR.

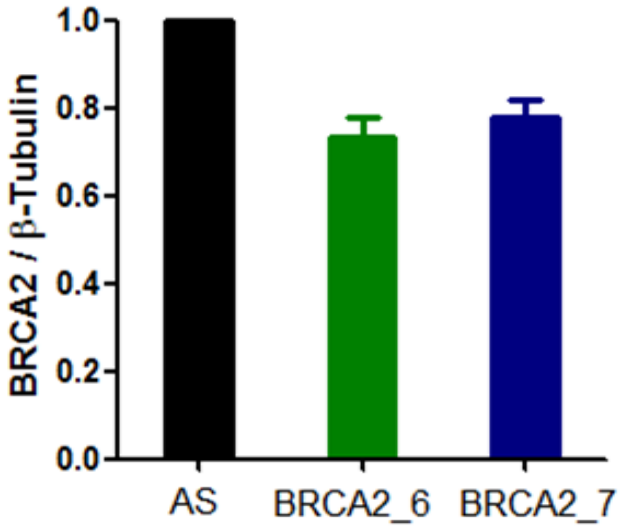


Figure 32: Assessment of BRCA2 screen siRNAs by quantitative real-time PCR

DU145 cells were transfected with 50 nM AllStars (AS) control siRNAs or two BRCA2 siRNAs that had been used in the original siRNA screen. After 48 hours, RNA was extracted, reverse transcribed and measured by qPCR to assess BRCA2 expression. Graph shows mean ± SEM of single experiment preformed in triplicate, corrected for β-tubulin expression.

To further investigate a possible link with BRCA2, an isogenic pair of DLD1 colorectal cancer cells was obtained that were either BRCA2 wild-type or BRCA2 deficient (Hucl *et al.*, 2008). These cells line model represented an alternative model in which to study the effects of impaired HR on the sensitivity to IGF-1R inhibition. **Figure 33** shows initial characterization of the DLD1 BRCA2 +/- and BRCA2 -/- cell lines in comparison with the prostate cancer cell line panel used previously (**Figure 27**). The BRCA2 wild type and null cells showed undetectable phosphorylated AKT, consistent with their PTEN wild-type status (**Figure 33**). Levels of IGF-1R, AKT, ERK 1/2, and RAD51 were similar, and the BRCA2 wild type cells contained a higher level of basal phosphorylated ERK 1/2 compared with the BRCA2 deficient cells (**Figure 33**). To investigate the HR status of the two cell lines, western blotting for BCRA2 was attempted, but BRCA2 protein was undetectable despite multiple attempts (not shown), possibly due to technical issues with the Western Blotting antibody. Given that loss of BRCA2 impairs HR (Powell and Kachnic, 2003), the effects of BRCA2

status was tested by measuring the ability of the cell lines to form RAD51 foci following ionizing radiation induced DSBs. DLD1 BRCA2 wild type cells successfully formed RAD51 foci following ionizing radiation, while RAD51 focus formation was reduced in DLD1 BRCA2 deficient cells (**Figure 34**). This confirms that the DLD1 cell lines showed the expected phenotype, and could be used to study the effects of HR status on sensitivity to IGF-1R inhibition. CellTiter Glo cell viability assay was used to assess the effects of IGF-1R inhibition in BRCA2 deficient or wild type backgrounds. **Figure 35** shows cumulative data from three independent CTG cell viability assays. DLD1 BRCA2 wild type cells showed a decrease in cell viability with increasing concentrations of IGF-1R inhibitor, and GI_{50} value of 117 nM (**Figure 35**). DLD1 BRCA2 deficient cells were more sensitive to IGF-1R inhibition measured by a shift in the dose-response curve. The GI_{50} value was 66 nM, representing a 1.8 fold sensitisation. This modest but statistically significant sensitization to IGF-1R inhibition suggests that cells can be sensitised to IGF-1R inhibition not only by depletion of RAD51 but also by BRCA2 deficiency. This raises the prospect more generally that impaired homologous recombination may affect the sensitivity to IGF-1R inhibition.

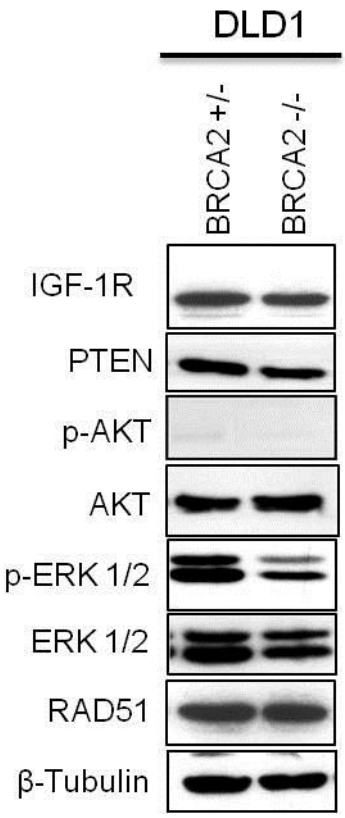


Figure 33: Characterization of DLD1 BRCA2 WT and Null cells

DLD1 BRCA2 wild type (+/-) and BRCA2 null (-/-) cells were lysed, 50 µg of lysates was separated by SDS-PAGE and immunoblotted for components of the IGF-1R axis: IGF-1R, phospho-AKT (serine 473), total AKT, phospho-ERK 1/2, total ERK 1/2, PTEN, and also BRCA2, AR and RAD51. β-Tubulin was used as a loading control. BRCA2 protein could not be detected in either cell line.

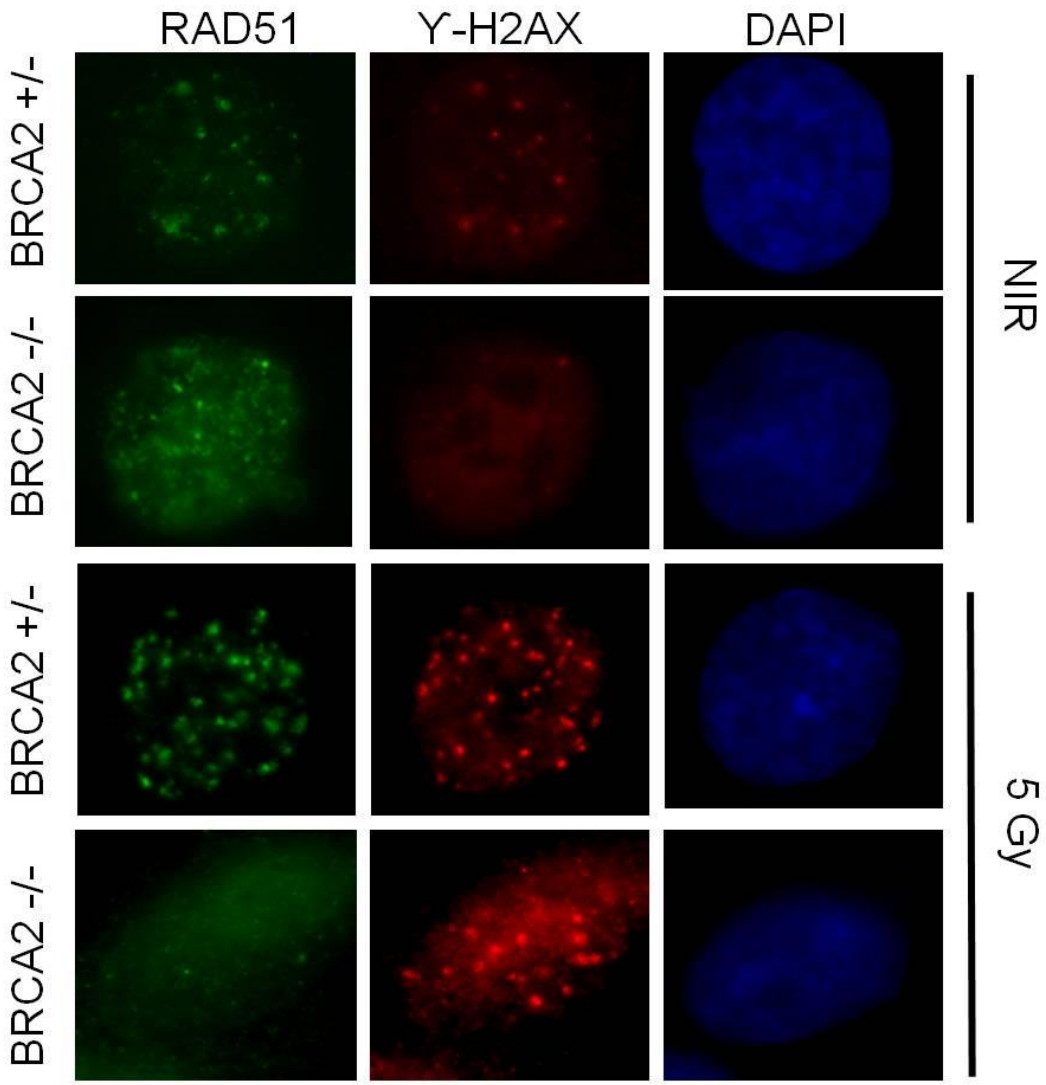


Figure 34: BRCA2 deficient cells fail to form radiation induced RAD51 foci

DLD1 BRCA2 proficient and deficient cells were either mock irradiated or irradiated at 5 Gray. Following 4 hours incubation cells were fixed, permeabilized and co-stained for RAD51 (Green) and ɣH2AX (Red). DLD1 BRCA2 wild type cells (+/-) formed radiation-induced RAD51 foci while DLD1 BRCA2 null cells (-/-) showed diffuse nuclear RAD51 with reduced focus formation. ɣH2AX was used as a marker for DNA damage. Representative images are shown.

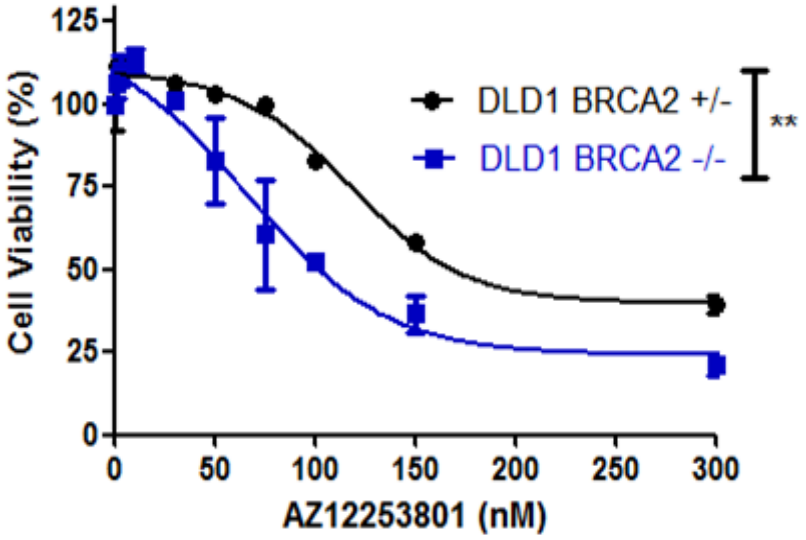


Figure 35: BRCA2 status affects sensitivity to IGF-1R inhibition

BRCA2 wild type (+/-) or BRCA2 null (-/-) DLD1 colorectal cancer cells were seeded at 2,000 cells per well in triplicate, the following day treated with IGF-1R inhibitor and 5 days later cell viability was measured by luminescence. Graphs show cell viability expressed as a percent of viability in solvent-treated cells. Results represent the mean ±SEM of three independent experiments each with triplicate data points. Two way ANOVA was used to compare the sensitivity of BRCA2 +/- or BRCA2 -/- cells to IGF-1R inhibition. ** $p<0.001$.

5.2.7 Investigating whether small molecule CDK1 inhibitor mimics effects of RAD51 depletion in enhancing sensitivity to IGF-1R inhibition

A key step in HR is the loading of the RAD51 nucelofilament onto chromatin; this is accomplished with the assistance of BRCA2 and RAD52. Prior to this, both BRCA2 and BRCA1 undergo phosphorylation on serine residues by cyclin dependent kinases (CDK) (Esashi *et al.*, 2005; Johnson *et al.*, 2009). Esashi *et al.*, showed that in addition to controlling cell cycle progression, CDK2 also phosphorylates serine 3291 of BRCA2, and this phosphorylation blocks the interaction between the C-terminus of BRCA2 and RAD51 (Esashi *et al.*, 2005; Esashi *et al.*, 2007). CDK2 has recently been shown to directly bind the c-terminus of Mre11 and this interaction is required for CtIP phosphorylation and subsequent BRCA1 interaction (Buis *et al.*, 2012). CDK2 is also capable of phosphorylating Nbs1 on a consensus CDK recognition site at serine 432, and mutation of this site leads to increased radiosensitivity (Wohlbold *et al.*, 2012). CDK1 phosphorylates BRCA1 at serines 1189, 1191, and 1497, and CDK1 depletion or inhibition causes decreased phosphorylation of Chk1 and Chk2, and impairs the ability of BRCA1 to localize at the site of DNA DSBs (Johnson *et al.*, 2009). Furthermore, the association of BRCA1 with the MRN complex is restricted to the S and G2 phases of the cell cycle, and is regulated closely by CDK1 activity (Chen *et al.*, 2008). **Figure 36** summarizes the role of CDKs in HR mediated repair of DNA DSBs.

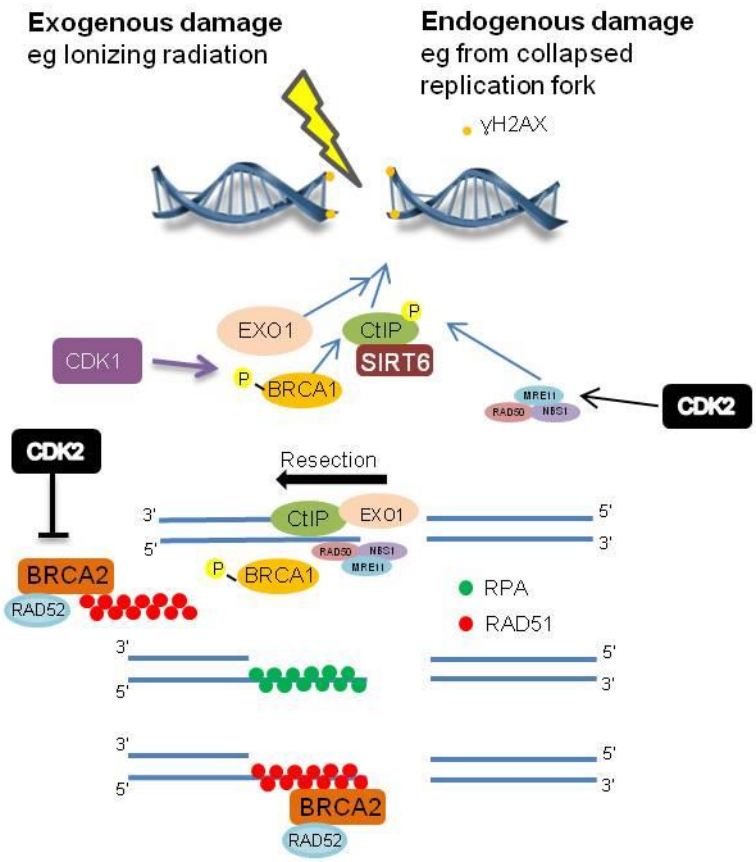


Figure 36: Effects of CDK1 in Homologous recombination DSB repair

Cyclin dependent kinases (CDKs) regulate cell cycle progression: CDK1 regulates the transition between G2 and Mitosis, while CDK2 controls progression into S and G2 phases of the cell cycle (Hochegger *et al.*, 2008). In addition to their roles in cell cycle control, CDK1 and 2 have been show to affect HR mediated repair. CDK1 is capable of phosphorylating BRCA1 on serines 1189, 1191, and 1497, which affects the ability of BRCA1 to localize at the site of damage and to interact with the MRN complex (Johnson *et al.*, 2009). CDK2 phosphorylates BRCA2 on serine 3291 and this inhibits the interaction between BRCA2 and RAD51 nucleoprotein (Esashi *et al.*, 2005; Esashi *et al.*, 2007).

Consistent with the importance of CDK1 in phosphorylating BRCA1, a small molecule CDK1 inhibitor was reported to impair HR mediated repair of DSBs (Johnson *et al.*, 2011). In that report, U2OS osteosarcoma cells treated with CDK1 inhibitor (R0-3306) showed a significant decrease in HR measured by a reporter assay, compared to control treated cells (Johnson *et al.*, 2011). Furthermore, CDK1 inhibited cells failed to properly recruit BRCA1 and RAD51 to the site of DNA DSBs following ɣ irradiation (Johnson *et al.*, 2011). Therefore, it was possible that a small

molecule CDK1 inhibitor could phenocopy the effects of RAD51 depletion in DU145 cells.

Before testing the effects of CDK1 inhibition on the sensitivity to IGF-1R inhibition, Celltiter Glo (CTG) assays were used to determine the GI_{50} concentration of the CDK1 inhibition R0-3306. Cells treated with CDK1 inhibitor showed a dose-dependent decrease in viability and the GI_{50} value was 1 μM (**Figure 37**). To check whether 1 μM CDK1 inhibitor impaired HR in DU145 cells, immunofluorescence was used to measure RAD51 focus formation. **Figure 38** shows images of cells pre-treated with solvent or CDK1 inhibitor and then irradiated. Solvent control treated DU145 cells formed RAD51 foci in response to irradiation. In cells that were pre-treated with 1 μM CDK1 inhibitor, γH2AX foci formed as in control treated cells, but there was a clear suppression of RAD51 focus formation, consistent with HR attenuation (**Figure 38**).

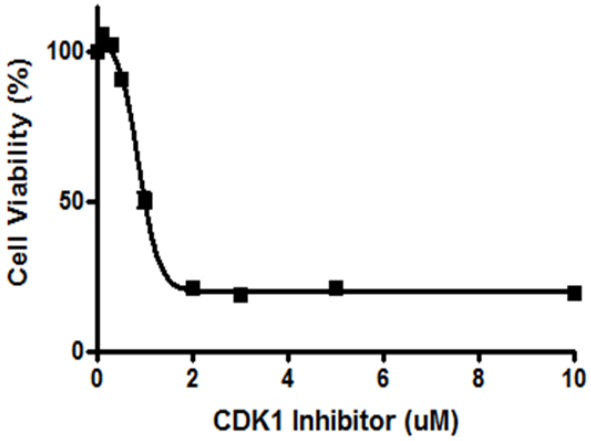


Figure 37: Effects of CDK1 inhibition on viability of DU145 prostate cancer cells
DU145 prostate cancer cells were treated with 0-10μM CDK1 inhibitor R0-3306 and cell viability was measured by luminescence 5 days later. Viability was expressed as percent survival in the absence of drug, and points represent mean ± SEM of three independent experiments, each with triplicate data points. DU145 viability decreased with increasing concentration of CDK1 inhibitor, and the GI_{50} was 1 μM.

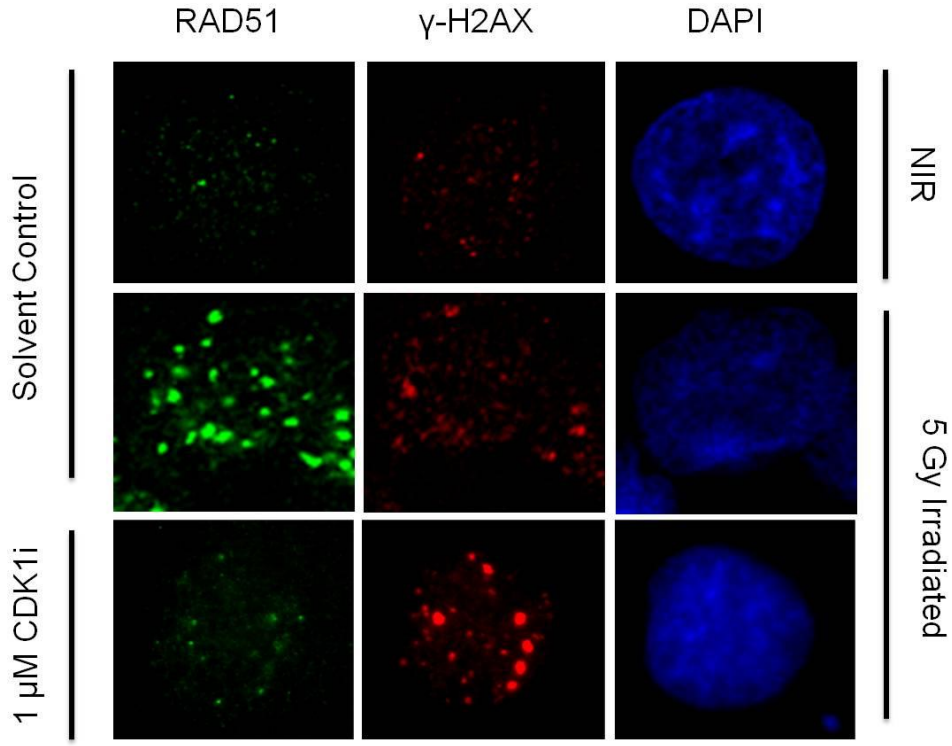


Figure 38: CDK1 inhibition impairs RAD51 focus formation
DU145 cells were seeded at 200,000 cells in 24 well plate and following day were either treated with solvent control or 1 μM CDK1 inhibitor. After 1 hour pre-treatment cells were irradiated at 5 Gy and, following 4 hours incubation cells were fixed, permeabilized and co-stained for RAD51 (Green) and γH2AX (Red) foci. DU145 cells formed radiation induced RAD51 foci while DU145 cells pre-treated with 1 μM CDK1, failed to successfully form

radiation induced RAD51 foci. γH2AX was used as a marker for cells containing damaged DNA and DAPI was used to stain nuclei.

Having confirmed that 1 μM R0-3306 suppressed RAD51 focus formation, as reported (Johnson *et al.*, 2011), this concentration of R0-3306 was used in CTG arrays to assess the effects of CDK1 inhibition on sensitivity to AZ12253801. Control treated DU145 cells treated with IGF-1R inhibitor showed a decrease in survival with increasing concentration of IGF-1R inhibitor (GI_{50} = 131 nM) (**Figure 39**). Co-treatment with CDK1 inhibitor further sensitized DU145 prostate cancer cells to IGF-1R inhibition, as calculated by the shift in GI_{50} value to 54 nM (**Figure 39**). This 2.4 fold sensitisation is similar to the results obtained using RAD51 depletion (**Table 10**), or BRCA2 deficiency (**Figure 35**). Sensitization to AZ12253801 was particularly apparent at low AZ12253801 concentrations, with a 13 fold difference in GI_{80} values (107 nM in control cells vs. 8 nM in R0-3306-treated cells). Thus CDK1 inhibition phenocopied effects of RAD51 depletion in sensitizing prostate cancer cells to AZ12253801.

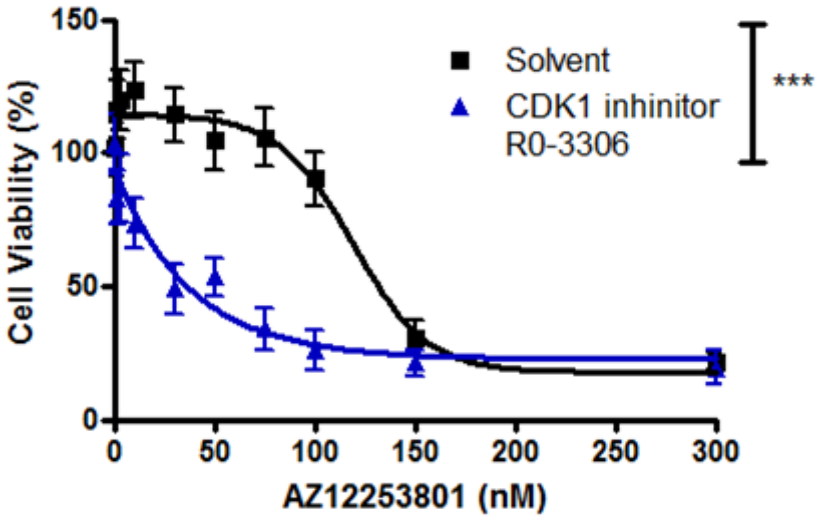


Figure 39: CDK1 inhibition sensitises DU145 prostate cancer cells to IGF-1R inhibition

DU145 prostate cancer cells were treated with 0-300 nM AZ12253801 in the presence or absence of 1 μM CDK1 inhibitor R0-3306 and cell viability was measured by luminescence 5 days later. Cell viability was expressed as percent survival in the absence of AZ12253801. Graph represents mean ±SEM viability from 3 independent experiments, each with triplicate data points. The pooled data were curve-fitted to allow extrapolation of GI_{50} values. DU145 viability decreased with increasing concentration of IGF-1R inhibitor alone (GI_{50} = 131 nM), while addition of CDK1 inhibitor (1 μM) increased the sensitivity of DU145 cells to IGF-1R inhibitor (GI_{50} = 54 nM). *** $p<0.001$ by two-way ANOVA.

5.3 Discussion

The work presented in this chapter validated RAD51 as a hit in the screen for proteins whose depletion increases the sensitivity of DU145 prostate cancer cells to IGF-1R inhibition sensitisation was shown by two independent assays: clonogenic assay and cell viability assay. Subsequent assays in a panel of prostate cancer cells lines: PC3, LNCaP and 22RV1, suggested that RAD51 influences AZ12253801 sensitivity in PTEN wild-type prostate cancer cells. Previous reports have shown a link between PTEN status and homologous recombination. One report in glioblastomas observed in PTEN null tumours decreased RAD51 expression and impaired homologous recombination (Mukherjee and Karmakar, 2012). However, in this project, differences in RAD51 protein levels were not observed to vary with PTEN status in the panel of prostate cancer cell lines. This finding is consistent with a previous report showing that PTEN status does not affect RAD51 mRNA or protein expression in primary prostate cancer cells (Fraser *et al.*, 2011). Moreover, PTEN deficient breast cancers, acting via activated AKT, exhibited decreased nuclear CHK1-RAD51 interaction and the accumulation of DSBs (Jia *et al.*, 2012; Puc *et al.*, 2005). AKT1 itself has also been shown to suppress HR via a cytoplasmic retention of BRCA1 and RAD51 (Plo *et al.*, 2008). Future work could further investigate the effects of PTEN status on RAD51 mediated sensitisation to IGF-1R inhibition using an isogenic PTEN cell line model.

Further work presented here used two additional approaches to suppress HR. The first was a BRCA2 wild-type and BRCA2 deficient isogenic cell line model. BRCA2 deficient cells were more sensitive to IGF-1R inhibition than BRCA2 proficient cells. This suggests that impaired HR could be a factor mediating sensitivity to IGF-1R inhibition. To further investigate this effect, a small molecule inhibitor of CDK1 was

used to impair HR (Johnson *et al.*, 2009; Johnson *et al.*, 2011). Pre-treatment with CDK1 inhibitor phenocopied the effects of RAD51 depletion in sensitising DU145 prostate cancer cells to AZ12253801. Taken together the data thus far suggest that the combined inhibition of CDK1 and IGF-1R could be tested in PTEN wild-type prostate cancer models *in vivo*. Given that at least 50% of prostate cancers retain wild-type PTEN (Hollander *et al.*, 2011), these findings suggest relevance to the majority of clinical cases of prostate cancer.

Finally, the work presented here was carried out in the absence of exogenous damage, suggesting that the 3 different approaches to block HR may have impacted on repair of any DSBs arising from endogenous sources such as stalled replication forks, which are repaired by HR (Saleh-Gohari *et al.*, 2005). It is possible that IGFs are affecting HR-mediated DSB repair via regulation of cyclin D1 and CDKs, both of which have been shown to affect HR (Frederick and Wood, 2004; Jirawatnotai *et al.*, 2011; Johnson *et al.*, 2011; Warsito *et al.*, 2012), or by some other mechanism as yet unidentified. Thus the observed synthetic sickness may have arisen from the combined effects of IGF-1R inhibition and HR suppression (via RAD51 depletion, BRCA2 deficiency or CDK1 inhibition) to block repair of endogenous DSBs. In future it will be informative to perform additional studies involving exogenous damaging agents, to guide the possible use of combination treatment with IGF-1R and CKD1 or PARP inhibitors with irradiation.

Chapter 6: Conclusion and Future Directions

The work presented here focused on the role of the IGF axis in the response to DNA damage, with the aim of informing the clinical use of IGF-1R inhibitors in combination with conventional chemotherapy and radiotherapy in prostate cancer. Based on previous work (Macaulay *et al.*, 2001), the initial approach focused on identifying whether IGF-1R signalling can influence ATM activation and function via AKT. However, insufficient evidence was generated to support this hypothesis in prostate cancer cells, and therefore this study was discontinued. Subsequently, two further investigations were taken on in parallel, to explore the contribution of IGF-1R in prostate cancer. The first was to understand the function of nuclear IGF-1R by identifying potential nuclear binding partners using mass spectrometry. The second approach was to investigate RAD51 as a hit in a screen for proteins that affect sensitivity to IGF-1R inhibition.

The work presented in **Chapter 4** confirmed previous reports from our group and another laboratory, showing the presence of full-length α and β subunits of the IGF-1R in the nucleus of prostate cancer cells (Aleksic *et al.*, 2010; Sehat *et al.*, 2010). After optimization of nuclear extraction and large scale immunoprecipitation, MS analysis identified several transcription factors as candidate IGF-1R binding partners in cells growing in complete medium, or treated with IGF-1 or exposed to irradiation-induced DNA damage. Identification of transcription factors suggests a possible role for nuclear IGF-1R in the regulation of transcription via binding to chromatin. This is consistent with the known role of nuclear EGFR (Massie and Mills, 2006; Wang *et al.*, 2010) and with a recent report showing that nuclear IGF-1R binds to the transcription

factor LEF1 and increases TCF/LEF promoter activity and expression of cyclin D1 and axin2 (Warsito *et al.*, 2012).

Due to time limitations it was possible to perform preliminary validation on only one candidate binding partner. TF II-I a general transcription factor that binds to and functions via the Initiator element (Inr) (Roy *et al.*, 1991). The activity of TF II-I is influenced by post translational modifications such as SUMOylation (Zhao *et al.*, 2004b) and phosphorylation by EGFR on tyrosine 248 (Y248) (Cheriyath *et al.*, 2002; Roy, 2007). Further, this EGFR induced Y248 phosphorylation is important for TF II-I association with ERKs, and given that ERKs do not have an intrinsic nuclear localization signal but translocate to the nucleus upon activation, it has postulated that ERKs are transported to the nucleus via direct interaction with TFII-I (Roy, 2012). In future work, it will be interesting to explore whether TF II-I can similarly chaperone IGF-1R to the nucleus. To study the apparent IGF-induced phosphorylation of TF II-I, phospho-peptide MS analysis, mutagenesis and immunofluorescence staining may prove useful to understand the functional significance of this post-translational modification. Plasmids encoding the wild-type or Y248F (EGFR phospho-site mutant) TF II-I are already commercially available, but plasmids encoding mutants at other phosphorylation site(s) would need to be generated.

Data presented in this thesis, together with published work, suggest that nuclear IGF-1R might be an additional molecular mechanism by which IGF-1R promotes cell proliferation and thus contributes to the malignant phenotype. A further understanding of the biology of nuclear IGF-1R might reveal new targets for treatment, and secondly may clarify whether nuclear IGF-1R has the potential to be a predictive or prognostic biomarker in prostate cancers. Work from our lab showed that nuclear IGF-1R is associated with adverse prognosis in clear cell renal cancer

(Aleksic *et al.*, 2010). More recent studies in hepatocellular carcinoma (HCC) showed increased levels of nuclear IGF-1R following treatment with EGFR inhibitor Gefitinib, suggesting that nuclear IGF-1R translocation may contribute to Gefitinib resistance (Bodzin *et al.*, 2012). Another recent study, in a small group of sarcoma patients treated with IGF-1R monoclonal antibodies, found that exclusively nuclear IGF-1R was associated with response to IGF-1R antibody, with better progression free survival and overall survival (Asmane *et al.*, 2012). This raises the possibility that nuclear IGF-1R may help to identify sarcoma patients who may benefit from treatment with anti-IGF-1R antibodies. If this applies more widely to prostate cancer and other tumor types, this could be extremely valuable clinically as a predictive biomarker, the lack of which is currently the major obstacle to effective clinical use of IGF-1R inhibitory drugs (Basu *et al.*, 2011; Yee, 2012).

The final project investigated another aspect of the link between IGF-1R and the response to DNA repair, based on a siRNA screen conducted by our laboratory in collaboration with Professor Alan Ashworth and Dr. Chris Lord at Breakthrough Breast Cancer. The aim was to identify proteins that when depleted increased the sensitivity of DU145 prostate cancer cells to IGF-1R inhibition. Because of the interest of our group in the possible involvement of IGF-1R in the DNA damage response in prostate cancer (Rochester *et al.*, 2005; Turney *et al.*, 2012), the screen included a library of siRNAs to deplete DNA repair proteins. RAD51, a key protein in homologous recombination repair, was one of the proteins identified by this screen, and was the focus of the work presented in **Chapter 5**. The identification of RAD51 as a protein that mediates resistance to IGF-1R inhibition is interesting given previous work from our laboratory and others showing that the IGF-1R axis can influence homologous recombination (Trojanek *et al.*, 2006; Trojanek *et al.*, 2003; Turney *et al.*, 2012). Typically, synthetic interactions are reported to occur between

genes in separate but compensatory pathways, such as BRCA2 and PARP (Bryant *et al.*, 2005; Farmer *et al.*, 2005), but can also occur between genes in the same biochemical pathway (Brough *et al.*, 2011). The siRNA screen was performed in the absence of exogenous damage, but it is well known that DSBs can arise endogenously as a result of reactive oxygen species or endogenous reactive chemicals, leading to stalling and collapse of replication forks, which are repaired by homologous recombination (De Bont and van Larebeke, 2004; Errico and Costanzo, 2012; Jones and Petermann, 2012). The initial report of cell cycle dependent phosphorylation of BRCA2 (Esashi *et al.*, 2005; Esashi *et al.*, 2007) has been followed by recent data describing a complex interplay between proteins involved in cell cycle regulation and HR (Jirawatnotai *et al.*, 2011; Johnson *et al.*, 2011; Shechter *et al.*, 2004; Yata *et al.*, 2012). The tight regulation of HR during the cell cycle ensures that the integrity of the genome is maintained during replication, a time when cells are particularly vulnerable to DNA damage leading to mutations. It is possible that the ability of IGF-1R to influence cell cycle progression could directly or indirectly influence homologous recombination repair. If IGF-1R inhibitor AZ12253801 inhibits HR repair of endogenous DSBs arising as a consequence of stalled replication forks, it is possible that this defect would be exacerbated by RAD51 depletion, potentially explaining why RAD51 was identified as a screen hit. Preliminary experiments have tested whether AZ12253801 caused a delay in repair of endogenous damage, comparable to the delay in repair of irradiation-induced DSBs that follow IGF-1R depletion or inhibition (Turney *et al.*, 2012), Chitnis *et al.* in preparation). Indeed, while DU145 cells showed occasional ɣH2AX foci in undamaged cells, there was clear accumulation of ɣH2AX foci after 24hr of AZ12253801 treatment, compared with solvent-treated controls. It would be important to check whether IGF-1R depletion has similar effects, to link this result firmly to the IGF-1R. If confirmed,

these data suggest that IGF-1R inhibition not only delays repair of radiation-induced DSBs (Turney *et al.*, 2012), but also of endogenous DSBs.

Subsequent work tested whether other approaches to impair HR could sensitize prostate cancer cells to IGF-1R inhibition. Sensitivity to AZ12253801 was enhanced in BRCA2 null cells, compared with BRCA2 proficient isogenic cells. Furthermore, a small molecule inhibitor of CDK1 phenocopied the effects of RAD51 depletion and sensitized DU145 prostate cancer cells to IGF-1R inhibition. These findings suggest, firstly, that prostate cancer patients whose tumours are BRCA deficient may respond to IGF-1R inhibition. Secondly, these results may help to guide development of novel treatments. The data shown here would support further evaluation of the combination of IGF-1R and CDK1 inhibitors, and may also help to inform use of IGF-1R inhibitors with DNA-damaging chemotherapy.

The use of DNA damaging agents in cancer therapy is well established. For example, platinum agents, including cisplatin, carboplatin and oxaliplatin, cause DNA intra-strand and interstrand cross links which ultimately lead to induction of apoptosis. Another DNA damaging agent is gemcitabine, a nucleoside analog that stalls replication forks and requires functional HR for their repair (Rosell *et al.*, 2006). Indeed, IGF-1R mAb has recently been showed to sensitize pancreatic cancer cells to gemcitabine (Kawanami *et al.*, 2012). Platinum agents and gemcitabine are not used clinically in the management of prostate cancer, although radiotherapy is an important treatment both for localised and metastatic disease. Taken together with the data presented here, inhibition of IGF-1R and CDK1 in combination with a DNA damaging agent, either chemotherapy or radiotherapy, would be the next logical step to explore *in vitro* and *in vivo*, with the ultimate aim of translating this work to clinical trials in prostate cancer.

Bibliography

Adams TE, Epa VC, Garrett TP, Ward CW (2000). Structure and function of the type 1 insulin-like growth factor receptor. *Cell Mol Life Sci* **57:** 1050-93.

Ahn JY, Rong R, Liu X, Ye K (2004). PIKE/nuclear PI 3-kinase signaling mediates the antiapoptotic actions of NGF in the nucleus. *EMBO J* **23:** 3995-4006.

Ahnesorg P, Smith P, Jackson SP (2006). XLF interacts with the XRCC4-DNA ligase IV complex to promote DNA nonhomologous end-joining. *Cell* **124:** 301-13.

Aleksic T, Chitnis MM, Perestenko OV, Gao S, Thomas PH, Turner GD *et al* (2010). Type 1 insulin-like growth factor receptor translocates to the nucleus of human tumor cells. *Cancer Research* **70:** 6412-9.

Alessi DR, Caudwell FB, Andjelkovic M, Hemmings BA, Cohen P (1996). Molecular basis for the substrate specificity of protein kinase B; comparison with MAPKAP kinase-1 and p70 S6 kinase. *FEBS Lett* **399:** 333-8.

Alison MR, Sarraf CE (1992). Apoptosis: a gene-directed programme of cell death. *J R Coll Physicians Lond* **26:** 25-35.

All-Ericsson C, Girnita L, Seregard S, Bartolazzi A, Jager MJ, Larsson O (2002). Insulin-like growth factor-1 receptor in uveal melanoma: a predictor for metastatic disease and a potential therapeutic target. *Invest Ophthalmol Vis Sci* **43:** 1-8.

Arteaga CL, Kitten LJ, Coronado EB, Jacobs S, Kull FC, Jr., Allred DC *et al* (1989). Blockade of the type I somatomedin receptor inhibits growth of human breast cancer cells in athymic mice. *J Clin Invest* **84:** 1418-23.

Ashworth T, Roy AL (2009). Phase specific functions of the transcription factor TFII-I during cell cycle. *Cell Cycle* **8:** 596-605.

Asmane I, Watkin E, Alberti L, Duc A, Marec-Berard P, Ray-Coquard I *et al* (2012). Insulin-like growth factor type 1 receptor (IGF-1R) exclusive nuclear staining: A predictive biomarker for IGF-1R monoclonal antibody (Ab) therapy in sarcomas. *Eur J Cancer* **48:** 3027-35.

Aus G, Damber JE, Hugosson J (2005). Prostate biopsy and anaesthesia: an overview. *Scand J Urol Nephrol* **39:** 124-9.

Bajgelman MC, Strauss BE (2006). The DU145 human prostate carcinoma cell line harbors a temperature-sensitive allele of p53. *Prostate* **66:** 1455-62.

Baserga R (1999). The IGF-I receptor in cancer research. *Exp Cell Res* **253:** 1-6.

Baserga R, Resnicoff M, Dews M (1997). The IGF-I receptor and cancer. *Endocrine* **7:** 99-102.

Basu B, Olmos D, de Bono JS (2011). Targeting IGF-1R: throwing out the baby with the bathwater? *Br J Cancer* **104:** 1-3.

Benecke H, Flier JS, Moller DE (1992). Alternatively spliced variants of the insulin receptor protein. Expression in normal and diabetic human tissues. *J Clin Invest* **89:** 2066-70.

Bjorndahl M, Cao R, Nissen LJ, Clasper S, Johnson LA, Xue Y *et al* (2005). Insulin-like growth factors 1 and 2 induce lymphangiogenesis in vivo. *Proc Natl Acad Sci U S A* **102:** 15593-8.

Bodzin AS, Wei Z, Hurtt R, Gu T, Doria C (2012). Gefitinib resistance in HCC mahlavu cells: upregulation of CD133 expression, activation of IGF-1R signaling pathway, and enhancement of IGF-1R nuclear translocation. *J Cell Physiol* **227:** 2947-52.

Bozulic L, Hemmings BA (2009). PIKKing on PKB: regulation of PKB activity by phosphorylation. *Curr Opin Cell Biol* **21:** 256-61.

Brough R, Frankum JR, Costa-Cabral S, Lord CJ, Ashworth A (2011). Searching for synthetic lethality in cancer. *Curr Opin Genet Dev* **21:** 34-41.

Bryant HE, Schultz N, Thomas HD, Parker KM, Flower D, Lopez E *et al* (2005). Specific killing of BRCA2-deficient tumours with inhibitors of poly(ADP-ribose) polymerase. *Nature* **434:** 913-7.

Bubendorf L, Schopfer A, Wagner U, Sauter G, Moch H, Willi N *et al* (2000). Metastatic patterns of prostate cancer: an autopsy study of 1,589 patients. *Hum Pathol* **31:** 578-83.

Buck E, Gokhale PC, Koujak S, Brown E, Eyzaguirre A, Tao N *et al* (2010). Compensatory insulin receptor (IR) activation on inhibition of insulin-like growth factor-1 receptor (IGF-1R): rationale for cotargeting IGF-1R and IR in cancer. *Mol Cancer Ther* **9:** 2652-64.

Buck E, Mulvihill M (2011). Small molecule inhibitors of the IGF-1R/IR axis for the treatment of cancer. *Expert Opin Investig Drugs* **20:** 605-21.

Buck E, Mulvihill M (2012). Small molecule inhibitors of the IGF-1R/IR axis for the treatment of cancer. *Expert Opin Investig Drugs* **20:** 605-21.

Buis J, Stoneham T, Spehalski E, Ferguson DO (2012). Mre11 regulates CtIP-dependent double-strand break repair by interaction with CDK2. *Nat Struct Mol Biol* **19:** 246-52.

Buratowski S (2009). Progression through the RNA polymerase II CTD cycle. *Mol Cell* **36:** 541-6.

Calsou P, Delteil C, Frit P, Drouet J, Salles B (2003). Coordinated assembly of Ku and p460 subunits of the DNA-dependent protein kinase on DNA ends is necessary for XRCC4-ligase IV recruitment. *J Mol Biol* **326:** 93-103.

Canman CE, Lim DS, Cimprich KA, Taya Y, Tamai K, Sakaguchi K *et al* (1998). Activation of the ATM kinase by ionizing radiation and phosphorylation of p53. *Science* **281:** 1677-9.

Carlson H, Ota S, Song Y, Chen Y, Hurlin PJ (2002). Tbx3 impinges on the p53 pathway to suppress apoptosis, facilitate cell transformation and block myogenic differentiation. *Oncogene* **21:** 3827-35.

Carmeliet P, Jain RK (2000). Angiogenesis in cancer and other diseases. *Nature* **407:** 249-57.

Carnero A (2010). The PKB/AKT pathway in cancer. *Curr Pharm Des* **16:** 34-44.

Carver BS, Chapinski C, Wongvipat J, Hieronymus H, Chen Y, Chandarlapaty S *et al* (2011). Reciprocal feedback regulation of PI3K and androgen receptor signaling in PTEN-deficient prostate cancer. *Cancer Cell* **19:** 575-86.

Castedo M, Perfettini JL, Roumier T, Andreau K, Medema R, Kroemer G (2004). Cell death by mitotic catastrophe: a molecular definition. *Oncogene* **23:** 2825-37.

Chan JM, Stampfer MJ, Giovannucci E, Gann PH, Ma J, Wilkinson P *et al* (1998). Plasma insulin-like growth factor-I and prostate cancer risk: a prospective study. *Science* **279:** 563-6.

Chen BP, Uematsu N, Kobayashi J, Lerenthal Y, Krempler A, Yajima H *et al* (2007). Ataxia telangiectasia mutated (ATM) is essential for DNA-PKcs phosphorylations at the Thr-2609 cluster upon DNA double strand break. *J Biol Chem* **282:** 6582-7.

Chen L, Nievera CJ, Lee AY, Wu X (2008). Cell cycle-dependent complex formation of BRCA1.CtIP.MRN is important for DNA double-strand break repair. *J Biol Chem* **283:** 7713-20.

Cheriyath V, Desgranges ZP, Roy AL (2002). c-Src-dependent transcriptional activation of TFII-I. *J Biol Chem* **277:** 22798-805.

Cheriyath V, Roy AL (2000). Alternatively spliced isoforms of TFII-I. Complex formation, nuclear translocation, and differential gene regulation. *J Biol Chem* **275:** 26300-8.

Cheriyath V, Roy AL (2001). Structure-function analysis of TFII-I. Roles of the N-terminal end, basic region, and I-repeats. *J Biol Chem* **276:** 8377-83.

Chitnis MM, Yuen JS, Protheroe AS, Pollak M, Macaulay VM (2008). The type 1 insulin-like growth factor receptor pathway. *Clin Cancer Res* **14:** 6364-70.

Chlenski A, Nakashiro K, Ketels KV, Korovaitseva GI, Oyasu R (2001). Androgen receptor expression in androgen-independent prostate cancer cell lines. *Prostate* **47:** 66-75.

Chu K, Cheng CJ, Ye X, Lee YC, Zurita AJ, Chen DT *et al* (2008). Cadherin-11 promotes the metastasis of prostate cancer cells to bone. *Mol Cancer Res* **6:** 1259-67.

Clemmons DR (2007). Modifying IGF1 activity: an approach to treat endocrine disorders, atherosclerosis and cancer. *Nat Rev Drug Discov* **6:** 821-33.

Collett-Solberg PF, Cohen P (1996). The role of the insulin-like growth factor binding proteins and the IGFBP proteases in modulating IGF action. *Endocrinol Metab Clin North Am* **25:** 591-614.

Confalonieri S, Salcini AE, Puri C, Tacchetti C, Di Fiore PP (2000). Tyrosine phosphorylation of Eps15 is required for ligand-regulated, but not constitutive, endocytosis. *J Cell Biol* **150:** 905-12.

Cortot AB, Repellin CE, Shimamura T, Capelletti M, Zejnullahu K, Ercan D *et al* (2012). Resistance to Irreversible EGFR Tyrosine Kinase Inhibitors through a Multistep Mechanism Involving the IGF1R Pathway. *Cancer Res*.

Culig Z, Hobisch A, Cronauer MV, Radmayr C, Hittmair A, Zhang J *et al* (1996). Regulation of prostatic growth and function by peptide growth factors. *Prostate* **28:** 392-405.

Damber JE (2004). Decreasing mortality rates for prostate cancer: possible role of hormonal therapy? *BJU Int* **93:** 695-701.

Damber JE, Aus G (2008). Prostate cancer. *Lancet* **371:** 1710-21.

Danial NN (2008). BAD: undertaker by night, candyman by day. *Oncogene* **27 Suppl 1:** S53-70.

De Bont R, van Larebeke N (2004). Endogenous DNA damage in humans: a review of quantitative data. *Mutagenesis* **19:** 169-85.

De Valck D, Jin DY, Heyninck K, Van de Craen M, Contreras R, Fiers W *et al* (1999). The zinc finger protein A20 interacts with a novel anti-apoptotic protein which is cleaved by specific caspases. *Oncogene* **18:** 4182-90.

DeChiara TM, Efstratiadis A, Robertson EJ (1990). A growth-deficiency phenotype in heterozygous mice carrying an insulin-like growth factor II gene disrupted by targeting. *Nature* **345:** 78-80.

Denham JW, Steigler A, Lamb DS, Joseph D, Turner S, Matthews J *et al* (2011). Short-term neoadjuvant androgen deprivation and radiotherapy for locally advanced prostate cancer: 10-year data from the TROG 96.01 randomised trial. *Lancet Oncol* **12:** 451-9.

Denicourt C, Dowdy SF (2004). Cip/Kip proteins: more than just CDKs inhibitors. *Genes Dev* **18:** 851-5.

Denley A, Cosgrove LJ, Booker GW, Wallace JC, Forbes BE (2005). Molecular interactions of the IGF system. *Cytokine Growth Factor Rev* **16:** 421-39.

Denton D, Nicolson S, Kumar S (2012). Cell death by autophagy: facts and apparent artefacts. *Cell Death Differ* **19:** 87-95.

Desgranges ZP, Ahn J, Lazebnik MB, Ashworth T, Lee C, Pestell RC *et al* (2005). Inhibition of TFII-I-dependent cell cycle regulation by p53. *Mol Cell Biol* **25:** 10940-52.

Desgranges ZP, Roy AL (2006). TFII-I: connecting mitogenic signals to cell cycle regulation. *Cell Cycle* **5:** 356-9.

Desjardins R, Smetana K, Steele WJ, Busch H (1963). Isolation of Nucleoli of the Walker Carcinosarcoma and Liver of the Rat Following Nuclear Disruption in a French Pressure Cell. *Cancer Res* **23:** 1819-23.

Dickey JS, Redon CE, Nakamura AJ, Baird BJ, Sedelnikova OA, Bonner WM (2009). H2AX: functional roles and potential applications. *Chromosoma* **118:** 683-92.

Dittmann K, Mayer C, Fehrenbacher B, Schaller M, Raju U, Milas L *et al* (2005). Radiation-induced epidermal growth factor receptor nuclear import is linked to activation of DNA-dependent protein kinase. *J Biol Chem* **280:** 31182-9.

Djiogue S, Nwabo Kamdje AH, Vecchio L, Kipanyula MJ, Farahna M, Aldebasi YH *et al* (2012). Insulin resistance and cancer: the role of insulin and insulin-like growth factors. *Endocr Relat Cancer*.

Downward J (2004). PI 3-kinase, Akt and cell survival. *Semin Cell Dev Biol* **15:** 177-82.

Du K, Montminy M (1998). CREB is a regulatory target for the protein kinase Akt/PKB. *J Biol Chem* **273:** 32377-9.

Du LQ, Wang Y, Wang H, Cao J, Liu Q, Fan FY (2010). Knockdown of Rad51 expression induces radiation- and chemo-sensitivity in osteosarcoma cells. *Med Oncol*.

Dunn SE, Hardman RA, Kari FW, Barrett JC (1997). Insulin-like growth factor 1 (IGF-1) alters drug sensitivity of HBL100 human breast cancer cells by inhibition of apoptosis induced by diverse anticancer drugs. *Cancer Research* **57:** 2687-93.

Echevarria W, Leite MF, Guerra MT, Zipfel WR, Nathanson MH (2003). Regulation of calcium signals in the nucleus by a nucleoplasmic reticulum. *Nat Cell Biol* **5:** 440-6.

Eggenschwiler J, Ludwig T, Fisher P, Leighton PA, Tilghman SM, Efstratiadis A (1997). Mouse mutant embryos overexpressing IGF-II exhibit phenotypic features of the Beckwith-Wiedemann and Simpson-Golabi-Behmel syndromes. *Genes Dev* **11:** 3128-42.

Egloff S, Zaborowska J, Laitem C, Kiss T, Murphy S (2012). Ser7 phosphorylation of the CTD recruits the RPAP2 Ser5 phosphatase to snRNA genes. *Mol Cell* **45:** 111-22.

Elmore S (2007). Apoptosis: a review of programmed cell death. *Toxicol Pathol* **35:** 495-516.

Errico A, Costanzo V (2012). Mechanisms of replication fork protection: a safeguard for genome stability. *Crit Rev Biochem Mol Biol* **47:** 222-35.

Esashi F, Christ N, Gannon J, Liu Y, Hunt T, Jasin M *et al* (2005). CDK-dependent phosphorylation of BRCA2 as a regulatory mechanism for recombinational repair. *Nature* **434:** 598-604.

Esashi F, Galkin VE, Yu X, Egelman EH, West SC (2007). Stabilization of RAD51 nucleoprotein filaments by the C-terminal region of BRCA2. *Nat Struct Mol Biol* **14:** 468-74.

Farmer H, McCabe N, Lord CJ, Tutt AN, Johnson DA, Richardson TB *et al* (2005). Targeting the DNA repair defect in BRCA mutant cells as a therapeutic strategy. *Nature* **434:** 917-21.

Feldser D, Agani F, Iyer NV, Pak B, Ferreira G, Semenza GL (1999). Reciprocal positive regulation of hypoxia-inducible factor 1alpha and insulin-like growth factor 2. *Cancer Res* **59:** 3915-8.

Feng Z, Scott SP, Bussen W, Sharma GG, Guo G, Pandita TK *et al* (2011). Rad52 inactivation is synthetically lethal with BRCA2 deficiency. *Proc Natl Acad Sci U S A* **108:** 686-91.

Fizazi K, Scher HI, Molina A, Logothetis CJ, Chi KN, Jones RJ *et al* (2012). Abiraterone acetate for treatment of metastatic castration-resistant prostate cancer: final overall survival analysis of the COU-AA-301 randomised, double-blind, placebo-controlled phase 3 study. *Lancet Oncol* **13:** 983-92.

Forbes BE, Hartfield PJ, McNeil KA, Surinya KH, Milner SJ, Cosgrove LJ *et al* (2002). Characteristics of binding of insulin-like growth factor (IGF)-I and IGF-II analogues to the type 1 IGF receptor determined by BIAcore analysis. *Eur J Biochem* **269:** 961-8.

Fortschegger K, Shiekhattar R (2011). Plant homeodomain fingers form a helping hand for transcription. *Epigenetics* **6:** 4-8.

Fraser M, Zhao H, Luoto KR, Lundin C, Coackley C, Chan N *et al* (2011). PTEN deletion in prostate cancer cells does not associate with loss of RAD51 function: implications for radiotherapy and chemotherapy. *Clin Cancer Res* **18:** 1015-27.

Frederick TJ, Wood TL (2004). IGF-I and FGF-2 coordinately enhance cyclin D1 and cyclin E-cdk2 association and activity to promote G1 progression in oligodendrocyte progenitor cells. *Mol Cell Neurosci* **25:** 480-92.

Friedlander TW, Ryan CJ (2012). Targeting the androgen receptor. *Urol Clin North Am* **39:** 453-64.

Fujiwara K, Iwado E, Mills GB, Sawaya R, Kondo S, Kondo Y (2007). Akt inhibitor shows anticancer and radiosensitizing effects in malignant glioma cells by inducing autophagy. *Int J Oncol* **31:** 753-60.

Fukuda R, Hirota K, Fan F, Jung YD, Ellis LM, Semenza GL (2002). Insulin-like growth factor 1 induces hypoxia-inducible factor 1-mediated vascular endothelial growth factor expression, which is dependent on MAP kinase and phosphatidylinositol 3-kinase signaling in colon cancer cells. *J Biol Chem* **277:** 38205-11.

Garcia MA, Koonrugsa N, Toda T (2002). Two kinesin-like Kin I family proteins in fission yeast regulate the establishment of metaphase and the onset of anaphase A. *Curr Biol* **12:** 610-21.

Girnita L, Girnita A, Larsson O (2003). Mdm2-dependent ubiquitination and degradation of the insulin-like growth factor 1 receptor. *Proc Natl Acad Sci U S A* **100:** 8247-52.

Goodarzi AA, Noon AT, Deckbar D, Ziv Y, Shiloh Y, Lobrich M *et al* (2008). ATM signaling facilitates repair of DNA double-strand breaks associated with heterochromatin. *Mol Cell* **31:** 167-77.

Graefen M, Ohori M, Karakiewicz PI, Cagiannos I, Hammerer PG, Haese A *et al* (2004). Assessment of the enhancement in predictive accuracy provided by systematic biopsy in predicting outcome for clinically localized prostate cancer. *J Urol* **171:** 200-3.

Greer SN, Metcalf JL, Wang Y, Ohh M (2012). The updated biology of hypoxia-inducible factor. *EMBO J* **31:** 2448-60.

Gualberto A, Hixon ML, Karp DD, Li D, Green S, Dolled-Filhart M *et al* (2011). Pre-treatment levels of circulating free IGF-1 identify NSCLC patients who derive clinical benefit from figitumumab. *Br J Cancer* **107:** 2024.

Gualberto A, Karp DD (2009). Development of the monoclonal antibody figitumumab, targeting the insulin-like growth factor-1 receptor, for the treatment of patients with non-small-cell lung cancer. *Clin Lung Cancer* **10:** 273-80.

Gudmundsdottir K, Lord CJ, Witt E, Tutt AN, Ashworth A (2004). DSS1 is required for RAD51 focus formation and genomic stability in mammalian cells. *EMBO Rep* **5:** 989-93.

Hanahan D, Weinberg RA (2000). The hallmarks of cancer. *Cell* **100:** 57-70.

Hanahan D, Weinberg RA (2011). Hallmarks of cancer: the next generation. *Cell* **144:** 646-74.

Hartman JLt, Garvik B, Hartwell L (2001). Principles for the buffering of genetic variation. *Science* **291:** 1001-4.

He M, Wen L, Campbell CE, Wu JY, Rao Y (1999). Transcription repression by Xenopus ET and its human ortholog TBX3, a gene involved in ulnar-mammary syndrome. *Proc Natl Acad Sci U S A* **96:** 10212-7.

Hellawell GO, Turner GD, Davies DR, Poulsom R, Brewster SF, Macaulay VM (2002). Expression of the type 1 insulin-like growth factor receptor is up-regulated in primary prostate cancer and commonly persists in metastatic disease. *Cancer Res* **62:** 2942-50.

Hendrickson AW, Haluska P (2009). Resistance pathways relevant to insulin-like growth factor-1 receptor-targeted therapy. *Curr Opin Investig Drugs* **10:** 1032-40.

Hewish M, Chau I, Cunningham D (2009). Insulin-like growth factor 1 receptor targeted therapeutics: novel compounds and novel treatment strategies for cancer medicine. *Recent Pat Anticancer Drug Discov* **4:** 54-72.

Hewitt SC, Li Y, Li L, Korach KS (2010). Estrogen-mediated regulation of Igf1 transcription and uterine growth involves direct binding of estrogen receptor alpha to estrogen-responsive elements. *J Biol Chem* **285:** 2676-85.

Hickson I, Zhao Y, Richardson CJ, Green SJ, Martin NM, Orr AI *et al* (2004). Identification and characterization of a novel and specific inhibitor of the ataxia-telangiectasia mutated kinase ATM. *Cancer Research* **64:** 9152-9.

Hill MM, Adrain C, Duriez PJ, Creagh EM, Martin SJ (2004). Analysis of the composition, assembly kinetics and activity of native Apaf-1 apoptosomes. *EMBO J* **23:** 2134-45.

Hochegger H, Takeda S, Hunt T (2008). Cyclin-dependent kinases and cell-cycle transitions: does one fit all? *Nat Rev Mol Cell Biol* **9:** 910-6.

Hoelz A, Debler EW, Blobel G (2011). The structure of the nuclear pore complex. *Annu Rev Biochem* **80:** 613-43.

Hollander MC, Blumenthal GM, Dennis PA (2011). PTEN loss in the continuum of common cancers, rare syndromes and mouse models. *Nat Rev Cancer* **11:** 289-301.

Hucl T, Rago C, Gallmeier E, Brody JR, Gorospe M, Kern SE (2008). A syngeneic variance library for functional annotation of human variation: application to BRCA2. *Cancer Res* **68:** 5023-30.

Hudelist G, Wagner T, Rosner M, Fink-Retter A, Gschwantler-Kaulich D, Czerwenka K *et al* (2007). Intratumoral IGF-I protein expression is selectively upregulated in breast cancer patients with BRCA1/2 mutations. *Endocr Relat Cancer* **14:** 1053-62.

Huo H, Guo X, Hong S, Jiang M, Liu X, Liao K (2003). Lipid rafts/caveolae are essential for insulin-like growth factor-1 receptor signaling during 3T3-L1 preadipocyte differentiation induction. *J Biol Chem* **278:** 11561-9.

Hussein MR (2004). The TP53 tumor suppressor gene and melanoma tumorigenesis: is there a relationship? *Tumour Biol* **25:** 200-7.

Isaacs WB, Carter BS, Ewing CM (1991). Wild-type p53 suppresses growth of human prostate cancer cells containing mutant p53 alleles. *Cancer Res* **51:** 4716-20.

Isebaert SF, Swinnen JV, McBride WH, Haustermans KM (2011). Insulin-like growth factor-type 1 receptor inhibitor NVP-AEW541 enhances radiosensitivity of PTEN wild-type but not PTEN-deficient human prostate cancer cells. *Int J Radiat Oncol Biol Phys* **81:** 239-47.

Jackson SP (2002). Sensing and repairing DNA double-strand breaks. *Carcinogenesis* **23:** 687-96.

Jeon JH, Kim SK, Kim HJ, Chang J, Ahn CM, Chang YS (2008). Insulin-like growth factor-1 attenuates cisplatin-induced gammaH2AX formation and DNA double-strand breaks repair pathway in non-small cell lung cancer. *Cancer Lett* **272:** 232-41.

Jernberg-Wiklund H, Nilsson K (2007). Control of apoptosis in human multiple myeloma by insulin-like growth factor I (IGF-I). *Adv Cancer Res* **97:** 139-65.

Jia Y, Song W, Zhang F, Yan J, Yang Q (2012). Akt1 inhibits homologous recombination in Brca1-deficient cells by blocking the Chk1-Rad51 pathway. *Oncogene*.

Jiang Y, Wang L, Gong W, Wei D, Le X, Yao J *et al* (2004). A high expression level of insulin-like growth factor I receptor is associated with increased expression of transcription factor Sp1 and regional lymph node metastasis of human gastric cancer. *Clin Exp Metastasis* **21:** 755-64.

Jirawatnotai S, Hu Y, Michowski W, Elias JE, Becks L, Bienvenu F *et al* (2011). A function for cyclin D1 in DNA repair uncovered by protein interactome analyses in human cancers. *Nature* **474:** 230-4.

Johnson N, Cai D, Kennedy RD, Pathania S, Arora M, Li YC *et al* (2009). Cdk1 participates in BRCA1-dependent S phase checkpoint control in response to DNA damage. *Mol Cell* **35:** 327-39.

Johnson N, Li YC, Walton ZE, Cheng KA, Li D, Rodig SJ *et al* (2011). Compromised CDK1 activity sensitizes BRCA-proficient cancers to PARP inhibition. *Nat Med* **17:** 875-82.

Jones RM, Petermann E (2012). Replication fork dynamics and the DNA damage response. *Biochem J* **443:** 13-26.

Juergens H, Daw NC, Geoerger B, Ferrari S, Villarroel M, Aerts I *et al* (2011). Preliminary efficacy of the anti-insulin-like growth factor type 1 receptor antibody figitumumab in patients with refractory Ewing sarcoma. *J Clin Oncol* **29:** 4534-40.

Kaelin WG (2007). Von Hippel-Lindau disease. *Annu Rev Pathol* **2:** 145-73.

Kaelin WG, Jr. (2005). The concept of synthetic lethality in the context of anticancer therapy. *Nat Rev Cancer* **5:** 689-98.

Kanter-Lewensohn L, Dricu A, Wang M, Wejde J, Kiessling R, Larsson O (1998). Expression of the insulin-like growth factor-1 receptor and its anti-apoptotic effect in malignant melanoma: a potential therapeutic target. *Melanoma Res* **8:** 389-97.

Kanter-Lewensohn L, Girnita L, Girnita A, Dricu A, Olsson G, Leech L *et al* (2000). Tamoxifen-induced cell death in malignant melanoma cells: possible involvement of the insulin-like growth factor-1 (IGF-1) pathway. *Mol Cell Endocrinol* **165:** 131-7.

Karimi-Busheri F, Rasouli-Nia A, Allalunis-Turner J, Weinfeld M (2007). Human polynucleotide kinase participates in repair of DNA double-strand breaks by nonhomologous end joining but not homologous recombination. *Cancer Res* **67:** 6619-25.

Karp DD, Paz-Ares LG, Novello S, Haluska P, Garland L, Cardenal F *et al* (2009). Phase II study of the anti-insulin-like growth factor type 1 receptor antibody CP-751,871 in combination with paclitaxel and carboplatin in previously untreated, locally advanced, or metastatic non-small-cell lung cancer. *J Clin Oncol* **27:** 2516-22.

Kass EM, Jasin M (2010). Collaboration and competition between DNA double-strand break repair pathways. *FEBS Lett* **584:** 3703-8.

Kawanami T, Takiguchi S, Ikeda N, Funakoshi A (2012). A humanized anti-IGF-1R monoclonal antibody (R1507) and/or metformin enhance gemcitabine-induced apoptosis in pancreatic cancer cells. *Oncol Rep* **27:** 867-72.

Key TJ, Appleby PN, Reeves GK, Roddam AW (2010). Insulin-like growth factor 1 (IGF1), IGF binding protein 3 (IGFBP3), and breast cancer risk: pooled individual data analysis of 17 prospective studies. *Lancet Oncol* **11:** 530-42.

Kim DW, Cochran BH (2000). Extracellular signal-regulated kinase binds to TFII-I and regulates its activation of the c-fos promoter. *Mol Cell Biol* **20:** 1140-8.

Kim IA, Bae SS, Fernandes A, Wu J, Muschel RJ, McKenna WG *et al* (2005). Selective inhibition of Ras, phosphoinositide 3 kinase, and Akt isoforms increases the radiosensitivity of human carcinoma cell lines. *Cancer Res* **65:** 7902-10.

Kim J, Kim JH, Lee SH, Kim DH, Kang HY, Bae SH *et al* (2002). The novel human DNA helicase hFBH1 is an F-box protein. *J Biol Chem* **277:** 24530-7.

Kischkel FC, Hellbardt S, Behrmann I, Germer M, Pawlita M, Krammer PH *et al* (1995). Cytotoxicity-dependent APO-1 (Fas/CD95)-associated proteins form a death-inducing signaling complex (DISC) with the receptor. *EMBO J* **14:** 5579-88.

Kleiner DE, Stetler-Stevenson WG (1999). Matrix metalloproteinases and metastasis. *Cancer Chemother Pharmacol* **43 Suppl:** S42-51.

Knorz VJ, Spalluto C, Lessard M, Purvis TL, Adigun FF, Collin GB *et al* (2010). Centriolar association of ALMS1 and likely centrosomal functions of the ALMS motif-containing proteins C10orf90 and KIAA1731. *Mol Biol Cell* **21:** 3617-29.

Koch CA, Agyei R, Galicia S, Metalnikov P, O'Donnell P, Starostine A *et al* (2004). Xrcc4 physically links DNA end processing by polynucleotide kinase to DNA ligation by DNA ligase IV. *EMBO J* **23:** 3874-85.

Kojic M, Holloman WK (2004). BRCA2-RAD51-DSS1 interplay examined from a microbial perspective. *Cell Cycle* **3:** 247-8.

Kooijman R (2006). Regulation of apoptosis by insulin-like growth factor (IGF)-I. *Cytokine Growth Factor Rev* **17:** 305-23.

Krejci L, Altmannova V, Spirek M, Zhao X (2012). Homologous recombination and its regulation. *Nucleic Acids Res* **40:** 5795-818.

Kroemer G, Galluzzi L, Vandenabeele P, Abrams J, Alnemri ES, Baehrecke EH *et al* (2009). Classification of cell death: recommendations of the Nomenclature Committee on Cell Death 2009. *Cell Death Differ* **16:** 3-11.

Kubbutat MH, Jones SN, Vousden KH (1997). Regulation of p53 stability by Mdm2. *Nature* **387:** 299-303.

Kull FC, Jr., Jacobs S, Su YF, Svoboda ME, Van Wyk JJ, Cuatrecasas P (1983). Monoclonal antibodies to receptors for insulin and somatomedin-C. *J Biol Chem* **258:** 6561-6.

Lamarche N, Hall A (1994). GAPs for rho-related GTPases. *Trends Genet* **10:** 436-40.

Laplante M, Sabatini DM (2012). mTOR signaling in growth control and disease. *Cell* **149:** 274-93.

Larsson O, Girnita A, Girnita L (2005). Role of insulin-like growth factor 1 receptor signalling in cancer. *Br J Cancer* **92:** 2097-101.

Laursen LS, Kjaer-Sorensen K, Andersen MH, Oxvig C (2007). Regulation of insulin-like growth factor (IGF) bioactivity by sequential proteolytic cleavage of IGF binding protein-4 and -5. *Mol Endocrinol* **21:** 1246-57.

Lavin MF (2008). Ataxia-telangiectasia: from a rare disorder to a paradigm for cell signalling and cancer. *Nat Rev Mol Cell Biol* **9:** 759-69.

Lavoie JN, L'Allemain G, Brunet A, Muller R, Pouyssegur J (1996a). Cyclin D1 expression is regulated positively by the p42/p44MAPK and negatively by the p38/HOGMAPK pathway. *J Biol Chem* **271:** 20608-16.

Lavoie JN, Rivard N, L'Allemain G, Pouyssegur J (1996b). A temporal and biochemical link between growth factor-activated MAP kinases, cyclin D1 induction and cell cycle entry. *Prog Cell Cycle Res* **2:** 49-58.

Li J, Yuan J (2008). Caspases in apoptosis and beyond. *Oncogene* **27:** 6194-206.

Lin SY, Makino K, Xia W, Matin A, Wen Y, Kwong KY *et al* (2001). Nuclear localization of EGF receptor and its potential new role as a transcription factor. *Nat Cell Biol* **3:** 802-8.

Litvinov IV, Antony L, Dalrymple SL, Becker R, Cheng L, Isaacs JT (2006). PC3, but not DU145, human prostate cancer cells retain the coregulators required for tumor suppressor ability of androgen receptor. *Prostate* **66:** 1329-38.

Litzenburger BC, Creighton CJ, Tsimelzon A, Chan BT, Hilsenbeck SG, Wang T *et al* (2011). High IGF-IR activity in triple-negative breast cancer cell lines and tumorgrafts correlates with sensitivity to anti-IGF-IR therapy. *Clin Cancer Res* **17:** 2314-27.

Liu JP, Baker J, Perkins AS, Robertson EJ, Efstratiadis A (1993). Mice carrying null mutations of the genes encoding insulin-like growth factor I (Igf-1) and type 1 IGF receptor (Igf1r). *Cell* **75:** 59-72.

Lo HW, Hung MC (2007). Nuclear EGFR signalling network in cancers: linking EGFR pathway to cell cycle progression, nitric oxide pathway and patient survival. *Br J Cancer* **96 Suppl:** R16-20.

Locksley RM, Killeen N, Lenardo MJ (2001). The TNF and TNF receptor superfamilies: integrating mammalian biology. *Cell* **104:** 487-501.

Lu J, Li XP, Dong Q, Kung HF, He ML (2010). TBX2 and TBX3: the special value for anticancer drug targets. *Biochim Biophys Acta* **1806:** 268-74.

Lucchesi JC (1968). Synthetic lethality and semi-lethality among functionally related mutants of Drosophila melanfgaster. *Genetics* **59:** 37-44.

Luo H, Li Y, Mu JJ, Zhang J, Tonaka T, Hamamori Y *et al* (2008). Regulation of intra-S phase checkpoint by ionizing radiation (IR)-dependent and IR-independent phosphorylation of SMC3. *J Biol Chem* **283:** 19176-83.

Macaulay VM, Salisbury AJ, Bohula EA, Playford MP, Smorodinsky NI, Shiloh Y (2001). Downregulation of the type 1 insulin-like growth factor receptor in mouse melanoma cells is associated with enhanced radiosensitivity and impaired activation of Atm kinase. *Oncogene* **20:** 4029-40.

Maehama T, Dixon JE (1998). The tumor suppressor, PTEN/MMAC1, dephosphorylates the lipid second messenger, phosphatidylinositol 3,4,5-trisphosphate. *J Biol Chem* **273:** 13375-8.

Malaguarnera R, Sacco A, Voci C, Pandini G, Vigneri R, Belfiore A (2012). Proinsulin binds with high affinity the insulin receptor isoform A and predominantly activates the mitogenic pathway. *Endocrinology* **153:** 2152-63.

Mandriota SJ, Jussila L, Jeltsch M, Compagni A, Baetens D, Prevo R *et al* (2001). Vascular endothelial growth factor-C-mediated lymphangiogenesis promotes tumour metastasis. *EMBO J* **20:** 672-82.

Manning BD, Cantley LC (2007). AKT/PKB signaling: navigating downstream. *Cell* **129:** 1261-74.

Mansfield RE, Musselman CA, Kwan AH, Oliver SS, Garske AL, Davrazou F *et al* (2011). Plant homeodomain (PHD) fingers of CHD4 are histone H3-binding modules with preference for unmodified H3K4 and methylated H3K9. *J Biol Chem* **286:** 11779-91.

Massie C, Mills IG (2006). The developing role of receptors and adaptors. *Nat Rev Cancer* **6:** 403-9.

Mathews LS, Norstedt G, Palmiter RD (1986). Regulation of insulin-like growth factor I gene expression by growth hormone. *Proc Natl Acad Sci U S A* **83:** 9343-7.

McElroy B, Powell JC, McCarthy JV (2007). The insulin-like growth factor 1 (IGF-1) receptor is a substrate for gamma-secretase-mediated intramembrane proteolysis. *Biochem Biophys Res Commun* **358:** 1136-41.

McEwan IJ, Gustafsson J (1997). Interaction of the human androgen receptor transactivation function with the general transcription factor TFIIF. *Proc Natl Acad Sci U S A* **94:** 8485-90.

McMenamin ME, Soung P, Perera S, Kaplan I, Loda M, Sellers WR (1999). Loss of PTEN expression in paraffin-embedded primary prostate cancer correlates with high Gleason score and advanced stage. *Cancer Res* **59:** 4291-6.

Menagh PJ, Turner RT, Jump DB, Wong CP, Lowry MB, Yakar S *et al* (2010). Growth hormone regulates the balance between bone formation and bone marrow adiposity. *J Bone Miner Res* **25:** 757-68.

Meyer G, Kim B, van Golen C, Feldman EL (2005). Cofilin activity during insulin-like growth factor I-stimulated neuroblastoma cell motility. *Cell Mol Life Sci* **62:** 461-70.

Minuto F, Del Monte P, Barreca A, Fortini P, Cariola G, Catrambone G *et al* (1986). Evidence for an increased somatomedin-C/insulin-like growth factor I content in primary human lung tumors. *Cancer Res* **46:** 985-8.

Misra UK, Wang F, Pizzo SV (2009). Transcription factor TFII-I causes transcriptional upregulation of GRP78 synthesis in prostate cancer cells. *J Cell Biochem* **106:** 381-9.

Moon SY, Zheng Y (2003). Rho GTPase-activating proteins in cell regulation. *Trends Cell Biol* **13:** 13-22.

Moschos SJ, Mantzoros CS (2002). The role of the IGF system in cancer: from basic to clinical studies and clinical applications. *Oncology* **63:** 317-32.

Mukherjee A, Karmakar P (2012). Attenuation of PTEN perturbs genomic stability via activation of Akt and down-regulation of Rad51 in human embryonic kidney cells. *Mol Carcinog*.

Muller H, Brenner H (2006). Urine markers as possible tools for prostate cancer screening: review of performance characteristics and practicality. *Clin Chem* **52:** 562-73.

Musselman CA, Kutateladze TG (2009). PHD fingers: epigenetic effectors and potential drug targets. *Mol Interv* **9:** 314-23.

Mutter GL (2001). Pten, a protean tumor suppressor. *Am J Pathol* **158:** 1895-8.

Neufeld TP (2010). TOR-dependent control of autophagy: biting the hand that feeds. *Curr Opin Cell Biol* **22:** 157-68.

Ng YY, Baert MR, Pike-Overzet K, Rodijk M, Brugman MH, Schambach A *et al* (2010). Correction of B-cell development in Btk-deficient mice using lentiviral vectors with codon-optimized human BTK. *Leukemia* **24:** 1617-30.

Nguyen DX, Bos PD, Massague J (2009). Metastasis: from dissemination to organ-specific colonization. *Nat Rev Cancer* **9:** 274-84.

Nisato RE, Tille JC, Pepper MS (2003). Lymphangiogenesis and tumor metastasis. *Thromb Haemost* **90:** 591-7.

O'Connor R, Kauffmann-Zeh A, Liu Y, Lehar S, Evan GI, Baserga R *et al* (1997). Identification of domains of the insulin-like growth factor I receptor that are required for protection from apoptosis. *Mol Cell Biol* **17:** 427-35.

Ohlsson C, Kley N, Werner H, LeRoith D (1998). p53 regulates insulin-like growth factor-I (IGF-I) receptor expression and IGF-I-induced tyrosine phosphorylation in an osteosarcoma cell line: interaction between p53 and Sp1. *Endocrinology* **139:** 1101-7.

Omlin A, de Bono JS (2012). Therapeutic options for advanced prostate cancer: 2011 update. *Curr Urol Rep* **13:** 170-8.

Ono M, Kuwano M (2006). Molecular mechanisms of epidermal growth factor receptor (EGFR) activation and response to gefitinib and other EGFR-targeting drugs. *Clin Cancer Res* **12:** 7242-51.

Oren M (1999). Regulation of the p53 tumor suppressor protein. *J Biol Chem* **274:** 36031-4.

Orio F, Jr., Terouanne B, Georget V, Lumbroso S, Avances C, Siatka C *et al* (2002). Potential action of IGF-1 and EGF on androgen receptor nuclear transfer and transactivation in normal and cancer human prostate cell lines. *Mol Cell Endocrinol* **198:** 105-14.

Osman F, Dixon J, Barr AR, Whitby MC (2005). The F-Box DNA helicase Fbh1 prevents Rhp51-dependent recombination without mediator proteins. *Mol Cell Biol* **25:** 8084-96.

Ott M, Robertson JD, Gogvadze V, Zhivotovsky B, Orrenius S (2002). Cytochrome c release from mitochondria proceeds by a two-step process. *Proc Natl Acad Sci U S A* **99:** 1259-63.

Ouyang L, Shi Z, Zhao S, Wang FT, Zhou TT, Liu B *et al* (2012). Programmed cell death pathways in cancer: a review of apoptosis, autophagy and programmed necrosis. *Cell Prolif* **45:** 487-98.

Pandini G, Genua M, Frasca F, Vigneri R, Belfiore A (2009). Sex steroids upregulate the IGF-1R in prostate cancer cells through a nongenotropic pathway. *Ann N Y Acad Sci* **1155:** 263-7.

Pandini G, Mineo R, Frasca F, Roberts CT, Jr., Marcelli M, Vigneri R *et al* (2005). Androgens up-regulate the insulin-like growth factor-I receptor in prostate cancer cells. *Cancer Res* **65:** 1849-57.

Park JS, Choi E, Lee SH, Lee C, Seo YS (1997). A DNA helicase from Schizosaccharomyces pombe stimulated by single-stranded DNA-binding protein at low ATP concentration. *J Biol Chem* **272:** 18910-9.

Pavelic K, Bukovic D, Pavelic J (2002). The role of insulin-like growth factor 2 and its receptors in human tumors. *Mol Med* **8:** 771-80.

Pawelczak KS, Bennett SM, Turchi JJ (2011). Coordination of DNA-PK activation and nuclease processing of DNA termini in NHEJ. *Antioxid Redox Signal* **14:** 2531-43.

Pierce AJ, Johnson RD, Thompson LH, Jasin M (1999). XRCC3 promotes homology-directed repair of DNA damage in mammalian cells. *Genes Dev* **13:** 2633-8.

Pitts TM, Tan AC, Kulikowski GN, Tentler JJ, Brown AM, Flanigan SA *et al* (2010). Development of an integrated genomic classifier for a novel agent in colorectal cancer: approach to individualized therapy in early development. *Clin Cancer Res* **16:** 3193-204.

Plo I, Laulier C, Gauthier L, Lebrun F, Calvo F, Lopez BS (2008). AKT1 inhibits homologous recombination by inducing cytoplasmic retention of BRCA1 and RAD51. *Cancer Res* **68:** 9404-12.

Pollak M (2012). The insulin and insulin-like growth factor receptor family in neoplasia: an update. *Nat Rev Cancer* **12:** 159-69.

Pollak MN, Schernhammer ES, Hankinson SE (2004). Insulin-like growth factors and neoplasia. *Nat Rev Cancer* **4:** 505-18.

Potratz JC, Saunders DN, Wai DH, Ng TL, McKinney SE, Carboni JM *et al* (2010). Synthetic lethality screens reveal RPS6 and MST1R as modifiers of insulin-like growth factor-1 receptor inhibitor activity in childhood sarcomas. *Cancer Res* **70:** 8770-81.

Powell SN, Kachnic LA (2003). Roles of BRCA1 and BRCA2 in homologous recombination, DNA replication fidelity and the cellular response to ionizing radiation. *Oncogene* **22:** 5784-91.

Prevo R, Deutsch E, Sampson O, Diplexcito J, Cengel K, Harper J *et al* (2008). Class I PI3 kinase inhibition by the pyridinylfuranopyrimidine inhibitor PI-103 enhances tumor radiosensitivity. *Cancer Res* **68:** 5915-23.

Puc J, Keniry M, Li HS, Pandita TK, Choudhury AD, Memeo L *et al* (2005). Lack of PTEN sequesters CHK1 and initiates genetic instability. *Cancer Cell* **7:** 193-204.

Pugazhenthi S, Nesterova A, Sable C, Heidenreich KA, Boxer LM, Heasley LE *et al* (2000). Akt/protein kinase B up-regulates Bcl-2 expression through cAMP-response element-binding protein. *J Biol Chem* **275:** 10761-6.

Rehman FL, Lord CJ, Ashworth A (2012). Synthetic lethal approaches to breast cancer therapy. *Nat Rev Clin Oncol* **7:** 718-24.

Reiss K, Ferber A, Travali S, Porcu P, Phillips PD, Baserga R (1991). The protooncogene c-myb increases the expression of insulin-like growth factor 1 and insulin-like growth factor 1 receptor messenger RNAs by a transcriptional mechanism. *Cancer Res* **51:** 5997-6000.

Reiss K, Khalili K, Giordano A, Trojanek J (2006). JC virus large T-antigen and IGF-I signaling system merge to affect DNA repair and genomic integrity. *J Cell Physiol* **206:** 295-300.

Reiss K, Wang JY, Romano G, Furnari FB, Cavenee WK, Morrione A *et al* (2000). IGF-I receptor signaling in a prostatic cancer cell line with a PTEN mutation. *Oncogene* **19:** 2687-94.

Renard CA, Labalette C, Armengol C, Cougot D, Wei Y, Cairo S *et al* (2007). Tbx3 is a downstream target of the Wnt/beta-catenin pathway and a critical mediator of beta-catenin survival functions in liver cancer. *Cancer Res* **67:** 901-10.

Riedemann J, Takiguchi M, Sohail M, Macaulay VM (2007). The EGF receptor interacts with the type 1 IGF receptor and regulates its stability. *Biochem Biophys Res Commun* **355:** 707-14.

Rinaldi S, Cleveland R, Norat T, Biessy C, Rohrmann S, Linseisen J *et al* (2010). Serum levels of IGF-I, IGFBP-3 and colorectal cancer risk: results from the EPIC cohort, plus a meta-analysis of prospective studies. *Int J Cancer* **126:** 1702-15.

Roberts CT, Jr. (2004). IGF-1 and prostate cancer. *Novartis Found Symp* **262:** 193-9; discussion 199-204, 265-8.

Rochester MA, Patel N, Turney BW, Davies DR, Roberts IS, Crew J *et al* (2007). The type 1 insulin-like growth factor receptor is over-expressed in bladder cancer. *BJU Int* **100:** 1396-401.

Rochester MA, Riedemann J, Hellawell GO, Brewster SF, Macaulay VM (2005). Silencing of the IGF1R gene enhances sensitivity to DNA-damaging agents in both PTEN wild-type and mutant human prostate cancer. *Cancer Gene Ther* **12:** 90-100.

Roddam AW, Allen NE, Appleby P, Key TJ, Ferrucci L, Carter HB *et al* (2008). Insulin-like growth factors, their binding proteins, and prostate cancer risk: analysis of individual patient data from 12 prospective studies. *Ann Intern Med* **149:** 461-71, W83-8.

Rohlik QT, Adams D, Kull FC, Jr., Jacobs S (1987). An antibody to the receptor for insulin-like growth factor I inhibits the growth of MCF-7 cells in tissue culture. *Biochem Biophys Res Commun* **149:** 276-81.

Romanelli RJ, LeBeau AP, Fulmer CG, Lazzarino DA, Hochberg A, Wood TL (2007). Insulin-like growth factor type-I receptor internalization and recycling mediate the sustained phosphorylation of Akt. *J Biol Chem* **282:** 22513-24.

Rosell R, Cobo M, Isla D, Camps C, Massuti B (2006). Pharmacogenomics and gemcitabine. *Ann Oncol* **17 Suppl 5:** v13-16.

Rowlands MA, Tilling K, Holly JM, Metcalfe C, Gunnell D, Lane A *et al* (2012). Insulin-like growth factors (IGFs) and IGF-binding proteins in active monitoring of localized prostate cancer: a population-based observational study. *Cancer Causes Control*.

Roy AL (2007). Signal-induced functions of the transcription factor TFII-I. *Biochim Biophys Acta* **1769:** 613-21.

Roy AL (2012). Biochemistry and biology of the inducible multifunctional transcription factor TFII-I: 10 years later. *Gene* **492:** 32-41.

Roy AL, Meisterernst M, Pognonec P, Roeder RG (1991). Cooperative interaction of an initiator-binding transcription initiation factor and the helix-loop-helix activator USF. *Nature* **354:** 245-8.

Rubini M, Werner H, Gandini E, Roberts CT, Jr., LeRoith D, Baserga R (1994). Platelet-derived growth factor increases the activity of the promoter of the insulin-like growth factor-1 (IGF-1) receptor gene. *Exp Cell Res* **211:** 374-9.

Saelens X, Festjens N, Vande Walle L, van Gurp M, van Loo G, Vandenabeele P (2004). Toxic proteins released from mitochondria in cell death. *Oncogene* **23:** 2861-74.

Salani B, Passalacqua M, Maffioli S, Briatore L, Hamoudane M, Contini P *et al* (2010). IGF-IR internalizes with Caveolin-1 and PTRF/Cavin in HaCat cells. *PLoS One* **5:** e14157.

Saleh-Gohari N, Bryant HE, Schultz N, Parker KM, Cassel TN, Helleday T (2005). Spontaneous homologous recombination is induced by collapsed replication forks that are caused by endogenous DNA single-strand breaks. *Mol Cell Biol* **25:** 7158-69.

Saltiel AR, Kahn CR (2001). Insulin signalling and the regulation of glucose and lipid metabolism. *Nature* **414:** 799-806.

Samani AA, Yakar S, LeRoith D, Brodt P (2007). The role of the IGF system in cancer growth and metastasis: overview and recent insights. *Endocr Rev* **28:** 20-47.

Sasaki H, Hayakawa J, Terai Y, Kanemura M, Tanabe-Kimura A, Kamegai H *et al* (2008). Difference between genomic actions of estrogen versus raloxifene in human ovarian cancer cell lines. *Oncogene* **27:** 2737-45.

Schayek H, Haugk K, Sun S, True LD, Plymate SR, Werner H (2009). Tumor suppressor BRCA1 is expressed in prostate cancer and controls insulin-like growth factor I receptor (IGF-IR) gene transcription in an androgen receptor-dependent manner. *Clin Cancer Res* **15:** 1558-65.

Schlomm T, Iwers L, Kirstein P, Jessen B, Kollermann J, Minner S *et al* (2008). Clinical significance of p53 alterations in surgically treated prostate cancers. *Mod Pathol* **21:** 1371-8.

Sehat B, Andersson S, Vasilcanu R, Girnita L, Larsson O (2007). Role of ubiquitination in IGF-1 receptor signaling and degradation. *PLoS One* **2:** e340.

Sehat B, Tofigh A, Lin Y, Trocme E, Liljedahl U, Lagergren J *et al* (2010). SUMOylation mediates the nuclear translocation and signaling of the IGF-1 receptor. *Sci Signal* **3:** ra10.

Seino S, Bell GI (1989). Alternative splicing of human insulin receptor messenger RNA. *Biochem Biophys Res Commun* **159:** 312-6.

Shalita-Chesner M, Katz J, Shemer J, Werner H (2001). Regulation of insulin-like growth factor-I receptor gene expression by tumor necrosis factor-alpha and interferon-gamma. *Mol Cell Endocrinol* **176:** 1-12.

Shechter D, Costanzo V, Gautier J (2004). ATR and ATM regulate the timing of DNA replication origin firing. *Nat Cell Biol* **6:** 648-55.

Shembade N, Harhaj NS, Liebl DJ, Harhaj EW (2007). Essential role for TAX1BP1 in the termination of TNF-alpha-, IL-1- and LPS-mediated NF-kappaB and JNK signaling. *EMBO J* **26:** 3910-22.

Sheppard K, Kinross KM, Solomon B, Pearson RB, Phillips WA (2012). Targeting PI3 kinase/AKT/mTOR signaling in cancer. *Crit Rev Oncog* **17:** 69-95.

Sherr CJ (1996). Cancer cell cycles. *Science* **274:** 1672-7.

Shi W, Feng Z, Zhang J, Gonzalez-Suarez I, Vanderwaal RP, Wu X *et al* (2010). The role of RPA2 phosphorylation in homologous recombination in response to replication arrest. *Carcinogenesis* **31:** 994-1002.

Shimasaki S, Ling N (1991). Identification and molecular characterization of insulin-like growth factor binding proteins (IGFBP-1, -2, -3, -4, -5 and -6). *Prog Growth Factor Res* **3:** 243-66.

Shimasaki S, Shimonaka M, Zhang HP, Ling N (1991). Identification of five different insulin-like growth factor binding proteins (IGFBPs) from adult rat serum and molecular cloning of a novel IGFBP-5 in rat and human. *J Biol Chem* **266:** 10646-53.

Shin SI, Freedman VH, Risser R, Pollack R (1975). Tumorigenicity of virus-transformed cells in nude mice is correlated specifically with anchorage independent growth in vitro. *Proc Natl Acad Sci U S A* **72:** 4435-9.

Sikes RA, Nicholson BE, Koeneman KS, Edlund NM, Bissonette EA, Bradley MJ *et al* (2004). Cellular interactions in the tropism of prostate cancer to bone. *Int J Cancer* **110:** 497-503.

Singh P, Srivastava A (2007). Update in palliative management of hormone refractory cancer of prostate. *Indian J Urol* **23:** 43-50.

Skjoth IH, Issinger OG (2006). Profiling of signaling molecules in four different human prostate carcinoma cell lines before and after induction of apoptosis. *Int J Oncol* **28:** 217-29.

Smith GC, d'Adda di Fagagna F, Lakin ND, Jackson SP (1999). Cleavage and inactivation of ATM during apoptosis. *Mol Cell Biol* **19:** 6076-84.

Sola S, Morgado AL, Rodrigues CM (2013). Death receptors and mitochondria: two prime triggers of neural apoptosis and differentiation. *Biochim Biophys Acta* **1830:** 2160-6.

Stachelscheid H, Ibrahim H, Koch L, Schmitz A, Tscharntke M, Wunderlich FT *et al* (2008). Epidermal insulin/IGF-1 signalling control interfollicular morphogenesis and proliferative potential through Rac activation. *EMBO J* **27:** 2091-101.

Stacker SA, Caesar C, Baldwin ME, Thornton GE, Williams RA, Prevo R *et al* (2001). VEGF-D promotes the metastatic spread of tumor cells via the lymphatics. *Nat Med* **7:** 186-91.

Stambolic V, Suzuki A, de la Pompa JL, Brothers GM, Mirtsos C, Sasaki T *et al* (1998). Negative regulation of PKB/Akt-dependent cell survival by the tumor suppressor PTEN. *Cell* **95:** 29-39.

Stenman UH, Abrahamsson PA, Aus G, Lilja H, Bangma C, Hamdy FC *et al* (2005). Prognostic value of serum markers for prostate cancer. *Scand J Urol Nephrol Suppl***:** 64-81.

Sun W, Lorenz A, Osman F, Whitby MC (2011). A failure of meiotic chromosome segregation in a fbh1Delta mutant correlates with persistent Rad51-DNA associations. *Nucleic Acids Res* **39:** 1718-31.

Sung P, Klein H (2006). Mechanism of homologous recombination: mediators and helicases take on regulatory functions. *Nat Rev Mol Cell Biol* **7:** 739-50.

Symeonidou IE, Taraviras S, Lygerou Z (2012). Control over DNA replication in time and space. *FEBS Lett* **586:** 2803-12.

Tanaka K, Sugiura Y, Ichishita R, Mihara K, Oka T (2011). KLP6: a newly identified kinesin that regulates the morphology and transport of mitochondria in neuronal cells. *J Cell Sci* **124:** 2457-65.

Tang Y, Zhang D, Fallavollita L, Brodt P (2003). Vascular endothelial growth factor C expression and lymph node metastasis are regulated by the type I insulin-like growth factor receptor. *Cancer Res* **63:** 1166-71.

Tanikawa M, Wada-Hiraike O, Nakagawa S, Shirane A, Hiraike H, Koyama S *et al* (2011). Multifunctional transcription factor TFII-I is an activator of BRCA1 function. *Br J Cancer* **104:** 1349-55.

Tannock IF, de Wit R, Berry WR, Horti J, Pluzanska A, Chi KN *et al* (2004). Docetaxel plus prednisone or mitoxantrone plus prednisone for advanced prostate cancer. *N Engl J Med* **351:** 1502-12.

Taya S, Inagaki N, Sengiku H, Makino H, Iwamatsu A, Urakawa I *et al* (2001). Direct interaction of insulin-like growth factor-1 receptor with leukemia-associated RhoGEF. *J Cell Biol* **155:** 809-20.

Tezuka M, Watanabe H, Nakamura S, Yu D, Aung W, Sasaki T *et al* (2001). Antiapoptotic activity is dispensable for insulin-like growth factor I receptor-mediated clonogenic radioresistance after gamma-irradiation. *Clin Cancer Res* **7:** 3206-14.

Thimmaiah KN, Easton JB, Germain GS, Morton CL, Kamath S, Buolamwini JK *et al* (2005). Identification of N10-substituted phenoxazines as potent and specific inhibitors of Akt signaling. *J Biol Chem* **280:** 31924-35.

Thompson IM, Jr., Tangen CM, Paradelo J, Lucia MS, Miller G, Troyer D *et al* (2006). Adjuvant radiotherapy for pathologically advanced prostate cancer: a randomized clinical trial. *JAMA* **296:** 2329-35.

Tilley WD, Bentel JM, Aspinall JO, Hall RE, Horsfall DJ (1995). Evidence for a novel mechanism of androgen resistance in the human prostate cancer cell line, PC-3. *Steroids* **60:** 180-6.

Tricoli JV, Rall LB, Karakousis CP, Herrera L, Petrelli NJ, Bell GI *et al* (1986). Enhanced levels of insulin-like growth factor messenger RNA in human colon carcinomas and liposarcomas. *Cancer Res* **46:** 6169-73.

Trojanek J, Ho T, Croul S, Wang JY, Chintapalli J, Koptyra M *et al* (2006). IRS-1-Rad51 nuclear interaction sensitizes JCV T-antigen positive medulloblastoma cells to genotoxic treatment. *Int J Cancer* **119:** 539-48.

Trojanek J, Ho T, Del Valle L, Nowicki M, Wang JY, Lassak A *et al* (2003). Role of the insulin-like growth factor I/insulin receptor substrate 1 axis in Rad51 trafficking and DNA repair by homologous recombination. *Mol Cell Biol* **23:** 7510-24.

Tsai WB, Chung YM, Takahashi Y, Xu Z, Hu MC (2008). Functional interaction between FOXO3a and ATM regulates DNA damage response. *Nat Cell Biol* **10:** 460-7.

Turner BC, Haffty BG, Narayanan L, Yuan J, Havre PA, Gumbs AA *et al* (1997). Insulin-like growth factor-I receptor overexpression mediates cellular radioresistance and local breast cancer recurrence after lumpectomy and radiation. *Cancer Res* **57:** 3079-83.

Turney BW, Kerr M, Chitnis MM, Lodhia K, Wang Y, Riedemann J *et al* Depletion of the type 1 IGF receptor delays repair of radiation-induced DNA double strand breaks. *Radiother Oncol* **103:** 402-9.

Turney BW, Kerr M, Chitnis MM, Lodhia K, Wang Y, Riedemann J *et al* (2012). Depletion of the type 1 IGF receptor delays repair of radiation-induced DNA double strand breaks. *Radiother Oncol* **103:** 402-9.

Turney BW, Turner GD, Brewster SF, Macaulay VM (2011). Serial analysis of resected prostate cancer suggests up-regulation of type 1 IGF receptor with disease progression. *BJU Int* **107:** 1488-99.

Ullrich A, Gray A, Tam AW, Yang-Feng T, Tsubokawa M, Collins C *et al* (1986). Insulin-like growth factor I receptor primary structure: comparison with insulin receptor suggests structural determinants that define functional specificity. *EMBO J* **5:** 2503-12.

Underwood LE, Thissen JP, Lemozy S, Ketelslegers JM, Clemmons DR (1994). Hormonal and nutritional regulation of IGF-I and its binding proteins. *Horm Res* **42:** 145-51.

Vakifahmetoglu H, Olsson M, Zhivotovsky B (2008). Death through a tragedy: mitotic catastrophe. *Cell Death Differ* **15:** 1153-62.

Van Aelst L, D'Souza-Schorey C (1997). Rho GTPases and signaling networks. *Genes Dev* **11:** 2295-322.

van der Burg B, Rutteman GR, Blankenstein MA, de Laat SW, van Zoelen EJ (1988). Mitogenic stimulation of human breast cancer cells in a growth factor-defined medium: synergistic action of insulin and estrogen. *J Cell Physiol* **134:** 101-8.

Van der Kwast TH, Collette L, Bolla M (2007). Adjuvant radiotherapy after surgery for pathologically advanced prostate cancer. *J Clin Oncol* **25:** 5671-2.

Vaseva AV, Moll UM (2012). Identification of p53 in Mitochondria. *Methods Mol Biol* **962:** 75-84.

Vecchi M, Polo S, Poupon V, van de Loo JW, Benmerah A, Di Fiore PP (2001). Nucleocytoplasmic shuttling of endocytic proteins. *J Cell Biol* **153:** 1511-7.

Walker JR, Corpina RA, Goldberg J (2001). Structure of the Ku heterodimer bound to DNA and its implications for double-strand break repair. *Nature* **412:** 607-14.

Wang H, Arun BK, Fuller GN, Zhang W, Middleton LP, Sahin AA (2008). IGFBP2 and IGFBP5 overexpression correlates with the lymph node metastasis in T1 breast carcinomas. *Breast J* **14:** 261-7.

Wang YN, Yamaguchi H, Hsu JM, Hung MC (2010). Nuclear trafficking of the epidermal growth factor receptor family membrane proteins. *Oncogene* **29:** 3997-4006.

Warsito D, Sjostrom S, Andersson S, Larsson O, Sehat B (2012). Nuclear IGF1R is a transcriptional co-activator of LEF1/TCF. *EMBO Rep* **13:** 244-50.

Werner H, Karnieli E, Rauscher FJ, LeRoith D (1996). Wild-type and mutant p53 differentially regulate transcription of the insulin-like growth factor I receptor gene. *Proc Natl Acad Sci U S A* **93:** 8318-23.

Wheeler DL, Dunn EF, Harari PM (2010). Understanding resistance to EGFR inhibitors-impact on future treatment strategies. *Nat Rev Clin Oncol* **7:** 493-507.

Wilt TJ, Brawer MK, Jones KM, Barry MJ, Aronson WJ, Fox S *et al* (2012). Radical prostatectomy versus observation for localized prostate cancer. *N Engl J Med* **367:** 203-13.

Wohlbold L, Merrick KA, De S, Amat R, Kim JH, Larochelle S *et al* (2012). Chemical genetics reveals a specific requirement for Cdk2 activity in the DNA damage response and identifies Nbs1 as a Cdk2 substrate in human cells. *PLoS Genet* **8:** e1002935.

Wu C, Liu X, Wang Y, Tian H, Xie Y, Li Q *et al* (2012a). Insulin-like factor binding protein-3 promotes the G1 cell cycle arrest in several cancer cell lines. *Gene* **512:** 127-33.

Wu W, Liu P, Li J (2012b). Necroptosis: an emerging form of programmed cell death. *Crit Rev Oncol Hematol* **82:** 249-58.

Wu Y, Zhao W, Zhao J, Pan J, Wu Q, Zhang Y *et al* (2007). Identification of androgen response elements in the insulin-like growth factor I upstream promoter. *Endocrinology* **148:** 2984-93.

Wu YC, Zhu M, Robertson DM (2012c). Novel nuclear localization and potential function of insulin-like growth factor-1 receptor/insulin receptor hybrid in corneal epithelial cells. *PLoS One* **7:** e42483.

Wu Z, Gioeli D, Conaway M, Weber MJ, Theodorescu D (2008). Restoration of PTEN expression alters the sensitivity of prostate cancer cells to EGFR inhibitors. *Prostate* **68:** 935-44.

Xie Y, Skytting B, Nilsson G, Brodin B, Larsson O (1999). Expression of insulin-like growth factor-1 receptor in synovial sarcoma: association with an aggressive phenotype. *Cancer Res* **59:** 3588-91.

Yamaguchi H, Yoshida S, Muroi E, Yoshida N, Kawamura M, Kouchi Z *et al* (2011). Phosphoinositide 3-kinase signaling pathway mediated by p110alpha regulates invadopodia formation. *J Cell Biol* **193:** 1275-88.

Yang H, Jeffrey PD, Miller J, Kinnucan E, Sun Y, Thoma NH *et al* (2002). BRCA2 function in DNA binding and recombination from a BRCA2-DSS1-ssDNA structure. *Science* **297:** 1837-48.

Yarden Y (2001). The EGFR family and its ligands in human cancer. signalling mechanisms and therapeutic opportunities. *Eur J Cancer* **37 Suppl 4:** S3-8.

Yarosh W, Barrientos T, Esmailpour T, Lin L, Carpenter PM, Osann K *et al* (2008). TBX3 is overexpressed in breast cancer and represses p14 ARF by interacting with histone deacetylases. *Cancer Res* **68:** 693-9.

Yata K, Lloyd J, Maslen S, Bleuyard JY, Skehel M, Smerdon SJ *et al* (2012). Plk1 and CK2 act in concert to regulate Rad51 during DNA double strand break repair. *Mol Cell* **45:** 371-83.

Yavari K, Taghikhani M, Maragheh MG, Mesbah-Namin SA, Babaei MH, Arfaee AJ *et al* (2010). SiRNA-mediated IGF-1R inhibition sensitizes human colon cancer SW480 cells to radiation. *Acta Oncol* **49:** 70-5.

Yee D (2012). Insulin-like growth factor receptor inhibitors: baby or the bathwater? *J Natl Cancer Inst* **104:** 975-81.

Yee D, Morales FR, Hamilton TC, Von Hoff DD (1991). Expression of insulin-like growth factor I, its binding proteins, and its receptor in ovarian cancer. *Cancer Res* **51:** 5107-12.

Yoon S, Seger R (2006). The extracellular signal-regulated kinase: multiple substrates regulate diverse cellular functions. *Growth Factors* **24:** 21-44.

Yu H, Spitz MR, Mistry J, Gu J, Hong WK, Wu X (1999). Plasma levels of insulin-like growth factor-I and lung cancer risk: a case-control analysis. *J Natl Cancer Inst* **91:** 151-6.

Yuen JS, Cockman ME, Sullivan M, Protheroe A, Turner GD, Roberts IS *et al* (2007). The VHL tumor suppressor inhibits expression of the IGF1R and its loss induces IGF1R upregulation in human clear cell renal carcinoma. *Oncogene* **26:** 6499-508.

Yuen JS, Macaulay VM (2008). Targeting the type 1 insulin-like growth factor receptor as a treatment for cancer. *Expert Opin Ther Targets* **12:** 589-603.

Zhang D, Samani AA, Brodt P (2003). The role of the IGF-I receptor in the regulation of matrix metalloproteinases, tumor invasion and metastasis. *Horm Metab Res* **35:** 802-8.

Zhang W, Zong CS, Hermanto U, Lopez-Bergami P, Ronai Z, Wang LH (2006). RACK1 recruits STAT3 specifically to insulin and insulin-like growth factor 1 receptors for activation, which is important for regulating anchorage-independent growth. *Mol Cell Biol* **26:** 413-24.

Zhao H, Dupont J, Yakar S, Karas M, LeRoith D (2004a). PTEN inhibits cell proliferation and induces apoptosis by downregulating cell surface IGF-IR expression in prostate cancer cells. *Oncogene* **23:** 786-94.

Zhao Y, Kwon SW, Anselmo A, Kaur K, White MA (2004b). Broad spectrum identification of cellular small ubiquitin-related modifier (SUMO) substrate proteins. *J Biol Chem* **279:** 20999-1002.

Zheng Y (2001). Dbl family guanine nucleotide exchange factors. *Trends Biochem Sci* **26:** 724-32.

Zong CS, Chan J, Levy DE, Horvath C, Sadowski HB, Wang LH (2000). Mechanism of STAT3 activation by insulin-like growth factor I receptor. *J Biol Chem* **275:** 15099-105.

Zou L, Elledge SJ (2003). Sensing DNA damage through ATRIP recognition of RPA-ssDNA complexes. *Science* **300:** 1542-8.